DESIGN AND PERFORMANCE ANALYSIS OF OPTICAL AND RF ANTENNA USING FDTD SIMULATION

By

Fahmida Ahmed
14371001

A thesis submitted to the Department of Electrical and Electronic Engineering in fulfillment of the requirements for the degree of M.Eng. in Electrical and Electronic Engineering

Electrical and Electronic Engineering
Brac University
July 2021

Declaration

It is hereby declared that

1. The thesis submitted is my/our own original work while completing degree at Brac University.
2. The thesis does not contain material previously published or written by a third party, except where this is appropriately cited through full and accurate referencing.
3. The thesis does not contain material which has been accepted, or submitted, for any other degree or diploma at a university or other institution.
4. I/We have acknowledged all main sources of help.

Student's Full Name & Signature:

_____

Fahmida Ahmed
14371001

Approval

The thesis/project titled "Design and performance analysis of optical and RF antenna using FDTD simulation" submitted by

1. Fahmida Ahmed (14371001)

of Spring, 2021 has been accepted as satisfactory in fulfillment of the requirement for the degree of M. Eng. in Electrical and Electronic Engineering on 06th July 2021.

Examining Committee:

Supervisor:
(Member)

_____
Abu S.M. Mohsin, Ph.D.
Assistant Professor, Department of Electrical and Electronic Engineering
Brac University

External Expert Examiner:
(Member)

_____
Mohammed Belal Hossain Bhuian, Ph.D.
Associate Professor, Department of Electrical and Electronic Engineering
Brac University

Departmental Head:
(Chair)

_____
Md. Mosaddequr Rahman, Ph.D.
Professor and Chairperson, Department of Electrical and Electronic Engineering
Brac University

Abstract / Executive Summary

Abstract: In this study, we have investigated the optical property of single and coupled plasmonic antenna using the finite-difference time-domain (FDTD) method. The extinction efficiency, plasmon coupling, and near and far-field enhancement have been investigated as a function of size and shape for dipole, bowtie, and rectangular nanoantenna. Additionally, we have investigated the patch and probe antenna in terms of return loss, near field power, input impedance, and directivity and observed how antenna parameters can be tuned by changing their dimensions. The findings of this study will be helpful to design a cost-effective and efficient plasmonic nanoantenna by replacing the typical RF antenna in terms of size, efficiency, cost, and convenience.

Keywords: Gold nanoparticle absorption, scattering, near field, far- field, nanoparticle plasmon coupling, field enhancement, directivity, gain and FDTD simulation.

Dedication

Dedicated to my son, parents who sacrificed a lot and my honorable supervisor, Dr. Abu. S.M. Mohsin who taught me all the way and put tremendous effort to guide me for this successful research.

Acknowledgement

Firstly, my gratitude to almighty ALLAH for his blessings (Alhamdulillah). With the unprecedented circumstances of COVID-19 and few unexpected incidents, this thesis was a long pending to me. Hence, it would not justice if I don't mention the inspirations and learnings, I got from my supervisor Dr. Abu S.M. Mohsin, Assistant Professor, Department of EEE, Brac University who motivated and guided me all the way for successful completion of the thesis. My sincere gratefulness to all the faculties of EEE of Brac University for their support and guidance. And my wholehearted appreciation to Sr. Management of Bangladesh Computer Council (BCC) [my employer] who allowed me to develop my educational standing. Last but not least, my family and friends who cares, encourages, sacrifices and always stands beside me to reach this stage. Thank you all!

Table of Contents

List of Tables

List of Figures

List of Acronyms

NPs	Nano particles
FDTD	Finite difference time domain
TFSF	Total-field-scattered-field source
TF	Total-field region
SF	Scattered-field region
SPR	Surface plasmon resonance
LSPR	Localized surface plasmon resonance
PH	Plasmon hybridization
PML	Perfectly matched layer
UV Radiation	Ultraviolet radiation
IR	Infrared radiation
TEM Mode	Transverse electromagnetic mode
TE Mode	Transverse electric mode
TM Mode	Transverse magnetic mode
PEC	Perfect electric conductor
OEWG	Open-ended-waveguide-probe

Chapter 1

Introduction

1.1 Introduction

Antenna is a device that transmits or receives radio electromagnetic waves. Antenna can be in all shapes and sizes. In this study, we investigated performance analysis of RF and optical nano antenna. RF antenna converts electric energy into radio waves which enables the communication between two points and optical nano antennas operating at optical frequencies at nano scale. These two antennas are used in different applications depend on their design and purposes.

We started our analysis with RF antenna. RF antenna is larger in size, no need of fabrication and it has longer wavelength compared to optical antenna. Also, it works in different mechanism. Compared to the RF antenna, optical nano antenna has couple of advantages. Especially, size is smaller than RF. It is tunable where RF is fixed in nature. It can be fabricated in any shape and size utilizing different fabrication technique techniques. Obviously, it is also cost effective and environment friendly.

So, there are couple of advantages of optical nano antenna over RF antenna and that's why we have investigated both the antennas. We simulated several kinds of optical and RF antenna and observed how the key performance parameter varies with respect to antenna size, shape and geometry. We have also investigated how we can tune the frequency varying size and shape. Nowadays researchers are moving towards antenna designing. A thorough study would imperative regarding antenna property and parameter analyzing. In that perspective, we have analyzed RF and optical antenna and observed key performance parameters. All the findings of our study will help us to replicate specific kind of RF antenna with optical antenna with better performance and flexibility.

1.2 Introduction to RF and optical nano antenna

RF antenna is used to convert electric energy into radio waves which enable communication between two ends. Depending on the application, antennas can design in various sizes and shapes. RF antenna is larger in size. They have a frequency range from KHz to GHz. Compared to an optical nanoantenna, there is no need of fabrications. In RF antenna, we studied patch and probe antenna. We analyze all the parameters of patch and probe antenna.

Nanoantenna is the latest development of transceiver components, which does not have an old history. This antenna is very small in size, used to enhance the extraordinary transmission. We studied single triangle, bowtie antenna, dipole antenna. Our main objectives are tuned optical properties of nanoantenna. The main advantage of nano antenna is – It's tunable in size and shape and it can be fabricated with different fabrication techniques or tools. But it has a major disadvantage, for small size, the capability of fabricating and characterizing them became challenging. Anyway, both antennas can design depending on which application you are using.

1.3 State of art of RF and optical antenna

Now we are moving towards fourth industrial revolution (IR 4.0) edge. Everything is becoming smaller with enhanced efficiency. That's why research trend is going to advanced technology zone. Antenna design is one of the major portions of advance technology mostly in communication sector. In the last decade, significant advancement in antenna technology has been achieved by wireless communication system. Moreover, evolution of wireless handheld devices is consequence of antenna's experimentation.

So far, thorough work has not been done in antenna designing. Until now, the details analysis of the antenna parameters has not worked properly. In addition, if we look at the journals that have worked with optical bowtie antenna, Mr. Linhan Lin and Mr. Yuebing Zheng worked on the single bowtie antenna and they investigated a structure's cross-section with fixed

dimensions and varied cut off frequency[1]. Same as for dipole antenna, journals worked about fixed dimensions. Mr. E. Doruk Onal and Mr. Kaan Guven worked on the dipole antenna with fixed dimensions. They didn't tune particles size, shape or dimensions [2]. Similarly, in another paper, Mr. Anil Kumar, Mr Keng H. Hsu, Mr. Pratik Chaturvedi, and Mr. Hyungjin Ma worked on fabrication and optical characterization of bowtie antennas. They investigated bowtie antenna's extinction efficiency by varying particles size and keeping antennas gap as fixed [3]. Moreover, RF antenna can perform in large frequency range. But in typical journal, we can see value of cut-off frequencies radiation patterns are low. Mr. H. M. Sandip Gajera and Mr. N. Patel worked on rectangular microstrip patch antenna. Its return loss (RL) at the desired frequency range is 2.4 GHz which is very low [4]. Similarly, another paper of RF antenna, Mr. A. K. Arya, Mr. A. Patnaik, and Mr. M. V. Kartikeyan worked for improvement of the performance of microstrip antennas. Here cut-off frequencies radiation patterns are also low [5].

For this reason, we are going to analyze the details of the antenna parameters. Antenna can be designed depending on purposes. Basically, dependent on its application both antennas have couple of advantages and disadvantages. It is possible to tune antennas frequency range, size and shape to get desired frequency. In this study our main objective is to analyze antenna's key performance parameters. Then we can get an overview, how can we design both of antenna and which antenna is better suited for which purpose.

1.4 Potential research questions

Antennas are a very important component of communication systems. For antenna designing and performance assessment, we studied many papers about antennas. These papers worked on designing an efficient antenna and developing it to up-to-date applications. After observing papers about antenna, we understand that this area has a lot of freedom to work and can acquire

significant results. Another important thing was no detailed study has been conducted on what kind of problems would occur if nanoparticles size, shape or geometry changed. In this paper we studied about optical nano and RF antenna. In case of optical nano antenna, we observed three types of antennas like single triangle antenna, bowtie antenna and dipole antenna. In the case of bowtie antennas, our observation is most of the studies have dealt with fixed dimensions particles, they have not tuned particle size, shape, dimensions. Additionally, in case of dipole antenna, in literature they are doing with single rectangle, but we are observed for dipole particle, we seen absorption, cross section, scattering for different separation and we observed dramatically change in particles cross sections, field enhancement, optical efficiency. There are lot of opportunities in nanoantenna designing if particles dimension and material are varied. In the case of RF antenna, details work on the improvement of cut-off frequency and wide range of frequency has not been done. This is the remarkable area for antenna designing. We will work on this point. In addition, we tuned the cutoff frequency or wavelength and observed radiation pattern by varying the dimension of RF antenna. Hence, we have done details investigation thoroughly. We think antenna designing are easier for specific application which would be our contribution in this field.

1.5 Research objectives

Research objective of our thesis are given below:

1. We studied the optical property of single, coupled, and dipole plasmonic antenna using FDTD method. We determined their extinction efficiency, plasmon coupling, and near and far-field enhancement as a function of size and separation.

2. We investigated optical property of patch and probe RF antenna. For parameter analyzing, we investigated the return loss, near field power, input impedance, and directivity. Hence, we examined how antenna performance parameters can be tuned by changing their dimensions.

The findings of this study will be helpful to design a cost-effective and efficient plasmonic nanoantenna by replacing the typical RF antenna in terms of size, efficiency, cost, and convenience.

1.6 Proposed methodology

We have studied optical property of single, coupled (bowtie nano antenna), dipole antenna of gold (au) nano particle. And analyze patch antenna and patch antennas' parameters. Hence, we do not have accessible proper analytical or equational methods. When we are going to see the coupling effect, it is possible for a single particle but not possible for a coupled particle. That's why, in terms of implementation we use finite difference time domain (FDTD) simulation for all investigation.

1.7 Thesis outline

Chapter 1 – We categorized our first chapter with basics liike introduction and motivation of our thesis, RF and plasmonic nano Antenna, antenna parameters, surface plasmon resonance, localized surface plasmon resonance, absorption, scattering and extinction Theory, plasmon hybridization theory for nano antenna etc. We added a comparison between RF and nano antenna along with highlighting our objectives.

Chapter 2 – This chapter is focused on theory and simulation. We have discussed about Simulation method for design and characterization of Nano particle. We first discussed about FDTD Theory, differential form of Maxwell's equations and the Yee Cell and software (FDTD parameters & solutions). Finally, we have showed some layout editor of FDTD simulation from our projects.

Chapter 3 – In this chapter we investigated the optical property of single and coupled (bowtie nano antenna) gold (Au) nano particle by finite difference time domain (FDTD) simulation. In

this study, we observed the optical cross section and field enhancement for single and coupled Au nanoparticle as a function of diameter, size and separation.

Chapter 4 – Same as chapter 3, here we investigated the optical property of characterization of dipole Nanoantenna, also observed the optical cross section and field enhancement for coupled dipole (Au) nanoparticle as a function of diameter, size and separation.

Chapter 5 – In this chapter we investigated the parameter of patch and probe antenna by finite difference time domain (FDTD) simulation. In this study we observed how antenna parameters can be tuned by changing their dimensions.

Chapter 6 – This is our last chapter where we summarized our whole paper. We concluded our investigations with some challenges and what can be our future work. Finally, we highlighted thesis conclusions.

Chapter 2

Theory of RF and optical nano antenna

2.1 Introduction

In this chapter, we will discuss RF and nano antenna's theory and their parameters. Our target is to design an effective antenna and so we needed to study the concept of RF and plasmonic nanoantenna and their theory or related calculations.

Antennas can be classified by different criteria. To classify based on their working frequency is one method which can be classified as RF and nano antenna. RF antennas have been used for radio waves or microwaves, whereas nanoantenna are operated the same way but with infrared or visible light.

2.2 Theory of RF antenna

RF antenna device works like either transmitter or receiver. When RF antenna generates electromagnetic wave then it works like transmitter. At the time to receive electromagnetic wave, then it works as receiver. Moreover, we can say, the antenna at the transmitter generates the radio wave. A voltage at the desired frequency is applied to the antenna. The voltage across the antenna elements and the current pass through them create the electric and magnetic waves, respectively. At the receiver, the electromagnetic wave passing over the antenna induces a small voltage. Thus, the antenna becomes the signal source for the receiver input. In many wireless applications, the antenna is switched between the transmitter and receiver. Signals can move from one antenna to another in several ways, based on the radio wave's frequency. At low frequencies (less than 3 MHz), propagation is by ground wave, where the signal embraces the earth's surface. Distance is limited to a hundred miles or so. AM radio waves are a good example of low-frequency propagation.

At frequencies in the 3- to 30-MHz range (short waves), signals travel to 30 to 250 miles into the ionosphere, where they're refracted back to earth. It's almost like radiating the signal so that it appears to be reflected-off of a conducting surface. Very long distances can be achieved as the signals can make several hops from the earth to the ionosphere and back several times.[6] Antennas can be classified depends on their physical structure and functionality:

Type of antenna	Examples	Applications
Wire Antennas	Dipole antenna, Monopole antenna, Helix antenna, Loop antenna	Personal applications, buildings, ships, automobiles, space crafts
Aperture Antennas	Waveguide (opening), Horn antenna	Flush-mounted applications, aircraft, space craft
Reflector Antennas	Parabolic reflectors, Corner reflectors	Microwave communication, satellite tracking, radio astronomy
Lens Antennas	Convex-plane, Concave-plane, Convex-convex, Concave lenses	Used for very high frequency applications
Micro strip Antennas	Circular-shaped, rectangular shaped metallic patch above the ground plane	Aircraft, spacecraft, satellites, missiles, cars, mobile phones etc.
Array Antennas	Yagi-Uda antenna, Micro strip patch array, Aperture array, Slotted wave guide array	Used for very high gain applications, mostly when needs to control the radiation pattern

Table 1.-Types of antennas depending on their applications. [7]

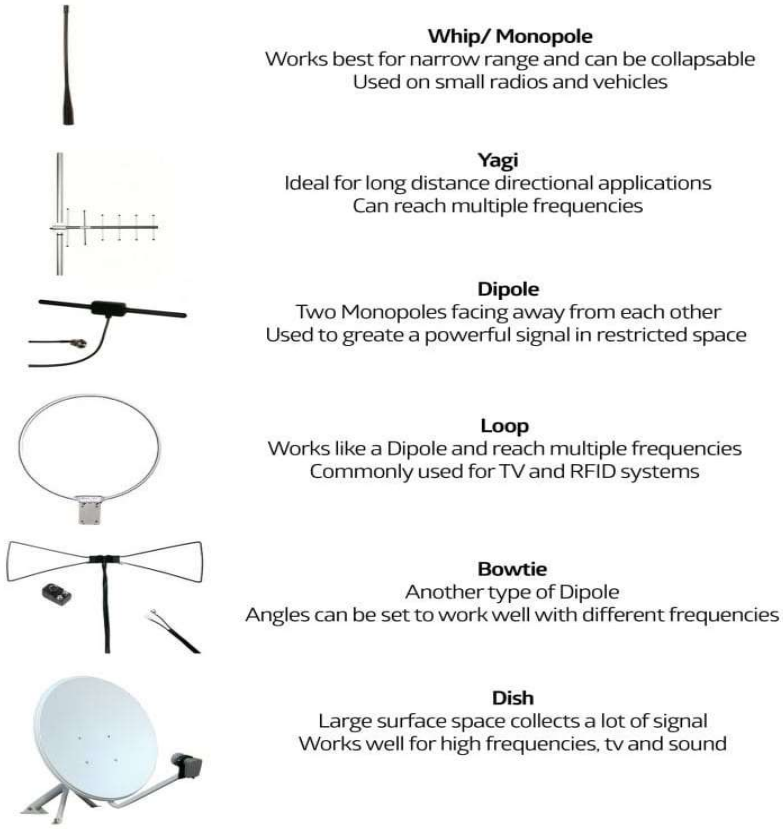

Figure 2.1- Some RF antennas.[8]

2.2.1 RF antenna parameters

Antenna measurement is a technique which means testing of an antenna. This technique ensures antenna's specifications. Typical antenna parameters are efficiency, gain, bandwidth, radiation pattern, beamwidth, polarization, impedance and near-far field region etc.[9]

Efficiency- The efficiency of an antenna is defined as the radiated power divided by the power delivered to the antenna. The efficiency can be expressed as-

$$\eta = P_{rad}/P_{in},$$

Here, if the antenna has 95% efficiency and 100W is being delivered to the antenna, then 95W will be converted into electromagnetic radiation.

Gain- Gain is how much input power is transmitted in the direction of peak radiation to that

of an isotropic source. The gain can be expressed as-

$$\mathbf{G=\eta.\ D},$$

The gain is calculated as the product of the efficiency (**η**) and the directivity (**D**). Here the efficiency of an antenna can take on any value between 0 and 1, and the directivity can take on any value greater than or equal to one, the gain can be any positive value. Antenna gain is expressed in decibels (dB), a logarithmic scale. From the gain factor G, one finds the gain in decibels as.

Bandwidth is a fundamental parameter of an antenna. The bandwidth of an antenna is the band of frequencies, over which it is considered to perform acceptably. In other word, bandwidth depends on the overall effectiveness of the antenna through a range of frequencies. Percentage of bandwidth can be defined by,

$$\mathbf{BW=100\times\frac{(F_H\times F_L)}{F_C}},$$

Here, F_H is the highest frequency band and F_L is the lowest frequency band and F_c is the center frequency band.

Radiation pattern delivers information that can describe how an antenna directs the energy which it radiates. Radiation patterns determine fields regions. If we want to describe radiation properties of an antenna in graphically such as amplitude, phase and polarization then we must use function of the angular space coordinates θ, Φ.

E-Plane, a linearly-polarized antenna plane consists two objects, one is the electric field vector (E aperture) and other one is direction of maximum radiation. Basically 'E' plane finds out the polarization of the radio wave. But for a vertically polarized antenna, the E-plane usually coincides with the vertical/elevation plane and horizontally polarized antenna, the E-Plane usually coincides with the horizontal/azimuth plane.

H-plane, a linearly polarized antenna which is the plane containing the magnetic field vector (H aperture) and the direction of maximum radiation. The magnetizing field or 'H' plane lies

at a right angle to the 'E' plane. But a vertically polarized antenna, the H-plane usually conforms to the horizontal/azimuth plane and horizontally polarized antenna, the H-plane usually conforms to the vertical/elevation plane.

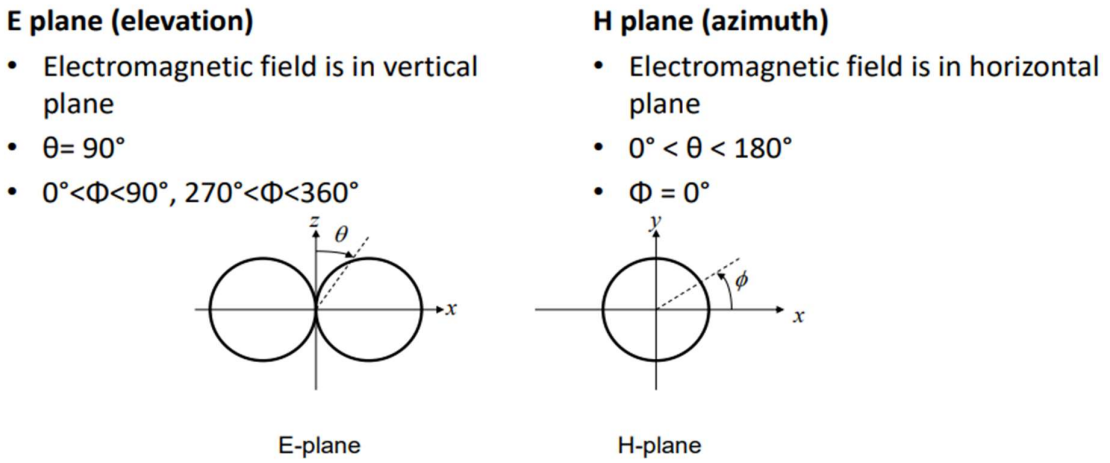

Figure 2.2 Radiation pattern of RF antennas[10]

Beam width usually measure in degree. Beam is a directional projection of light energy radiating from natural or artificial source. Beam width is the diameter of any specified line that is perpendicular to the beam axis and intersects it. Beams typically do not have sharp edges.

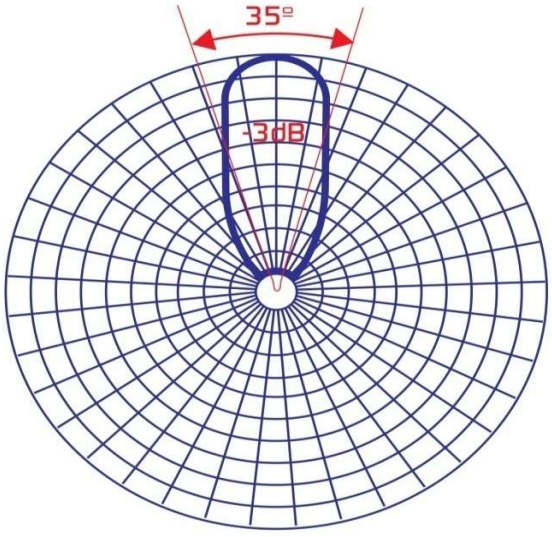

2.3 Figure: Beam width

Polarization is an important factor of antenna when designing and erecting radio antennas. Antenna polarization can be defined as the direction of the electric field of an electromagnetic

field. Basically, polarizations can be linear, circular, elliptical, cross and co-polarization. In linear polarization electric fields are generated vertical vs. horizontal. Linear polarization mostly used in radio communication applications and vertical polarization is often used for mobile radio communications. In circular polarization, electric fields are generated left-handed circular (LHC) vs. right-handed circular (RHC) and it's used for GPS system.

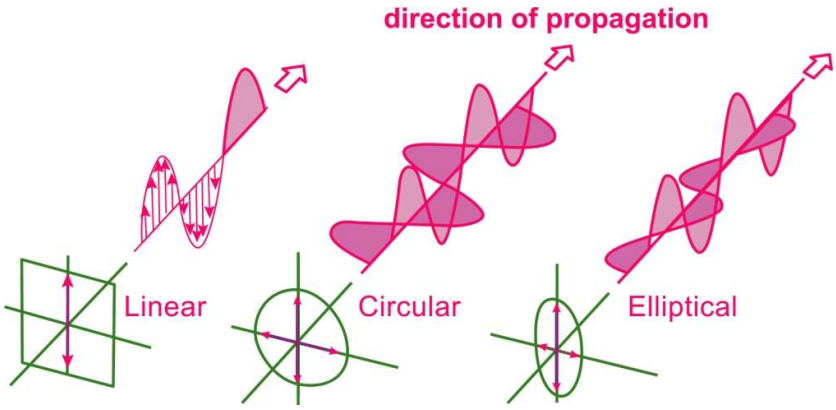

Figure 2.4: Types of polarization.[11]

Impedance is another parameter to describe antenna, it's a ratio between the voltage and the current at their input terminals. Electromagnetic power reached to antenna via transmission line. This power can be reflected and to avoid this reflection electromagnetic power backs to transmitter, and here antenna input impedance should match with transmission line. For matching with transmission line, input impedance usually set on 50ohm and 75ohm.

Field region is an important aperture of antenna. There are two regions in antenna – near field and far field. Near field communication can be considered the twin of far field communication. Both terms describe certain areas within an electromagnetic field formed around an antenna. In addition to the near and far field regions, a transition zone between the two also exists. Near field, as the name suggests, is very close to the antenna while far field is further away. The distance in the region from an antenna creates very different properties in how the electromagnetic field reacts. By taking advantage of these properties in the near field region, near field communication is possible.[12]

The far field region of an electromagnetic field starts approximately two wavelengths from the antenna and extends outward. As the distance increases, the strength of the electromagnetic field decreases equal to the square of the distance of the field from the antenna. If the signal is picked up by another antenna this has no effect on the original antenna signal.

Between the near and far field, transition zone exists, which retains properties of both near and far field communication depending on the distance. No exact distance exists for the transition zone. Changing of region based on several factors, such as the strength of the signal sent by the transmitting antenna.

The near field region is the region right next to the antenna. It is defined by the following equation:

Near Field Region $< \frac{2D^2}{\lambda}$

Where, D=Maximum linear dimension of the antenna and λ=Wavelength of the EM waves

In this region, the fields are sort of unpredictable and therefore no measurements are usually made in this region. This region is further divided into two parts:

Reactive near field: This is the region that is adjacent to the antenna. In this region, the E-Field and H-Field are 90 degrees out of phase with each other and are therefore reactive. To radiate or propagate, the E/H fields need to be orthogonal (perpendicular) and in phase with each other.

Reactive near field region $< 0.62 \frac{\sqrt{D^3}}{\sqrt{\lambda}}$

Where D=Maximum linear dimension of the antenna and λ=Wavelength of the EM waves

Radiative near field: This region is also known as the Fresnel Region. It is the region between the reactive near field and the far field. This is the region where the EM fields start to transition

from reactive to radiating fields. However, since they have not completely transitioned, the shape of the radiation pattern still varies with distance.[13]

$0.62\frac{\sqrt{D^3}}{\sqrt{\lambda}}$< Reactive near Field Region<$\frac{2D^2}{\lambda}$

Where D=Maximum linear dimension of the antenna and λ=Wavelength of the EM waves

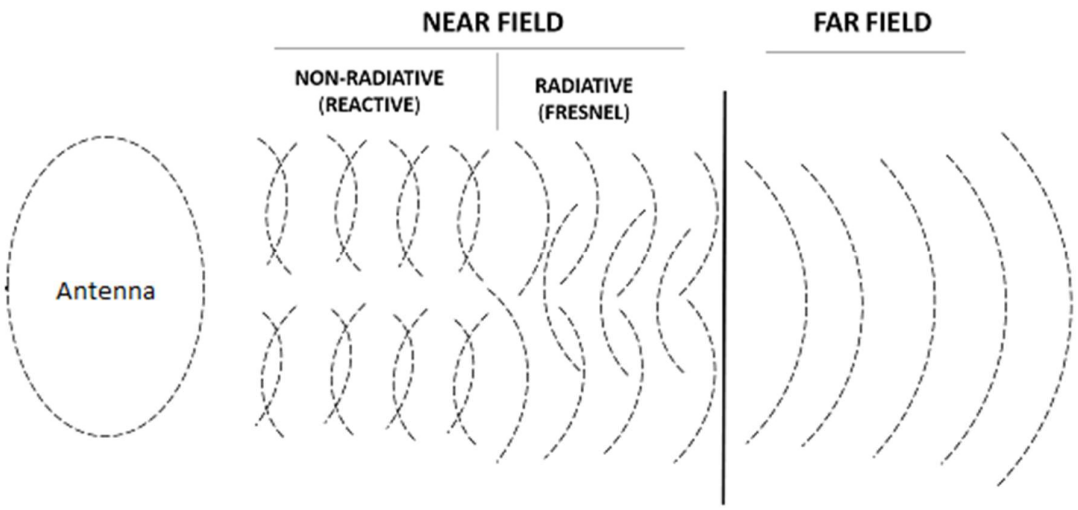

Figure 2.5: Field regions, i) Near field ii) Far field[14]

The Far Field Region is the region that comes after the radiative near field. In this region, the EM fields are controlled by radiating fields. The E and H-fields are perpendicularity to each other and to the direction of propagation as with plane waves. The far-field region is represented by the following equation:

Reactive Far Field Region > $\frac{2D^2}{\lambda}$

Where D=Maximum linear dimension of the antenna and λ=Wavelength of the EM waves.

Antennas are usually used to transfer signals at large distances which are considered to be in the far-field region. One condition that must be met when making measurements in the far field region is that the distance from the antenna must be much greater than the size of the antenna and the wavelength.

2.3 Theory of nano antenna

An antenna is a device used to propagate, receive, and/or transmit electromagnetic waves. Radio waves are just one type of electromagnetic wave. A sound wave may be translated into an electronic signal that is sent to a transmitter (antenna). The antenna creates an electromagnetic wave that carries the original embedded sound information through the atmosphere/space around it. An antenna at a different location, receives the electromagnetic wave, sending it to circuitry (your radio) that translates it to an electronic signal and then back to a sound wave.

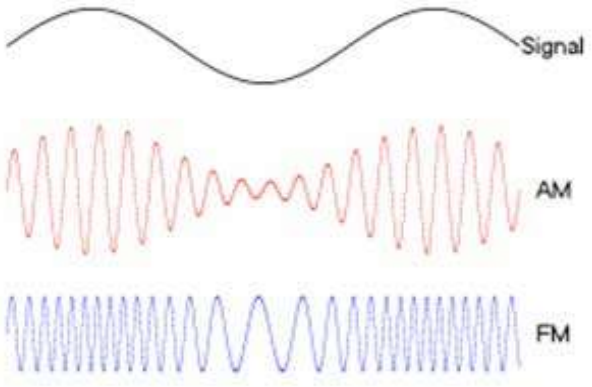

Figure 2.6: RF wave

A nanoantenna is an antenna that is very, very small, and is not used to carry our embedded sound waves from one place to another. A nano antenna operates same as RF antenna but works at higher frequency. It converted electrical signals into photons and radiated them in specific directions using a low footprint. Basically, plasmonic nanoantenna are made of gold and silver material because of their good metallic properties and low absorption.[15]

Antennas convert electrical signals to radio waves and emit them in a particular direction, allowing increased performance and reduced interference. This principle, which is useful in radio wave technology, could also be interesting for miniaturized light sources. After all, almost all internet-based communication utilizes optical light communication.

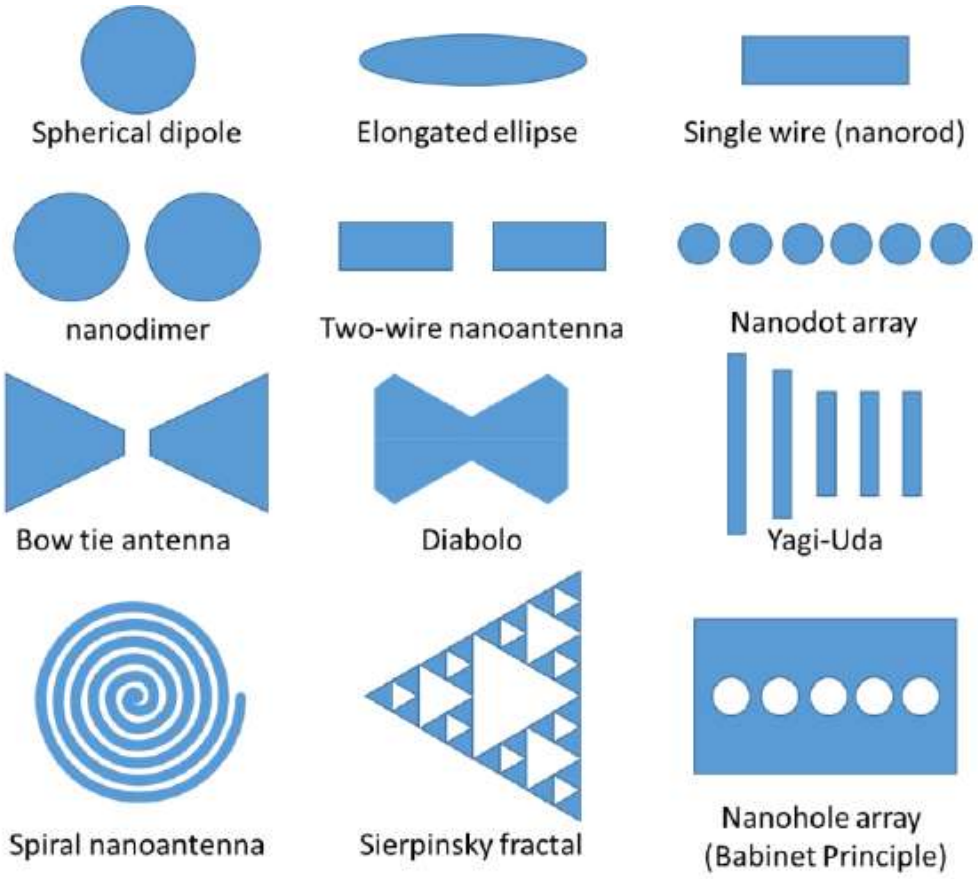

Figure 2.7: Some different types of experimental plasmonic nano antennas.

[16]

Nano antennas' application in modern science are expanded, such as medicine, photovoltaics, spectroscopy, near-field microscopy, photonics, sensory probes, therapeutic agents, drug delivery in biological and medical applications, electronic conductors and catalysis. Actually some of them already have employed optical antennas in operating devices (spectroscopy), while others are expected to start using them in the near future (medicine). Other fields like photovoltaics' and photonics are still experimental test sites with nano antennas.

Applications of optical nanoantenna in medicine for diagnostics and the treatment of malignant tumors, can improve the efficiency of solar cells, the enlargement of scattering cross sections and their application in the capacity of specialized probes for near-field microscopy.

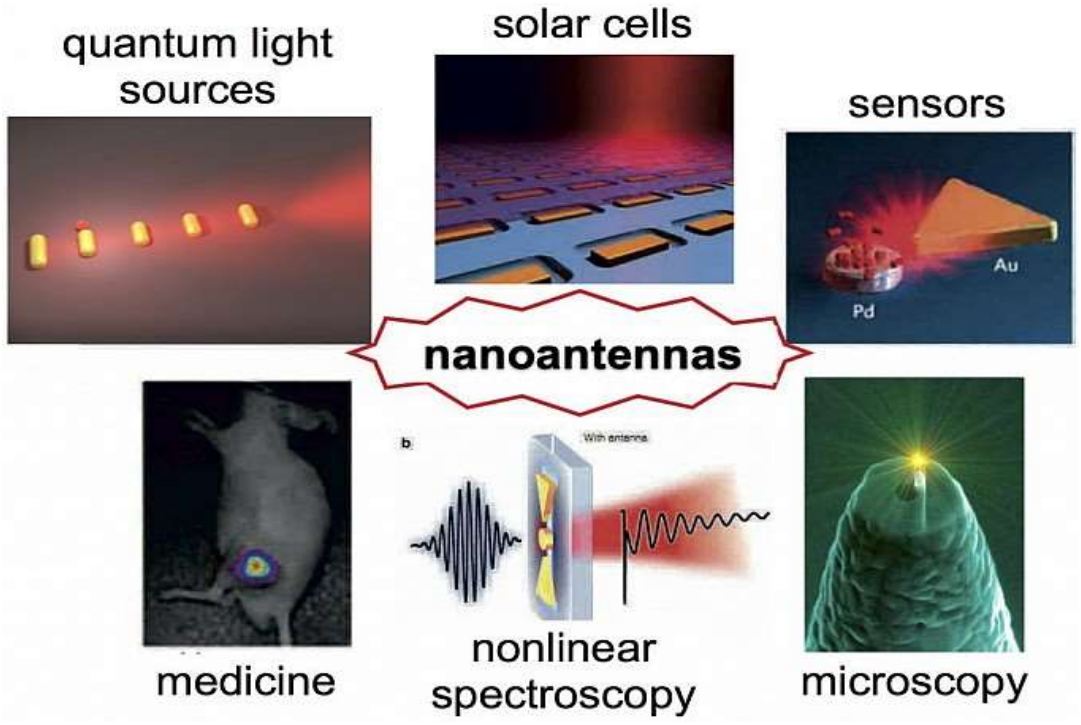

Figure 2.8: Examples and applications of optical nanoantennas in various areas, including solar cells, molecular and biomedical sensors, optical communication, and optical tweezers.[17]

2.3.1 Nano antenna parameters

Surface plasmon resonance

The unique optical properties of plasmonic nanoparticles have been observed for thousands of years. Since ancient times, artists have used colloidal nanoparticles of gold, silver, and copper to give color to pottery and stained glass. The beautiful range of colors results from adjustable optical properties in certain plasmonic nanoparticles. The phenomena that provides tunable control of nanoparticle light absorption and scattering is known as surface plasmon resonance (SPR).[18]

SPR occurs in plasmonic metal nanoparticles when the free surface electrons collectively oscillate, induced by light of specific wavelength. Figure 2.9 illustrates surface plasmon resonance (SPR) for a metallic sphere. When an incoming electromagnetic wave matches the

frequency of the oscillation of the electron cloud, SPR resonance occurs, and the light is absorbed.

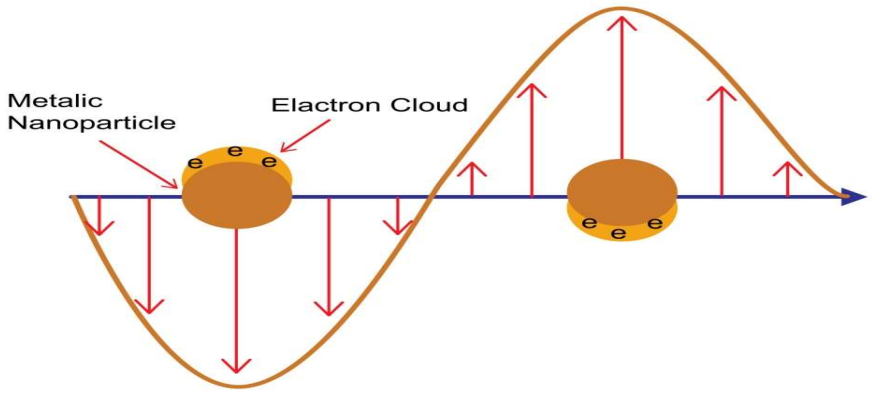

Figure 2.9: Schematic showing surface plasmon resonance (SPR) for a metallic sphere

This effect depends upon the polarizability of a particular nanoparticle. The polarizability is dependent upon numerous factors, including the size, shape, material composition, surface coating, and medium. Each of these factors can be tuned to change the resonance wavelength, though some of them can have larger effect than others.

For spherical plasmonic nanoparticles, the resonant wavelength depends on the particle's radius, material composition, and the refractive index of the medium. Increasing the radius or the medium's refractive index will cause a red shift of plasmon resonance (increases the wavelength at which plasmon resonance occurs).

According to Gans theory, polarizability, and therefore plasmon resonance wavelength, is highly dependent on both size and shape. When symmetry is broken, a particle gains additional modes of plasmon resonance. In the case of gold nanorods, this means that they have two SPR wavelengths: transverse and longitudinal. Figure 2.10 illustrates the two plasmon resonances of gold nanorods. The plasmonic gold nanorod is more easily polarized longitudinally, meaning the SPR occurs at a lower energy, and thus higher wavelength. As the aspect ratio (ratio of length to width) of a nanorod is increased for a fixed diameter, the longitudinal and

transverse plasmon resonances are both affected; however, the longitudinal axis is more polarizable and more sensitive to aspect ratio changes.

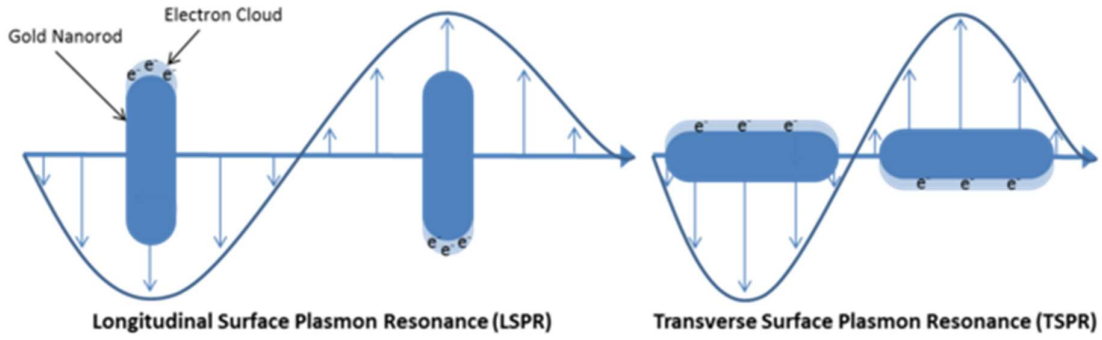

Figure 2.10: Schematic showing the two SPRs of gold nanorods

In gold nanorods, the longitudinal surface plasmon resonance (LSPR) wavelength can be tuned from 550nm to over 2000nm by adjusting to longer aspect ratios, while the transverse surface plasmon resonance (TSPR) remains relatively constant at approximately 510–520nm. As a convention, the peak LSPR (as opposed to TSPR) wavelength is often quoted to define gold nanorods with absorbance spanning the visible to near-infrared region (NIR)[19]

2.3.2 The physics of plasmon resonances

Effect of the plasmon resonance of free electrons in the metal nanoparticle can be understood by studying the polarizability (the ease with which charges, such as the conduction electrons on the metal nanoparticle surface, undergo charge distribution and form partial dipoles). For a spherical nanoparticle, the quasi-static polarizability of the nanoparticle is given by

$$\alpha = 4\pi\varepsilon_0 \, r^3 \, \frac{\varepsilon_1(\omega) - \varepsilon_2}{\varepsilon_1(\omega) + 2\varepsilon_1}$$

Where ε_1 is the wavelength dependent dielectric function of the nanoparticle and ε_2 is the dielectric function of the medium which remains roughly constant regardless of wavelength. When the condition Re = $-2\varepsilon_2$ is satisfied, the particle is driven into resonance resulting in a strong increase in the absorption and/or scattering at that wavelength. The resonance condition

depends on the wavelength dependent dielectric function of the nanoparticle as well as the dielectric function of the medium. Consequently, the nanoparticle optical properties are highly dependent on material composition, size, and the medium in which the particles are embedded. [18]

Nanoparticle optical properties are also sensitive to the proximity of other plasmonic materials. When two or more plasmonic nanoparticles are near each other (with edge-to-edge separations of one particle diameter or less) then surface plasmons couple occurred. Their surface Plasmon couple works as a conduction electron. Each particle of surface plasmons collectively oscillate.[20] This effect is similar to molecular orbital theory. The result of plasmon coupling is assuming that oscillating electrons are in the lowest energy state, because wavelength of the plasmon resonance of the coupled particles move on red-shift to longer wavelengths (lower energies).

2.3.3 Localized surface plasmon resonance

Surface plasmon resonance (SPR) and localized surface plasmon resonance (LSPR) both are controlling tools for nano particle. Because of their high sensitivity to the refractive index, that change is caused by their interactions with molecules.

A localized surface plasmon (LSP) is a result of the imprisonment of surface plasmon. In theory, size of surface plasmon's nanoparticle is comparable to smaller than the wavelength of light. It is used to stimulate the plasmon.

As per oscillation theory we know, when a small round metallic nanoparticle is illuminated by light, the oscillating electric field occurs because of the conduction electrons to oscillate coherently. When the electron cloud is replaced relative to its original position, a restoring force appears from coulombic attraction between electrons and nuclei. This force causes the electron cloud to oscillate. We can determine oscillation frequency by electron description like the consistency of electrons, the effective electron mass, and the size and shape of the charge

distribution etc. The LSP has two significant impacts. One is – electric fields near the particle's surface are greatly enhanced and other one is – the particle's optical absorption has a maximum point at the plasmon resonant frequency. Surface plasmon resonance can also be tuned by the shape of the nanoparticle [1]. The enhancement falls quickly with distance from the surface and for noble metal nanoparticles while the resonance occurs at visible wavelengths. Localized surface plasmon resonance creates brilliant colors in metal colloidal solutions [21].

For metals like silver and gold, the oscillation frequency is also affected by the electrons in d-orbitals. Gold is a popular choice in plasmonics, which studies the effect of coupling light to charges as it can support a surface plasmon over a wide range of wavelengths (300-1200 nm), and its peak absorption wavelength is easily changed [21]. For instance, the peak absorption wavelength of triangular silver nanoparticles was altered by changing the corner sharpness of the triangles. It underwent a blue shift as corner sharpness of the triangles decreased.

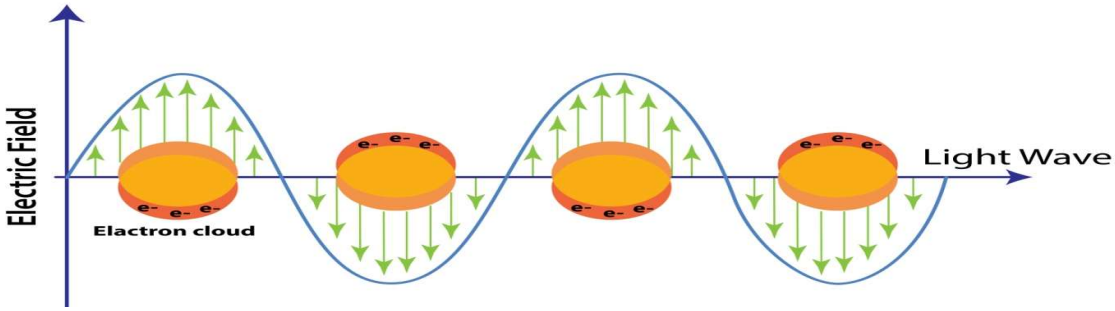

Figure 2.11: Schematic figure showing, light incident on a metal nanoparticle causes the conduction band electrons to oscillate. This is the localized surface plasmon.

2.3.4 Theory of absorption, scattering and extinction

Absorption is a process which can eliminate energy from the electromagnetic radiation field and transform it to another form. In other word we can say, an electromagnetic wave after passing through a matter, we can get certain results from two contributions – one is absorption other one is scattering. Moreover, scattering is a process, which conserves the total amount of energy, but the direction in which the radiation propagates may be altered. Last extinction is

the sum of scattering and absorption light, so it represents total effect of medium on radiation passing the medium.[22]

2.3.5 Plasmon hybridization theory

In this thesis, our objective is to design and characterization of nano-antenna by tuning their optical properties. Plasmon hybridization is a recently developed theory used to describe the collective oscillations of conduction electrons in metallic nanoparticles (plasmons). With Plasmon Hybridization (PH) and Finite-Difference Time-Domain (FDTD) method, we theoretically investigated the optical properties of some complex metallic (gold) nanostructures (coupled bowtie / dipole, patch antenna, probe antenna systems). [23]

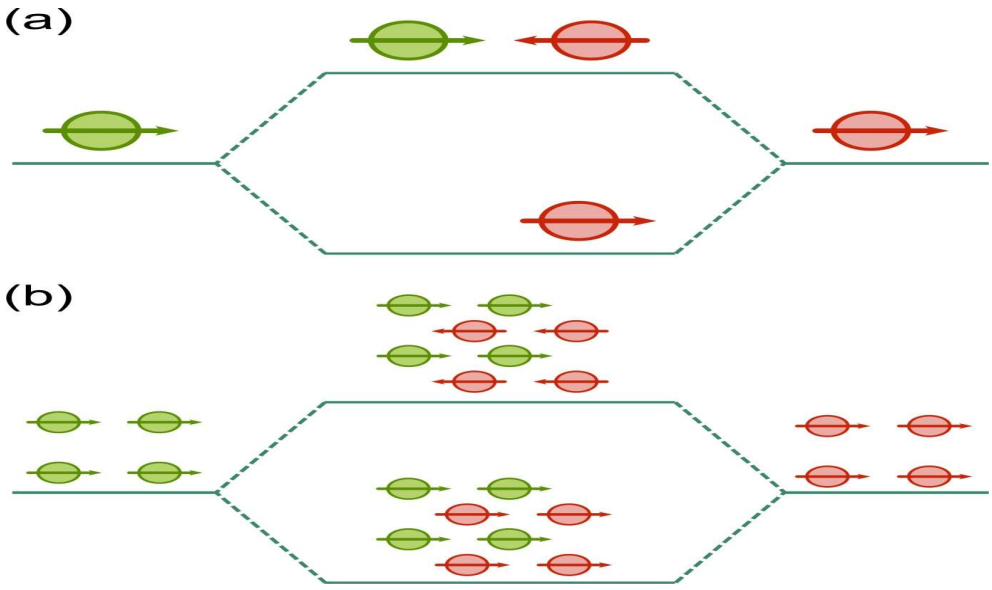

Figure 2.12: Summary of plasmon hybridization model. (a) Hybridization diagram for two identical plasmonic nanoparticles. When considered individually, each nanoparticle supports a dipolar mode. However, if the particles are placed together, the interaction between the dipolar modes leads to the formation of two hybridized modes, commonly referred to as bonding and antibonding, with energies determined by the strength of the interaction. (b) Hybridization diagram for two periodic arrays of plasmonic nanoparticles. Similar to the case of individual particles, the interaction between the lattice resonances of two identical arrays leads to the formation of hybridized lattice resonances when the arrays are placed in the same plane. [24]

In this thesis, we investigated that multiple peaks arise at strong coupling region which occurs due to hybridization of plasmon energy.

These are important parameter of nano antenna but similar to RF, some parameter concepts are used in nano antenna such as efficiency, gain, bandwidth, radiation pattern, polarization, impedance and near-far field region etc.

2.4 Comparison between RF and nano antenna

We have discussed various comparisons between RF and optical antenna, some of which are highlighted below:

Criteria	RF Antenna	Optical nano antenna
Size	From mm to cm	From um to nm
Radio Spectrum	3 Hz to 30000GHz	More than 30000GHz
Frequency Range	From KHz to GHz	In THz
Band width	Comparatively low bandwidth	High bandwidth
Antenna size	Big size	Very small size
Use in inter chip communication	Cannot use for inter chip communication	Can be use for inter chip communication
Speed	Comparatively low speed	High Speed Electronics circuit
Fabrication	No need to fabricate	Difficult to Fabricate
Wavelength	Longer wavelength	Small wavelength (High losses)
Causes waves	Current causes waives	Surface plasmon's causes waves
Excitation by	Feeding devices	Direct light excitation
Skin Depth	From 20 -30 nm	Skin Depth > diameter of antenna
Use in Area	Used in wireless communication	Can be use in advance technology like-medicine, photovoltaics, spectroscopy, near-field microscopy, photonics, sensory probes, therapeutic agents, drug delivery in biological and medical applications etc.

Table 2: Comparison between RF and Nano antenna

2.5 Conclusions

In this chapter, we have discussed about RF antenna and plasmonic nano antenna. We also highlighted about antenna parameters, antennas classification, surface plasmon resonance, localized surface plasmon resonance, absorption, scattering and extinction theory, plasmon hybridization theory etc. In addition, we tried to practice all equation regarding antenna. This chapter contains all the basic knowledge about antenna which will be helpful to complete our next chapters.

Chapter 3

Numerical simulation

3.1 Introduction

In this chapter, we discussed about numerical simulation theory and simulation method. Later we will discuss about simulation setup, how to do simulation and followed it step by step. For numerical simulation purpose we used Finite-difference Time-Domain (FDTD) technique using Lumerical Software.

3.2. FDTD theory

In the Finite Difference Time Domain (FDTD) method, a discretized form of Maxwell's equations is solved numerically and simultaneously in both the 3D space and time. During this process, the electric and magnetic fields are computed everywhere in the computational domain and as a function of time starting at t = 0. From knowledge of the primary fields in space and time, we can compute other secondary quantities including frequency domain characteristics such as scattering parameters, input impedance, far-field radiation patterns, radar cross section, etc.[25]

In terms of FDTD implementation, the full-wave techniques are used to solve problems in electromagnetic. It is well suited to modeling inhomogeneous materials and simulation of wideband antennas. Since it is a time domain method, Fourier techniques are applied to convert the time domain results into the frequency domain and thus a single FDTD simulation can be used to characterize a wideband frequency response.

FDTD is a finite domain numerical technique; the computational domain of the problem must be truncated. At the boundaries of the computational domain, proper boundary conditions must be enforced. In a shielded structure, all objects are enclosed within a perfect electric (or

magnetic) conductor box. In an open boundary problem like an antenna, some kind of absorbing boundary conditions such as a perfectly matched layer (PML) must be used to emulate the free space. The absorbing boundaries should act so that the incident fields and waves propagate through them without any back reflection. The FDTD simulation time depends directly on the size of the computational domain and on how close you can place the PML walls to the enclosed objects.

The FDTD computational domain must be discretized using an appropriate meshing scheme. A fixed-cell mesh generator is also available, where you can set constant cell dimensions along the three-principal axis for the entire computational domain. The variable mesh density is specified in terms of the effective wavelength inside material media. As a result, the mesh resolution and average mesh cell size differ in regions that are filled with different types of material. Electromagnetic simulator's adaptive mesher generates more cells in the areas that are occupied by dielectric materials, fewer cells in the free-space regions and no cells inside PEC regions. Electromagnetic simulator's default adaptive mesh generator also refines the mesh around curved segments of lines, surface or solids to produce a far more accurate representation of your geometry.[26]

The FDTD method provides a wideband simulation of your physical structure. In order to produce sufficient spectral information, an appropriate wideband temporal waveform is needed to excite the physical structure. This method is a grid-based differential numerical modeling method which is called the finite difference methods. The time-dependent Maxwell’s equations which are in partial differential form are changed into discrete forms and the resulting finite-difference equations can be solved in either way, either software or hardware. When we examined the Maxwell's differential equations, then we can see that the change in the E-field and H- field. Here E- field is time (the time derivative) is dependent on the change in the H-field across space (the curl).

3.3 Differential form of Maxwell's equations and the Yee Cell

Maxwell's equations for an isotropic, time-invariant and homogeneous medium are given by

$$\nabla \times E = -\frac{\partial B}{\partial t} - M$$

$$\nabla \times H = \frac{\partial h}{\partial t} + J$$

Where E and H are the electric and magnetic fields, respectively, D and B are the electric and magnetic flux densities, respectively, J and M are the volume electric and magnetic current densities, respectively, and the following constitutive relationships hold:

$$D = \epsilon E, \qquad J = \sigma E$$

$$B = \epsilon H, \qquad M = \sigma m H$$

Where ε is the permittivity, μ is the permeability, σ is the electric conductivity, and σ_m is the magnetic conductivity of the medium. In a medium without electric or magnetic losses these equations can be rewritten as:

$$\frac{\partial H}{\partial t} = -\frac{1}{\mu}\nabla \times E$$

$$\frac{\partial E}{\partial t} = \frac{1}{\in}\nabla \times H$$

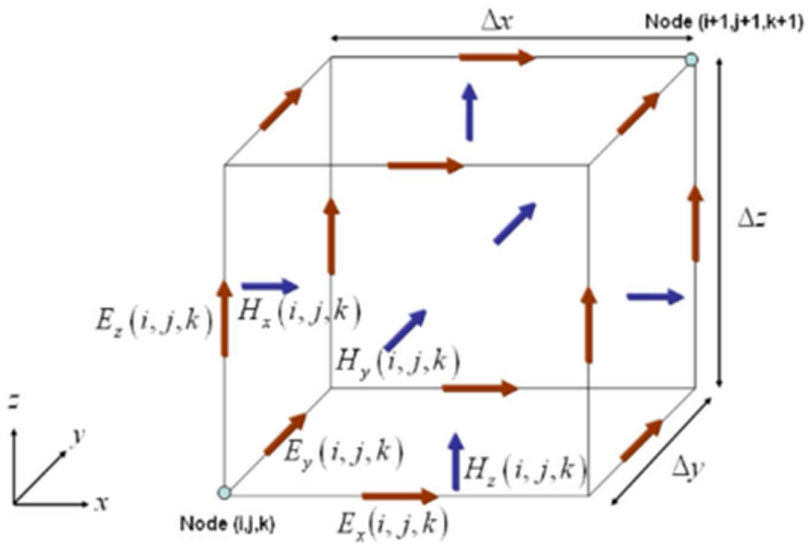

Figure: 3.1 Yee cell geometry [27]

$$H_x^{n+\frac{1}{2}}(i,j,k) = H_x^{n-\frac{1}{2}}(i,j,k) + \frac{\Delta t}{\mu(i,j,k)}\left[\frac{E_y^n(i,j,k+1) - E_y^n(i,j,k)}{\Delta z} - \frac{E_z^n(i,j+1,k) - E_z^n(i,j,k)}{\Delta y}\right.$$

$$H_y^{n+\frac{1}{2}}(i,j,k) = H_y^{n-\frac{1}{2}}(i,j,k) + \frac{\Delta t}{\mu(i,j,k)}\left[\frac{E_z^n(i+1,j,k) - E_z^n(i,j,k)}{\Delta x} - \frac{E_x^n(i,j,k+1) - E_x^n(i,j,k)}{\Delta z}\right.$$

$$H_z^{n+\frac{1}{2}}(i,j,k) = H_z^{n-\frac{1}{2}}(i,j,k) + \frac{\Delta t}{\mu(i,j,k)}\left[\frac{E_x^n(i,j+1,k) - E_x^n(i,j,k)}{\Delta y} - \frac{E_y^n(i+1,j,k) - E_y^n(i,j,k)}{\Delta x}\right.$$

$$E_x^{n+1}(i,j,k) = E_x^n(i,j,k) + \frac{\Delta t}{\varepsilon(i,j,k)}\left[\frac{H_z^{n+\frac{1}{2}}(i,j,k) - H_z^{n+\frac{1}{2}}(i,j-1,k)}{\Delta y} - \frac{H_y^{n+\frac{1}{2}}(i,j,k) - H_y^{n+\frac{1}{2}}(i,j,k-1)}{\Delta z}\right.$$

$$E_y^{n+1}(i,j,k) = E_y^n(i,j,k) + \frac{\Delta t}{\varepsilon(i,j,k)}\left[\frac{H_x^{n+\frac{1}{2}}(i,j,k) - H_z^{n+\frac{1}{2}}(i,j,k-1)}{\Delta z} - \frac{H_y^{n+\frac{1}{2}}(i,j,k) - H_y^{n+\frac{1}{2}}(i-1,j,k)}{\Delta x}\right.$$

$$E_z^{n+1}(i,j,k) = E_z^n(i,j,k) + \frac{\Delta t}{\varepsilon(i,j,k)}\left[\frac{H_y^{n+\frac{1}{2}}(i,j,k) - H_y^{n+\frac{1}{2}}(i-1,j,k)}{\Delta x} - \frac{H_x^{n+\frac{1}{2}}(i,j,k) - H_x^{n+\frac{1}{2}}(i,j-1,k)}{\Delta y}\right.$$

where i, j, k are the grid position indices along the X, Y, Z axis, respectively, n is the current time step index and Δx, Δy, Δz are the grid position indices along the X, Y, Z axis respectively. Similar expressions are obtained for the Y and Z components of the electric and magnetic fields. When physical structure involves lossy materials with nonzero electric conductivity σ and/or nonzero electric conductivity σ_m, the above update equations become more complicated.

In the case of anisotropic materials with tensorial constitutive parameters, the electric displacement vector D and magnetic induction vector B need to be involved in the update of Maxwell's equations at every step. These results in a total of twelve update equations at every step. In the case of dispersive materials with time-varying constitutive parameters, additional auxiliary differential equations are invoked and updated at every step. Applying the proper boundary conditions for all the materials inside the computational domain and at the boundaries of the domain itself, electromagnetic cube calculates and 'updates' all the necessary field components at every mesh node, at every step.[28]

3.4 Software: FDTD simulation solutions

FDTD simulation software is photonic simulation software that enables us to understand light, and predict how it behaves within complex structures, circuits, and systems. Using design tools, one can fabricate, improve and process as well as run tests without having to physically create the structures. These features allow designers check the accuracy of designs prior to manufacturing, create new product concepts, and explore long-term innovative photonics research such as quantum computing. It's an innovation of modeling optical materials that store vast amounts of information more efficiently; and engineers are designing high-speed communication systems that transmit information optically within datacenters and even between and within computer chips. Not only the designers able to create better performing components but also, they can do so in far less time, at lower costs, and with greater accuracy. Furthermore, our software's products allow optical, electrical, and thermal and circuit simulations.

It's delivered a broad range of state-of-the-art features to meet challenging user requirements for performance, usability and accuracy. We have used 3D Maxwell solver, capable to examine the interaction of UV, visible, and IR radiation. FDTD solutions can be used across a wide

range of nano photonic research areas, including plasmonics, particle and surface scattering and microscopy etc.

3.5 Software: FDTD simulation parameters

Using software design tools, one can fabricate, improve and process as well as run tests without having to physically create the structures.

For designing nano antenna, first needs to select shapes from structures. Then we need to choose material.

As a complete setup may contain a large number of objects where the object tree was designed to allow for organization and easy selection. Our objects are triangle in 3D; these objects are extruded in the z direction to a specific height. They are polygon objects, with the number of vertices set to 3. Here it must be mentioned that one of the selected triangles was rotated to give the structure of its desired shape. The rotation can be done with the help of the four windows in the layout, each showing a different view of the structure: xy, xz, yz and a 3D view of the design.

Simulation Region-After selection of objects material and structure, we set simulation region and mesh. Simulation objects are used to define simulation parameters like boundary conditions and mesh size. Simulation region defines most of simulation parameters including the size, boundary conditions and mesh size. In simulation region, generally mesh accuracy set at 1/2 mm.

Mesh-Mesh region is used to override the default mesh size in some part of the simulation region. Normally the meshing parameters are set in the simulation region. However, if some specific meshing conditions are required in part of the simulation region, a mesh override region can be specified.

In our designed structure, we set mesh as a mesh antenna that covers objects completely. It's a bigger mesh of the antenna. The mesh sizes were chosen with the simulation time and memory requirements in mind.

Boundary condition- In boundary condition there are seven techniques. We choose PML boundary condition. PML absorbing boundary conditions are impedance matched or comparable to the simulation region and it's all materials. This allows them to absorb light waves (both propagating and evanescent) with minimal reflections. An ideal PML boundary produces zero reflections, however, in practice; there will always be small reflections due to the discretization of the underlying PML equations.[25]

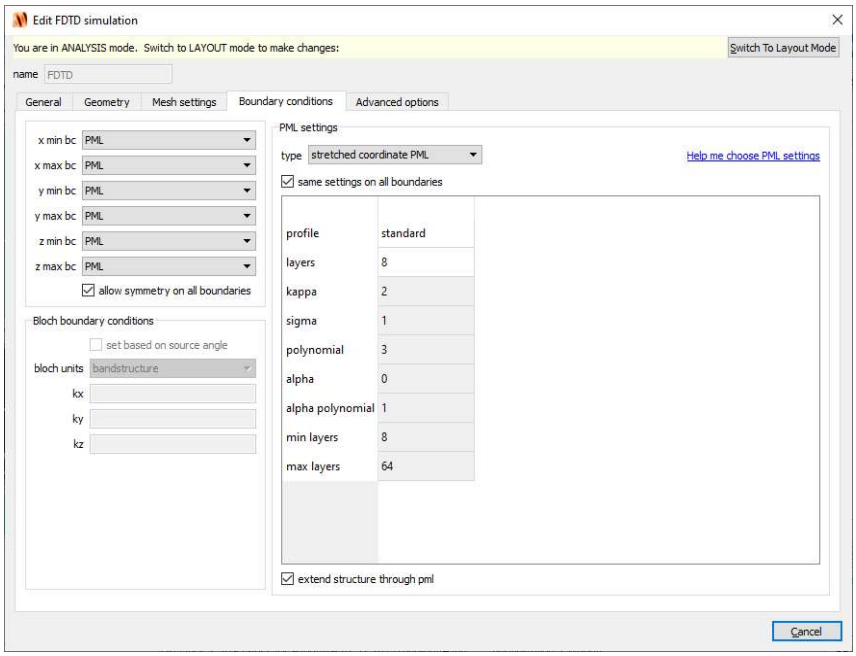

Figure 3.2: Screenshot of boundary condition setup in our FDTD simulation

PML boundary conditions are designed to absorb all incidents' light. For best performance, physical structures should extend completely through the PML boundary condition region. The default settings in FDTD will automatically extend any structures which lie on the PML boundary through the PML.

Source-For the purpose of illuminating our experimental setup, generally people used total-field scattered-field (TFSF) source with a wavelength range from 400nm to 1400nm. It must be noted that, source must be placed to the perpendicular (TE) to the z axis of the structure, in order to investigate the different simulation results.

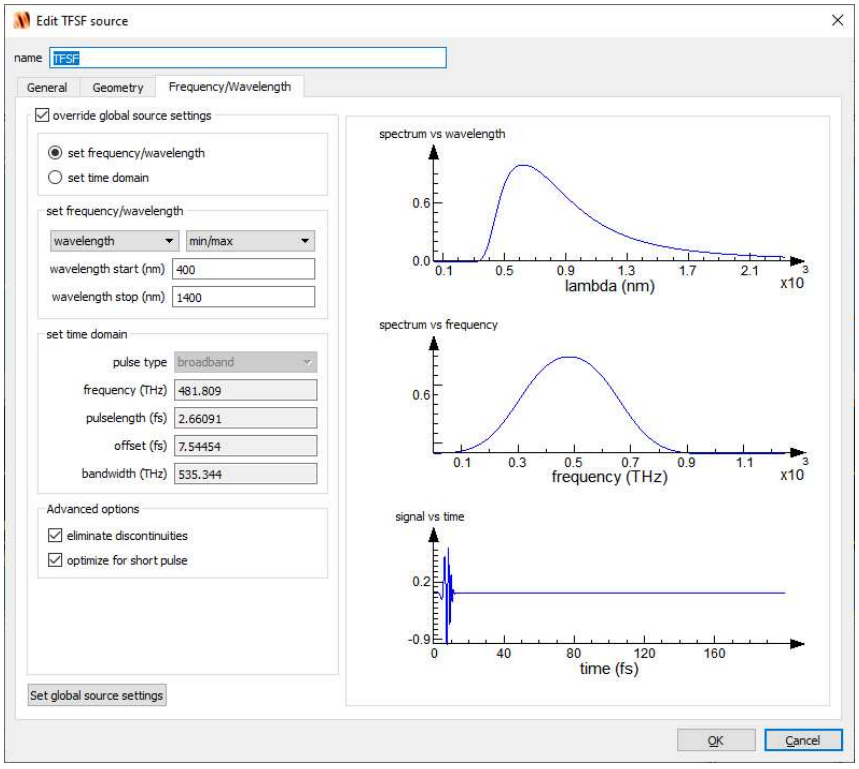

Figure 3.3: Screenshot of TFSF source setup in our FDTD simulation

Total-field scattered-field sources are used to distinct the computation region into two distinct regions – one region contains the total field, and second region contains only the scattered field. When we want to know about scattering behavior of object, then this type of source is useful.

Monitors-In FDTD order to obtain results, we have used time-domain monitors, index monitors and Frequency-domain power monitors. We use 3D monitors. Time-domain monitors provide time-domain information for field components over the course of the simulation. It can consist of point, line, or area monitors to capture this information over different spatial extents within the FDTD simulation region. Then we use the index monitor to record the n and k value

as a function of frequency or wavelength in the simulation. Index monitors are only available in two or three dimensions; there is no option for linear or point index monitors, thus we use modest memory requirements.

Frequency-domain power monitors this type of monitor can collect high-accuracy power flow information from the frequency domain of simulation results. These monitors are identical to frequency-domain profile monitors except that they automatically snap to the nearest FDTD mesh cell boundary when the simulation runs due to a different default setting of the spatial interpolation property in the advanced option. This is important when accurate power flow calculations are required. Less interpolation is required in this case, which results slightly more accurate power measurements.

Analysis Group-This group can be calculated the absorption cross section which located inside the TFSF source. The analysis group calculates the net power flow into the particle and hence the absorption crosses section using the optical theorem. Similarly, the scattering cross section can be calculated by an analysis group located outside the TFSF source. This group measures the net power scattered from the particle.

We add two analysis groups, named ‘total’ and ‘scat’. To obtain these plots, we increase the number of frequency points from global monitor settings to 50 from the edit tab of x-normal-profile. The extinction cross-section is the sum of the absorption and scattering cross-sections.

Here, we have shown layout figure (FDTD simulator) of single particle, length variation (fixed separation) coupled particles and separation variation (fixed length) coupled particles, separation variation (fixed length) dipole particles, patch antenna and probe antenna in our investigations.

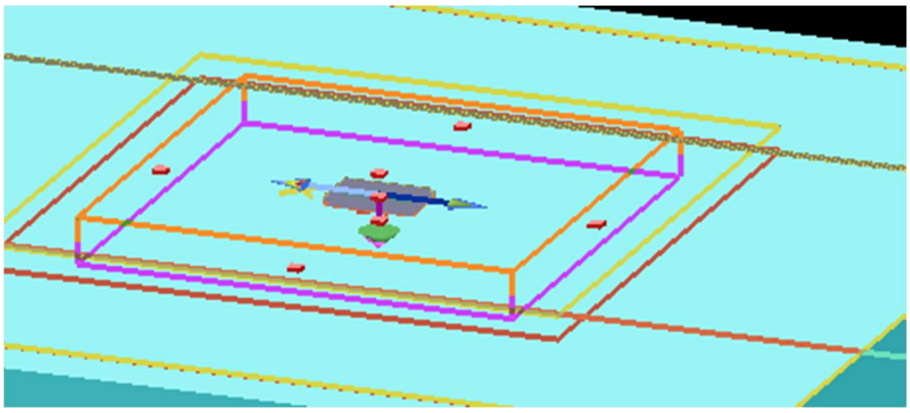

(i)

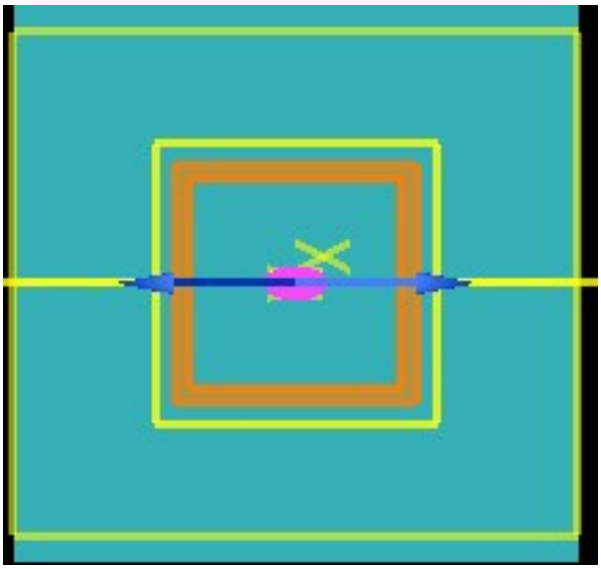

(ii)

Figure 3.4 (i) & (ii): Layout editor of FDTD (finite difference time domain) simulation layout for plasmonic single nano triangle gold (Au-Johnson and Christy) dimer– X-Y view (Left one), perspective view (right one). The yellow box represents the TF, the white box represents the TFSF and finally, the outer yellow box represents the SF. The pink and blue arrows represent the propagation direction and electric field

Similarly, for coupled particles FDTD layout

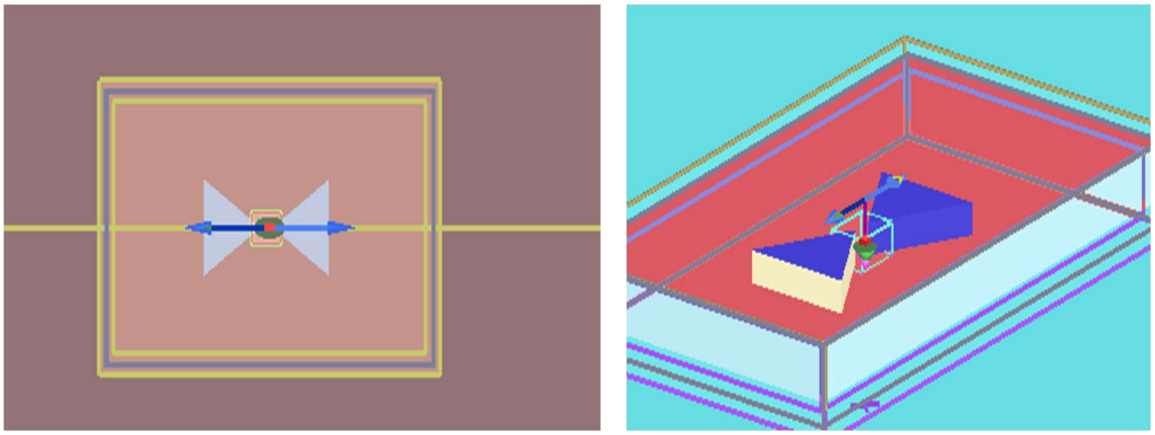

Figure 3.5: Layout editor of FDTD (finite difference time domain) simulation layout for bowtie nano antenna (two triangle gold (Au) particles) gap are fixed at 22 nm and length are varied in nm. Here triangle gold (Au-Johnson and Christy) – X-Y view (left one), perspective View (right one). The yellow box represents the TF, the white box represents the TFSF and finally, the outer yellow box represents the SF. The pink and blue arrows represent the propagation direction and electric field.

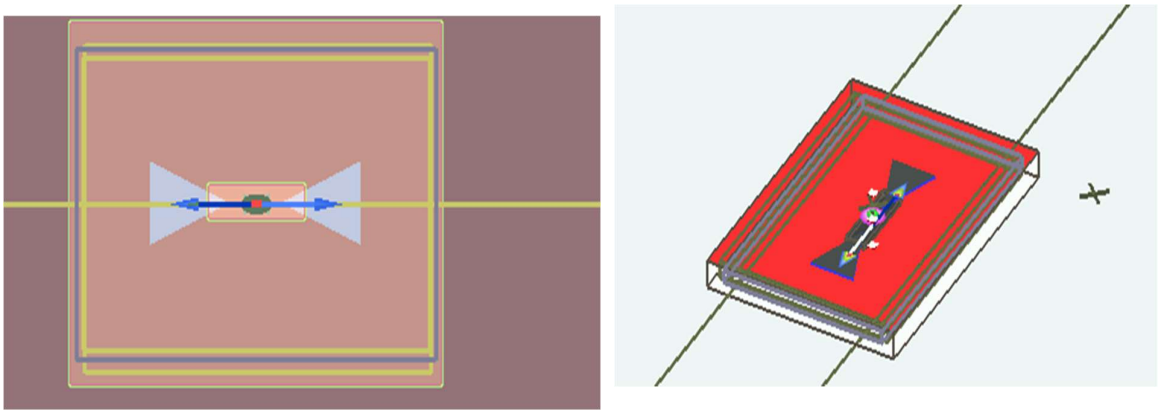

Figure 3.6: Layout editor of FDTD (finite difference time domain) simulation layout for bowtie nano antenna (two triangle gold (Au) particles) both particles length are fixed at 150 nm. Separation varied in d=1nm, 8 nm, 40 nm, 80 nm, 100 nm and 150nm. Here triangle gold (Au-Johnson and Christy) – X-Y view (Left one), perspective view (right one). The yellow box represents the TF, the white box represents the TFSF and finally, the outer yellow box represents the SF. The pink and blue arrows represent the propagation direction and electric field.

Similarly, for dipole particles FDTD layout.

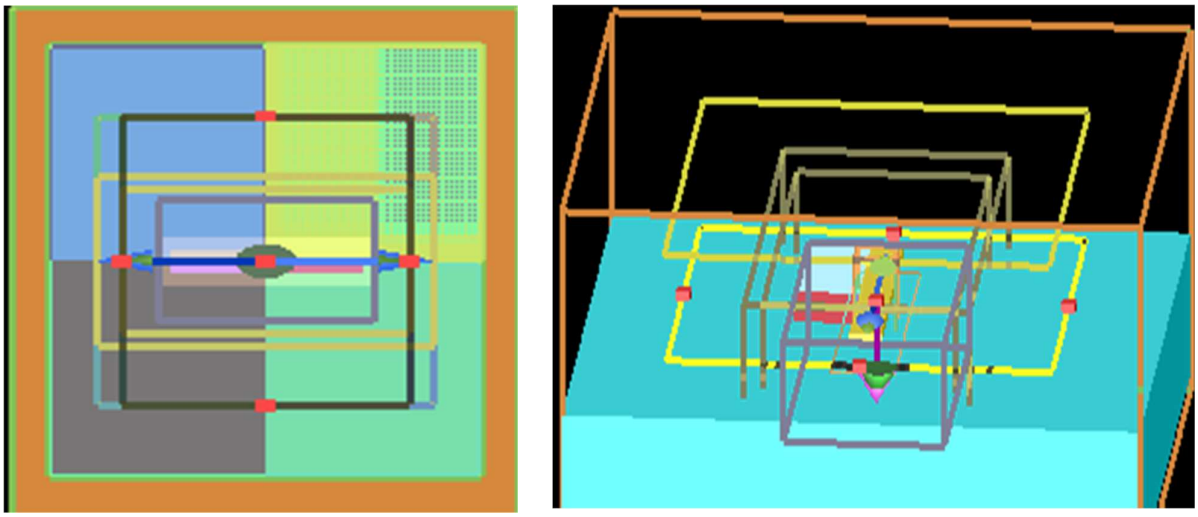

Figure 3.7: Layout editor of FDTD (finite difference time domain) simulation layout for dipole nano antenna (two dipole gold (Au) particles) both particles length is fixed at 400 nm, width at 100 nm and height at 50 nm. separation varied in d=1nm, 4nm, 8 nm, 16 nm, 32 nm, 64 nm and 128 nm. Here dipole gold (Au-Johnson and Christy) – X-Y view (left one), perspective view (Right one). The yellow box represents the TF, the white box represents the TFSF and finally, the outer yellow box represents the SF. The pink and blue arrows represent the propagation direction and electric field.

FDTD layout for Patch antenna,

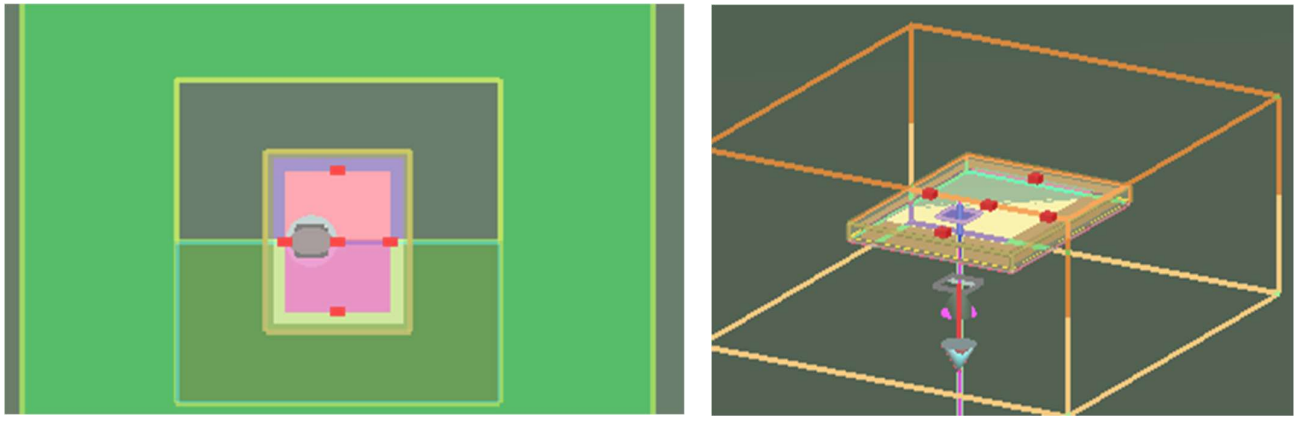

Figure 3.8: Layout editor of FDTD (finite difference time domain) simulation layout for patch nano antenna rectangular sheet of width (y span) 12.86 mm and length (x span) 10.06 mm substrate of 10.06X12.86X1.588 mm possessing a refractive index of 1.48, impedance 50Ω. Inner conductor radius a = 0.19107m and outer conductor radius b=1 mm. width at 100 nm and height at 50 nm. Here X-Y view (left one), perspective View (right one). The yellow box represents the TF, the white box represents the TFSF and finally, the outer yellow box represents the SF.

FDTD layout for Probe antenna,

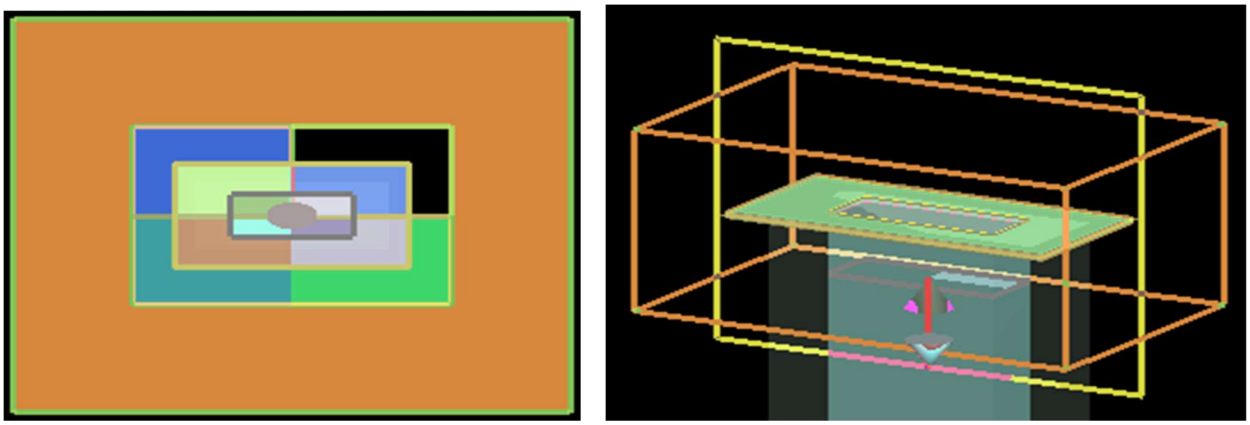

Figure 3.9: Layout editor of FDTD (finite difference time domain) simulation layout for probe nano antenna. Rectangular waveguide of width b=20.86mm and a=8.16mm. Here vacuum filled rectangular waveguide surrounded by a PEC wall which thickness was 2.5mm. PEC sheet of ground plane in finite dimension simulation which are g_x=40mm and g_y=20mm. Here X-Y view (left one), perspective view (right one). The yellow box represents the TF, the white box represents the TFSF and finally, the outer yellow box represents the SF.

3.6 Summary or simulation workflow

The overall workflow of the simulations can be summarized as below:

1. Set the physical layout (geometry and materials)
2. Add simulation region, boundary conditions and meshing
3. Add source, monitors, and the analysis groups
4. Check material explorer and Run the simulation and then
5. Open specific LSF files and run script file
6. Finally analyze the results

Figure-3.10: Simulation workflow.

3.7 Conclusions

In this chapter we observed FDTD theory and how Maxwell equation, the yee cell can be deriving for FDTD. We learned also FDTD software simulation method. Here, we showed FDTD layout editor of our upcoming chapters. Moreover, we articulated FDTD simulation workflow, and we have learned FDTD structure and theory. This chapter will be helpful for our subsequent chapter.

Chapter 4

Performance analysis of optical (bowtie and dipole) antenna

4.1 Introduction

In this chapter we investigated the optical property of single and coupled (bowtie nano antenna) gold (Au) nano particle by finite difference time domain (FDTD) simulation. In this study, we observed the optical cross section and field enhancement for single and coupled Au nanoparticle as a function of diameter, size and separation.

4.2 Characterization of nanoantenna

In this chapter, we characterized optical property of plasmonic gold (Au) nano particle. We characterized both single triangle nano particle and two nano particles (bowtie shaped antenna). We observed particles parameter like, far-field and near-field, field enhancement and cross sections. Our observation techniques are based on the finite difference time domain (FDTD) simulation software. We performed several finite difference time domain (FDTD) simulations in order to analyze the optical properties.

Field enhancement plays an important role in nano technology. The field enhancement is the ratio of the local electric field to that of the incident electric field when the optical fields present on such structures are induced by an incident wave. The local field enhancement relies on the size of the nano particles.

The near-field and far-field are regions of the electromagnetic field (EM) around an object. Near-field and far-field can be described as certain areas with an electromagnetic field formed around an antenna.

Near field is very close to the antenna while far field is further away.

In nano technology related literature, characterization of optical properties is discussed in various ways. These are applied in almost every sector like therapeutic agents, sensory probes, engineering, and medicine etc.

4.3 Simulation setup-FDTD

For our design of a nanoantenna of the bow-tie shape, we used two triangles from structures. We simulate both single and coupled nano particle of Gold (Au) (bowtie nano antenna) by FDTD software.

Here we choose Gold (Au) nano particle-Johnson and Christy. In case of objects, we select triangles glass substrate (refractive index 1.5). We changed particles length units to nanometer as our work involves nanostructures. The material of the structures faced tip to tip is gold (Au) of fixed height. Between the triangles, the gap size was 22nm which was later varied up to 300nm.

We firstly studied effect of single particle size by changing particles diameter. It's a gold (Au) triangle particle. We placed particle on glass substrate. We change the particles sizes in different nm (60, 80,100,150,200,240).

Secondly, we studied about coupled particles (bowtie antenna). We take two equalizer triangle gold particles and placed particles on glass substrate. Primarily we fixed particles separation at 22nm and changes particles diameter in different nm (100,150,200,240,300). Then we fixed both particles diameter at l= 150 nm and changes separation in different nm (1, 8, 40, 80,100,150).

In our simulations we set mesh accuracy at 2nm for single particle and length variation (fixed separation) coupled particles. We set mesh accuracy at 1nm for separation variation (fixed length) coupled particles. We choose PML boundary condition. We have used total-field

scattered-field (TFSF) source with a wavelength range from 400nm to 1400nm. It must be noted that, we have been placed the source perpendicular (TE) to the z axis of the structure. We have used time-domain monitors, index monitors and frequency-domain power monitors. We added two analysis groups, named 'total' and 'scat'. To observe particles cross sections, absorption cross section is determined within the origin of total field scatter field (TFSF) source. The source direction was set along the axis of AuNPs. Absorption cross section is calculated by an analysis group which is located inside the TFSF source. This group calculates the total power flow into the particle. Same way, the scattering cross section is calculated by an analysis group which is located outside of TFSF source. This group measures the net power scattered from the particle. The scattering cross section is located outside the TFSF origin and extinction cross section determine by the summing up of the absorption and the scattering cross section.

4.4 Simulation results and discussions

4.4.1 Single triangle particle simulation using FDTD

Single triangle with varying length:

We performed the FDTD simulation for single triangle shaped nanoparticle and observed the optical cross-section, near and far field enhancement as a function of varying length.

We know the optical and electronic properties of gold nanoparticles are tunable by changing their size. Our first simulation was effect of single particle size by changing particles length. We change the particles length in different nm (60, 80,100,150,200, and 240).

In this section, the numerical analytical result has been presented to observe how absorption, scattering and extinction enhancement factor's graph can be changes with changing particle's length. When we increase length of particles, then enhancement factors are also increased for

certain time. We can get the highest value or peak factor when wavelength is belonging to 650nm to 1050nm. We plot extinction σ_{ext} (figure C), absorption σ_{abs} (figure A), and scattering σ_{scat} (figure B), cross sections for Au nano particles.

Absorption enhancement factor as a function of varying length for a single triangular nanoparticle:

In Figure A shows absorption enhancement factor clearly when the length increases, the peak position of wavelength is red shifted (longer wavelength) of the surface plasmon resonance from around 650nm to 1050nm.

When length 60nm, absorption enhancement factor was 8, for length 80nm, enhancement factor was 11, for length 100nm enhancement factor was 9.5. Further way we can see for length 240nm enhancement factor was 1. In figure (A) clearly shows that, after length 80nm, enhancement factor was started decreasing. When particles length 80nm, factor was 11 and whenever particles length was 240nm, factor was 1. We can say in outline, it's around 8 times decreased. After a specific length (80 nm), when we expand particles length then absorption factor was linearly decreased. In common literature we found same trend. [29]

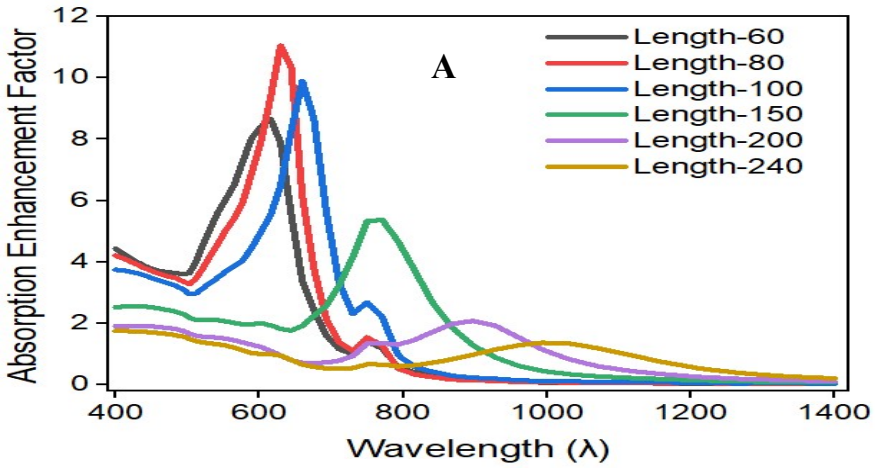

Figure 4.1 (A): Wavelength vs. absorption enhancement factor in FDTD simulation results for single gold (Au) particles and length are varied in nm. Figure (A) shows absorption spectrum of single gold nano particles, when length is l=60 nm, 80 nm, 100 nm, 150 nm, 200 nm and 240 nm.

Gold (Au) single particles show the band around 520 nm in the visible region. The band is affected by the particle size (Figure 4.1 (A)).Increasing particle size red shifts the wavelength and also it increases the intensity. For particles larger than 240nm, the band broadening is obvious due to the dominate contributions from higher order electron oscillations.

Gold nano particles' interaction with light is strongly dominated by their size. Here, light ray of oscillating electric fields produces blended to near nano particles. These nano particles interact with the free electrons. Because of combined oscillation of electron charge. That is in resonance with the frequency of visible light. These resonant oscillations are known as surface plasmon's. When we increase the particles size, then the wavelength of surface plasmon resonance related absorption are certainly shifts to longer wavelengths. As particle size continues to increase up to the load limit, surface plasmon resonance wavelengths proceed into the forward portion of the spectrum. As a result, most visible wavelengths are reflected. Here, the surface plasmon resonance can be tuned by varying the size of the nano particles.

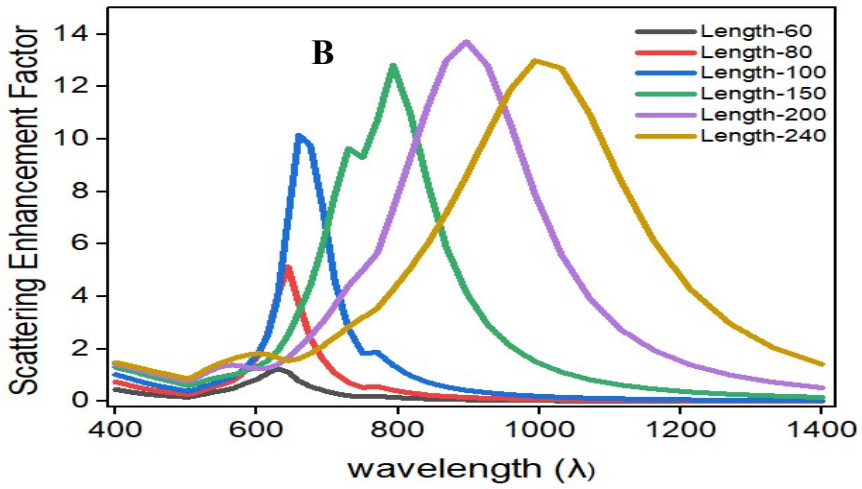

Figure 4.1 (B): wavelength vs. scattering enhancement factor in FDTD simulation results for single gold (Au) particles and length are varied in nm. Figure (B) shows scattering spectrum of single gold nano particles, when length is l=60 nm, 80 nm, 100 nm, 150 nm, 200 nm and 240 nm.

Scattering enhancement factor as a function of varying length for a single triangular nanoparticle:

Similarly, we can see in scattering enhancement factor's (figure (B)) graph, when we increase length of particles, enhancement factors are also increased for certain time. We can get the highest value or peak factor when wavelength is belong to 650nm to 1050nm. [28]

The optical scattering is also largely dependent on the size of the nano particles. When the size increases to 60nm, the scattering starts to show up (figure 4.1 (B)). From this relationship, it can be seen that, the proportion of the scattering to absorption increases for larger size of particles. In scattering enhancement factor, if we increased length of particle at 200nm (at wavelength 900) then we can find the highest value of scattering factor. The peak position of wavelength is red shifted (longer wavelength) of the surface plasmon resonance from around 650nm to 1050nm.

In figure (B) when length 60nm, scattering enhancement factor was 1, for length 80nm, enhancement factor was 5, for length 100 nm enhancement factor was 10.5. For length 200nm enhancement factor was 14. Further way, we can see enhancement factor was 13 for length 240nm. In figure (B) clearly shows after length 200nm enhancement factor was started decreasing. Here, scattering enhancement increasing rate was 13 times for increasing particles length. After a specific length (200nm) scattering factor was linearly decreased. In widely known literature, we found same trend.

Extinction enhancement factor as a function of varying length for a single triangular nanoparticle:

Here as usual the FDTD simulator has been employed to calculate extinction enhancement factor for isolated gold nanoparticles of different sizes (60–240 nm) (Figure 4.1 (C)). Same as

before, with increasing length of particles enhancement factors are also increased. When length of particle at 80nm (at wavelength 650), we can find the highest value of extinction factor.

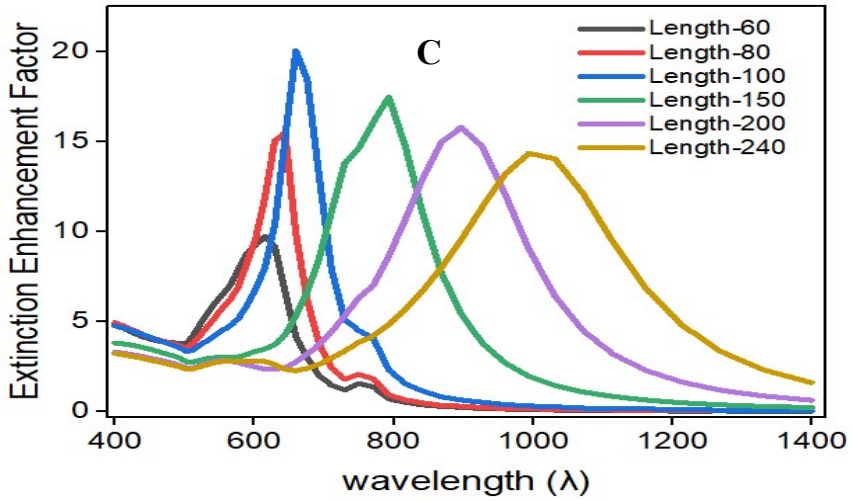

Figure 4.1 (C): Wavelength vs. extinction enhancement factor in FDTD simulation results for single gold (Au) particles and length are varied in nm. Figure (B) shows extinction spectrum of single gold nano particles, when length is l=60 nm, 80 nm, 100 nm, 150 nm, 200 nm and 240 nm.

The extinction cross section is (figure 4.9 C) defined as the sum of the scattering and absorption cross sections. The peak position of wavelength is red shifted (longer wavelength) of the surface plasmon resonance from around 650nm to 1050nm.

In figure (C) when length 60nm, extinction enhancement factor was 10, for length 80nm, enhancement factor was 16, for length 100nm enhancement factor was 20.5. For length 200nm, enhancement factor was 16. Further way, we see enhancement factor was 14 for length 240nm. In figure (B) clearly shows after length 100nm enhancement factor was starting decreased. Here extinction enhancement increasing rate was 1.4 times for increasing particles length. In literature, we found same trend. [3]

Cross section enhancement factor and SPR peak function of varying length for a single triangular nanoparticle:

From the below figure 4.1 (D), where cross section enhancement factor is plotted against length of the surrounding medium single Triangle.

We increase length of triangle, then peak of extinction, scattering, and absorption cross section's value are also increased.

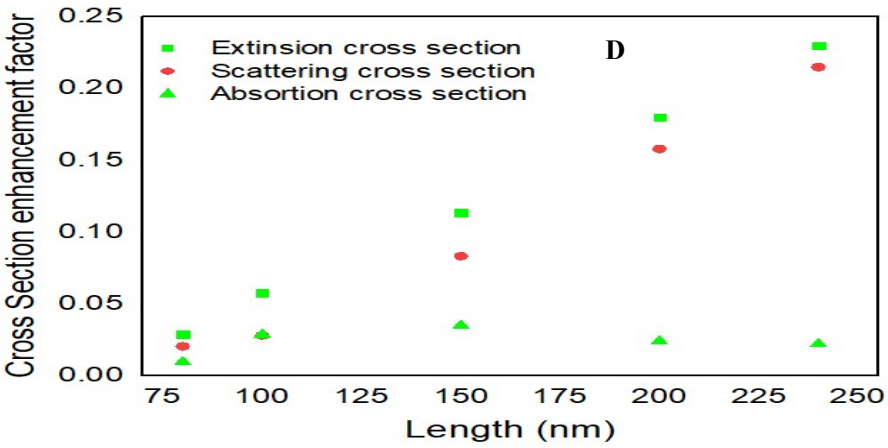

Figure 4.1 (D): *FDTD simulation results for comparison of cross section enhancement factor of single gold (Au) triangle particles and length are varied in nm. When length is l=60 nm, 80 nm, 100 nm, 150 nm, 200 nm and 240 nm. Here, extinction cross section – black series, scattering cross section – red series, absorption cross section – blue series.*

We can observe that the slopes for cross sections are slightly upward. Similarly, SPR peak of extinction, scattering, absorption is increased (figure 4.1 (E)) with increasing length and slopes are upward.

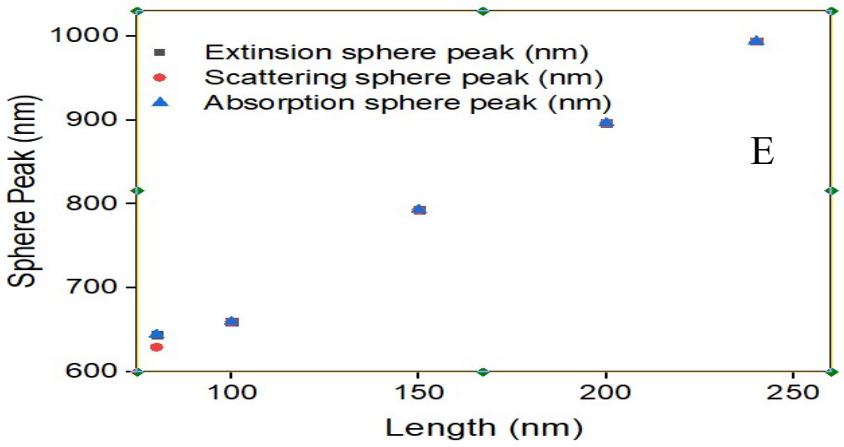

Figure 4.1 (E): *FDTD simulation results for SPR peak of single gold (Au) triangle particles and length are varied in nm. When length is l=60 nm, 80 nm, 100 nm, 150 nm, 200 nm and 240 nm. Here, extinction cross section – black series, scattering cross section – red series, absorption cross section – blue series.*

The comparison of cross section spectrum and SPR peak distinctly represents the interrelation of plasmonics (Au) nanoparticle optical properties including scattering cross-section, surface plasmon resonance (SPR) wavelength, extinction, absorption, and scattering cross-section's changes on sizes of nanoparticles. We can represent these results with the help of the table below.

Variations in length (nm)	Absorption		Scattering		Extinction	
	SPR Peak (nm)	Cross sections (μm^2)	SPR Peak (nm)	Cross sections (μm^2)	SPR Peak (μm^2)	Cross sections (μm^2)
80	644.131	0.00948	629.358	0.0204	644.131	0.028617
100	659.615	0.0285	659.615	0.028	659.615	0.0576
150	793.064	0.0349	793.064	0.0832	793.064	0.1135
200	896.732	0.024	896.732	0.158	896.732	0.18
240	994.203	0.022	994.203	0.215	994.203	0.23

Table-4.1: Comparative study of single gold nano particles (AuNPs) when varying the particles length in nm. Where column-1 represents variation of length, column-2 represents absorption SPR peak (nm) and cross-sectional area (μm^2), column 3 represents scattering SPR peak (nm) & cross-sectional area (μm^2) and column-4 represents extinction SPR peak (nm) & cross-sectional area (μm^2).

4.4.2 Coupling triangle particle simulation using FDTD

In terms of coupling (bowtie nanoantenna), it consists of two triangular pieces of gold, each about 100-300 nanometers long, whose tips face each other in the shape of a miniature bowtie.

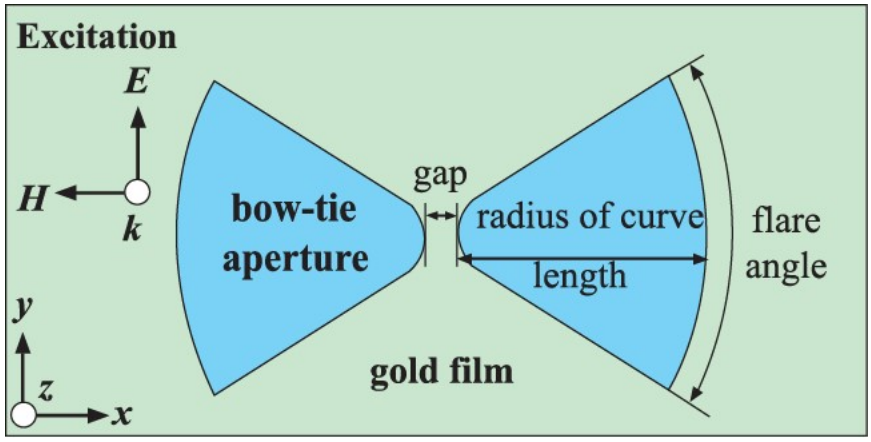

Figure 4.2: Schematic diagram of bowtie nanoantenna

The device operates like an antenna for a radio receiver, but instead of amplifying radio waves, the bowtie takes energy from beam of near-infrared light and squeezes it into a 22- nanometer gap that separates the two gold triangles. The result is a concentrated speck of light that is a thousand times more intense than the incoming near-infrared beam. [3]

Coupling triangle with varying length:

We performed the FDTD simulation for coupling triangle shaped (bowtie antenna) nanoparticle with varying length and observed the optical cross-section, near and far field enhancement as a function of varying length. [30]

Here we simulate of two metallic triangles. Here, triangles are facing face to face (tip to tip) and they are separated by a small Separation. It combines with the electromagnetic properties of sharp metal tips with those of coupled plasmon resonant nanoparticle pairs. [31]

We plot extinction σ_{ext}, absorption σ_{abs}, and scattering σ_{scat} cross sections for two Au nanoparticles.

Absorption enhancement factor as a function of varying length for a coupling triangular nanoparticle:

We fixed particles separation at 22nm and changes particles length in different nm (100,150,200,240,300).

FDTD simulation method has been used. Figure- 4.3 (A) shows the absorption enhancement factor for coupling effect when varying their triangles length. This inspection shows clearly when coupling triangles length increase the red shift (longer wavelength) of the surface plasmon resonance from around 700nm to 1250nm. For length 100nm, absorption enhancement factor was 3.4, when length 150nm enhancement factor was 1.3, for length 200nm enhancement factor was 0.8. Further way, we can see for length 300nm enhancement factor was 0.6. After length 100nm enhancement factor was started to decrease linearly. We

can say in outline, it's around 5.66 times decreased.[32]. Here, gold (Au) coupling particles show the band around 700 to 1200nm in the visible region. The band is affected by the particle size (figure 4.3 (A)). With increasing particle size, the red shift wavelength is found and increases the intensity. For particles larger than 300nm, the band broadening is obvious due to the dominating contributions from higher order electron oscillations.[33]

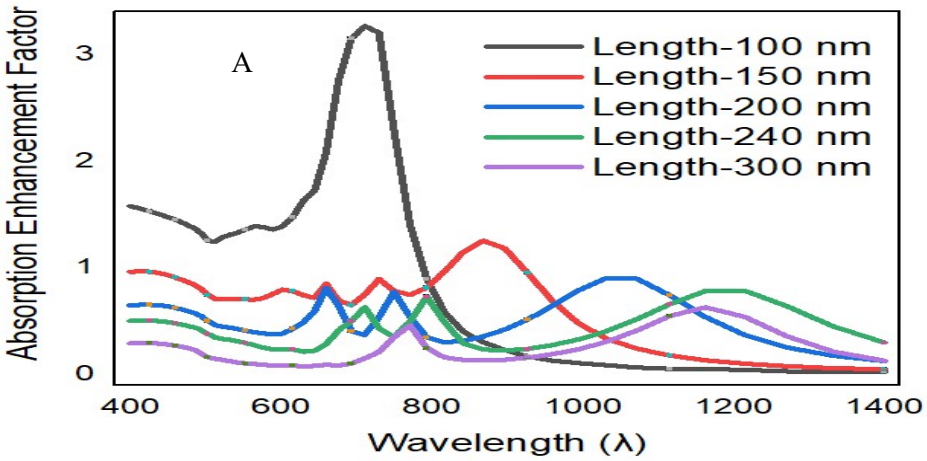

Figure 4.3 (A): Wavelength vs. absorption enhancement factor in FDTD simulation results of 22nm separation of gold (Au) coupling triangle particles when length, l = 100nm, 150nm, 200nm, 240nm and 300nm.

Scattering enhancement factor as a function of varying length for a coupling triangular nanoparticle:

To investigate the scattering cross-sectional coupling effect when particles length was varied from 100-300nm, FDTD simulation method has been used. We can see in scattering enhancement factors in figure 4.3 (B) graph, where we fixed separation at 22nm. When we increase length of particles then scattering factors are also increased for certain time. It shows clearly that, when the length increases, there has been a red shift (longer wavelength) of the surface plasmon resonance from around 650nm to 1200nm. We can get the highest value or peak factor when wavelength belongs to 650nm to 1200nm. After 120nm enhancement factors are decreased.[34]

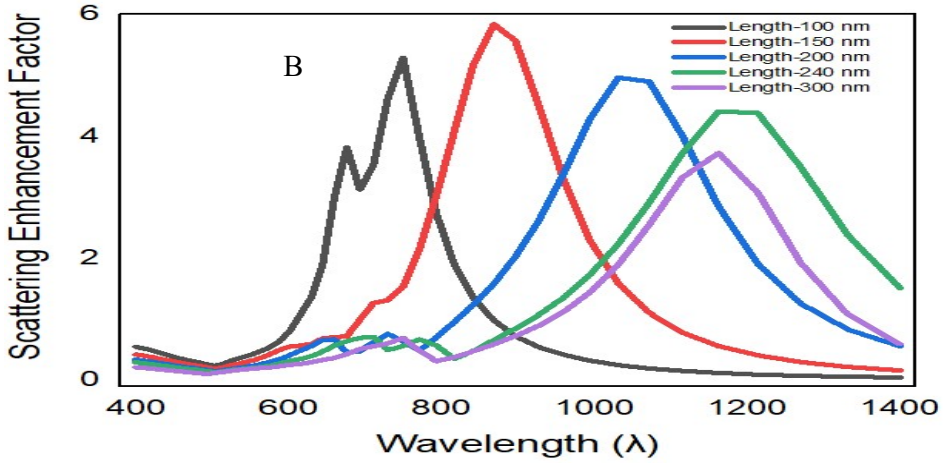

Figure 4.3 (B): wavelength vs. scattering enhancement factor in FDTD simulation results of 22nm separation of gold (Au) coupling triangle particle, when length, l =100 nm, 150nm, 200nm, 24 nm and 300nm.

In figure 4.3 (B) clearly shows after length 150nm, enhancement factor was started decreasing. Here scattering enhancement factor decreasing rate was around 0.68 times for increasing particles length. When we increased length of both particles at 150nm (at wavelength 900) then we can find the highest value of scattering factor.

Extinction enhancement factor as a function of varying length for a coupling triangular nanoparticle:

The extinction cross section is defined as the sum of the scattering and absorption cross sections. We fixed our particles separation at 22nm and varying length from 100nm to 300nm. As usual the FDTD simulator has been employed to calculate extinction enhancement factor for coupling gold nanoparticles (figure 4.3 (C)). The peak position of wavelength is red shifted (longer wavelength) of the surface plasmon resonance from around 750nm to 1200nm. In figure 4.3 (C) when length 100nm, extinction enhancement factor was 7.8, for length 150nm, enhancement factor was 7, for length 200nm enhancement factor was 5.5. Lastly, we can see for length 300nm, enhancement factor was 4.2nm.

It clearly shows that, after length 100nm enhancement factor was started decreasing. Here scattering enhancement decreasing rate was 0.53 times for increasing particles length. [35]

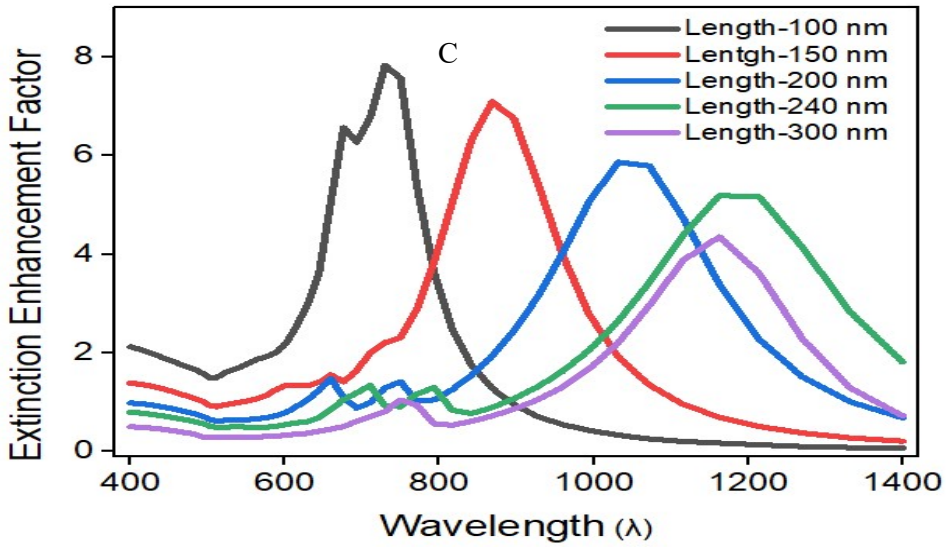

Figure 4.3 (C): wavelength vs. extinction enhancement factor in FDTD simulation results of 22 nm separation of gold (Au) coupling triangle particle, when length, l = 100nm, 150nm, 200nm, 240nm and 300 nm.

Cross section enhancement factor & SPR peak function of varying length for a couple triangular nanoparticle:

From the below figure 4.3 (D), where cross section enhancement factor is plotted against length of the surrounding medium of coupled triangle.

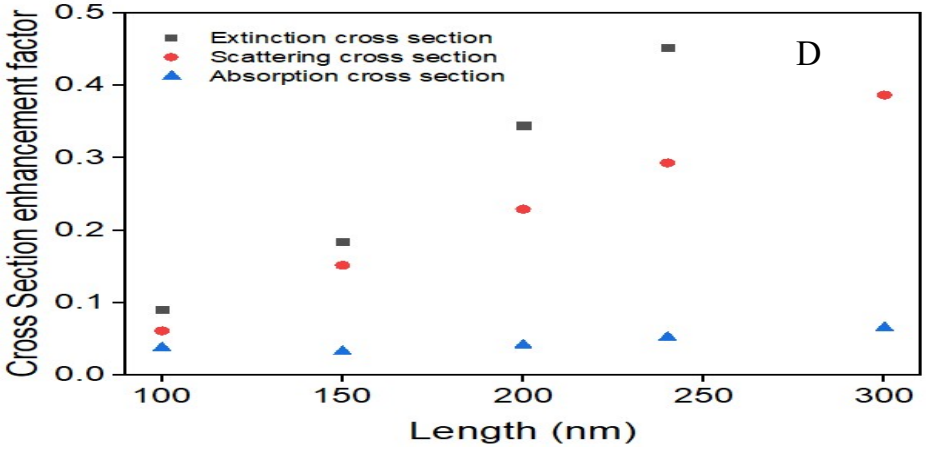

Figure 4.3 (D): FDTD simulation results for comparison of enhancement factor of cross section for coupling gold (Au) triangle particles where separation is fixed at 22 nm and length are varied in nm. When length is l=100 nm, 150 nm, 200 nm, 240 nm and 300 nm. Here, extinction cross section – black series, scattering cross section – red series, absorption cross section – blue series.

We increase the length of triangle, then peak of extinction, scattering, and absorption cross section's value are also linearly increased. We can observe that the slopes for cross sections are slightly upward. Similarly, SPR peak of extinction, scattering, absorption is increased (figure 4.3 (E)) with increasing length and upward slopes.

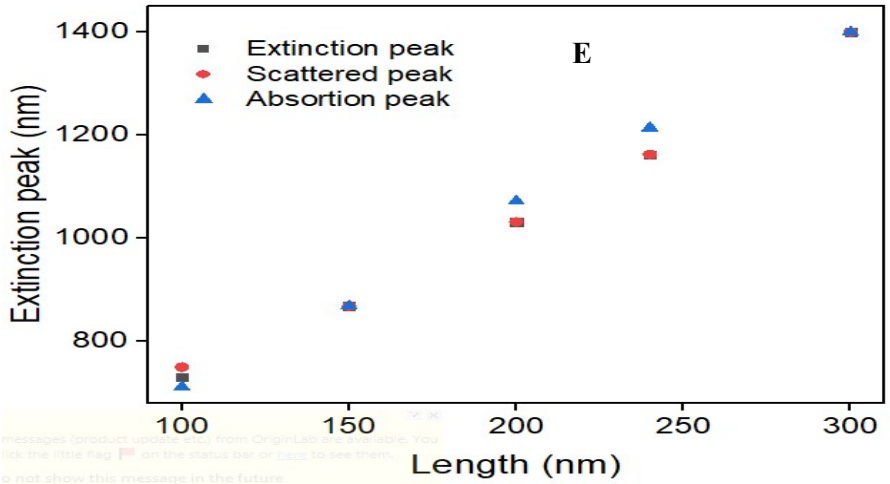

Figure 4.3 (E): FDTD simulation results for SPR peak & strength of coupling gold (Au) triangle particles where separation is fixed at 22 nm and length are varied in nm. When length is l=100nm, 150nm, 200nm, 240nm and 300nm. Here, extinction cross section – black series, scattering cross section – red series, absorption cross section – blue series.

The comparison of cross section spectrum and SPR peak distinctly represents the interrelation of plasmonics coupling (Au) nanoparticles optical properties including scattering cross-section, surface plasmon resonance (SPR) wavelength, extinction, and absorption and scattering cross-section's changes on sizes of nanoparticles.

Sphere peak and extinction efficiency function of varying length for a couple triangular nanoparticle:

Figure-4.3 (F) shows the couple Au nanoparticle sphere peak properties by varying their length (L =100nm, 150nm, 200nm, 250nm, 300nm) respectively. We increase length of triangles then sphere peaks' value are also linearly increased, when length was 100nm sphere peak was 739.78nm, when length was 300nm sphere peak was 1400nm. At that point we can say sphere peaks increasing rate around double for increasing particles length.

In figure-4.3 (G) extinction efficiencies have been displayed. It is seen that extinction efficiencies are linearly decreased with increasing length. At length 100nm, efficiency was 7.82 a.u.. Efficiency became 4.35 a.u .when length was 300nm.

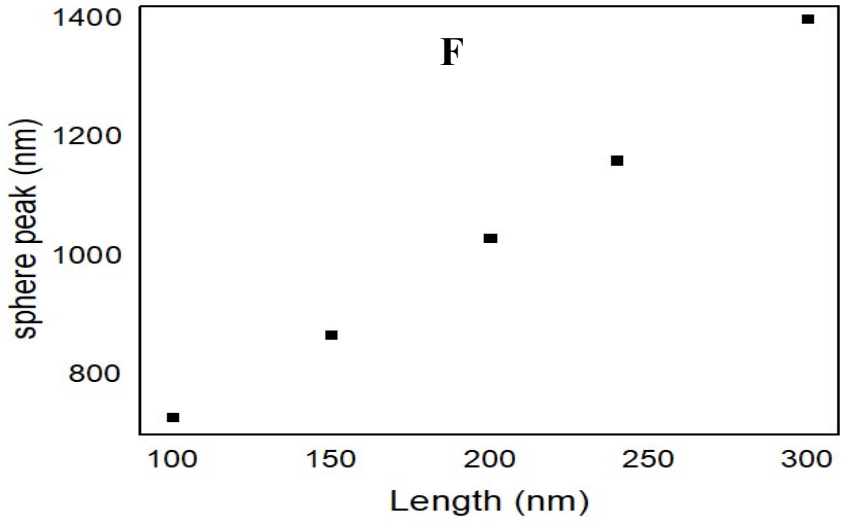

(F)

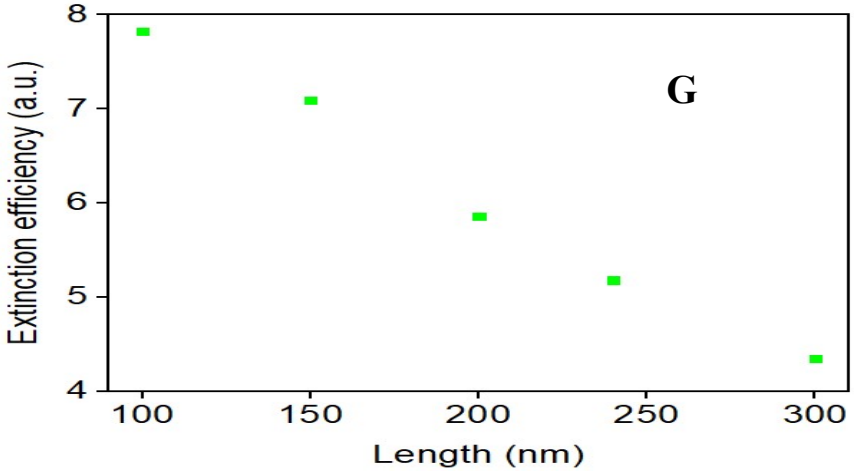

(G)

Figure 4.3 (F): FDTD simulation results for length vs sphere peak of coupling gold (Au) triangle particles where separation is fixed at 22 nm and length are varied in nm. When length is l=100nm, 150nm, 200nm, 240nm and 300nm. (G) Length vs. extinction efficiency of coupling gold (Au) triangle particles where separation is fixed at 22 nm and length are varied in nm. When length is l=100nm, 150nm, 200nm, 240nm and 300 nm.

Observing the result from figure-4.3 (G), it can be concluded that, extinction efficiencies decreasing rate was 0.55 times for increasing particles length.[3]

Here, we can represent these results with the help of the table given below.

Variations in length (nm)	Absorption		Scattering		Extinction	
	SPR Peak (nm)	Cross sections (μm^2)	SPR Peak (nm)	Cross sections (μm^2)	SPR Peak (nm)	Cross sections (μm^2)
100	710.881	0.0376	749.727	0.061	729.789	0.0903
150	868.355	0.0325	868.355	0.1516	868.355	0.1841
200	1071.88	0.04139	1031.58	0.2292	1031.58	0.2709
240	1214.16	0.0522	1162.71	0.2931	1162.71	0.3451
300	1400	0.06539	1400	0.387	1400	0.4524

Table-4.2: Comparative study of coupled gold nano particles (AuNPs) when varying the particles length in nm. Where column-1 represents variation of length, column-2 represents absorption SPR peak (nm) & cross-sectional area (μm^2), column 3 represents scattering SPR peak (nm) & cross-sectional area (μm^2) and column-4 represents extinction SPR peak (nm) & cross-sectional area (μm^2).

Coupling triangle with varying separation:

To observe the absorption, scattering, extinction cross sectional coupling effect when separation distance is from 1nm-150nm, FDTD simulation method has been used. We fixed both particles length at l= 150nm and changes separation in different nm (1, 8, 30, 80,100,150). We plot extinction σ_{ext}, absorption σ_{abs}, and scattering σ_{scat} cross sections for two Au nanoparticles.

Absorption enhancement factor as a function of varying separation for a coupling triangular nanoparticle:

Figure- 4.4 (A) shows the absorption coupling effect when varying their coupling distance. This inspection shows clearly when the separation decreases the red shift (longer wavelength) of the surface plasmon resonance from around 650nm to 1100nm. The red shift is due to coupling of plasmonic near field when two triangles approach each other and form bonding and antibonding plasmon modes. On the other side, there is an improvement in absorption cross sectional area from 1.4nm to 2.9nm when the separation decreases from 150nm to 1nm, which can be the observation of strong coupling and weak coupling. For absorption, the highest strong coupling is shown when peak value of wavelength is around 1031.58nm (figure 4.4(B)).

When separation distance is 8nm, peak value of wavelength is 927.027nm (figure 4.4(B)). This indicates that, a simple variation of separation distance can affect in a great extent of coupling effect.

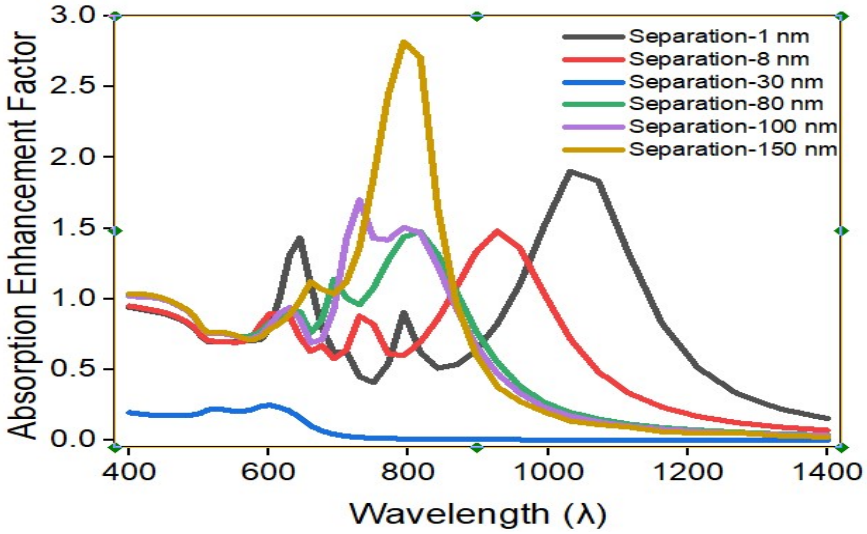

(A)

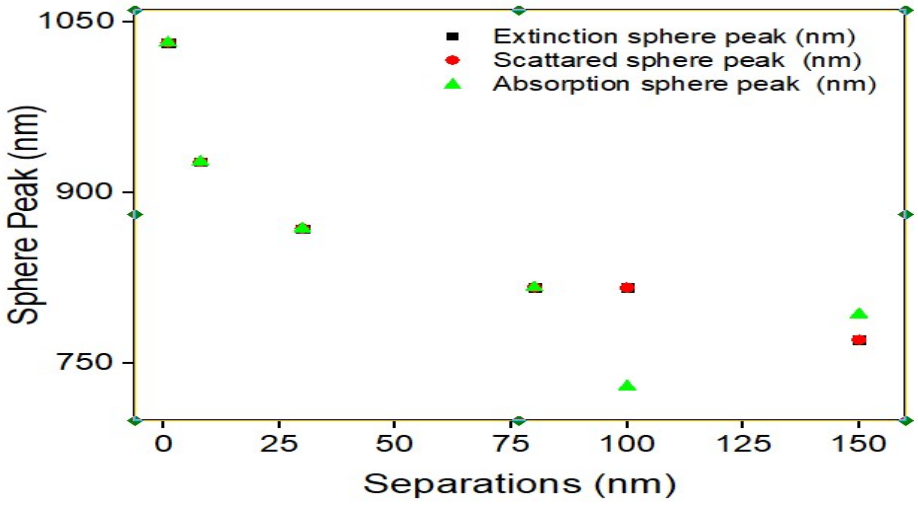

(B)

Figure 4.4 (A) FDTD simulation results of 150 nm lengths Au triangle plasmon coupling absorption spectrum, when separation distance, d = 1 nm, 8 nm, 30 nm, 80 nm, 100 nm and 150 nm (B) Plasmon absorption, scattering and extinction coupling effect – strong coupling to weak coupling of 150 nm length triangle (peak wavelength vs coupling separation).

On the other hand, weak coupling occurs from separation distance, d = 30nm, 80nm, 100nm, 150nm (very weak). Ironically, at length 150nm Au nano plasmon acts like single particle. When separation distance is 150nm, peak wavelength is around 800nm for absorption. We can

get the highest value or peak for absorption when wavelength belongs to 650nm to 1100nm. After wavelength 1100nm, enhancement factors are decreased. Here absorption enhancement increasing rate around 87% for increasing separation.

Scattering enhancement factor as a function of varying separation for a coupling triangular nanoparticle:

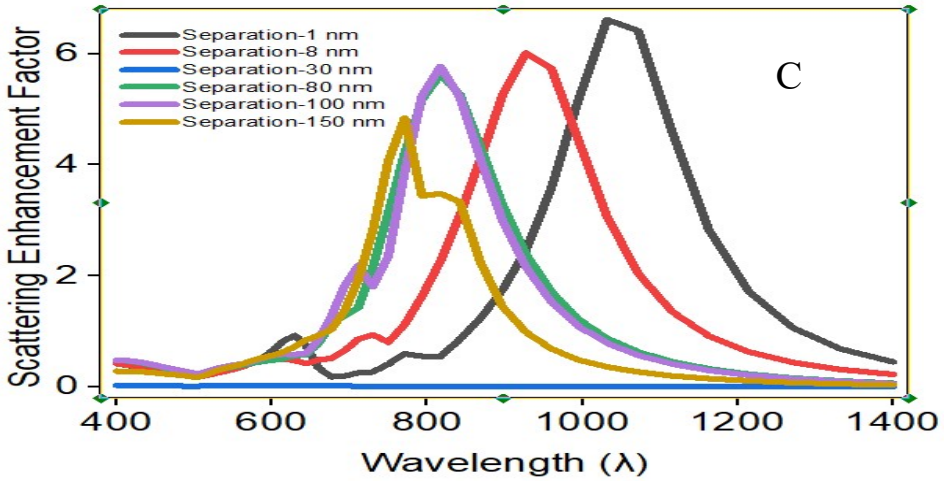

Figure 4.4 (C) FDTD simulation results of 150 nm lengths Au triangle plasmon coupling scattering spectrum, when separation distance, d = 1 nm, 8 nm, 30 nm, 80 nm, 100 nm and 150 nm.

Figure- 4.4 (C) and figure-4.4 (B) show the scattering coupling effect when varying their coupling separation. This inspection shows clearly when the separation decreases, there has been a red shift (longer wavelength) of the surface plasmon resonance from around 650nm to 1100nm. On the other side, there is an improvement in scattering cross sectional area from 1nm to 5nm. When the separation decreases from 150nm to 1nm, which can be the observation of strong coupling and weak coupling.

When separation distance is 8nm, peak value of wavelength is 927.027nm (figure 4.4(B)). This indicates that a simple variation of separation distance can affect in a great extent of coupling effect. On the other hand, weak coupling occurs from separation distance, d = 30nm, 80nm, 100nm, 150nm (very weak). At length 150nm Au nano plasmon acts like single particle. When separation distance is 150nm, peak wavelength is around 800nm for scattering. Here scattering enhancement factor's decreasing rate around 27.3% for increasing separation.

Extinction enhancement factor as a function of varying separation for a coupling triangular nanoparticle:

As we know extinction spectrum is a summation of absorption and scattering spectrum. We investigated the plasmon coupling of 150nm diameter AuNP dimer using FDTD simulation. In figure 4.4 (D)) we found red shift in SPR peak with decreasing inter–particle distance that means in weak coupling region. The red shift is occurred because coupling of plasmonic near field when two spheres approach each other, and it form bonding and antibonding plasmon modes. In extinction spectrum, the highest strong coupling is shown when peak value of wavelength is around 1000nm (figure 4.4(B)). When separation distance is 8nm, peak value of wavelength is 927.027nm (figure 4.4(B)).

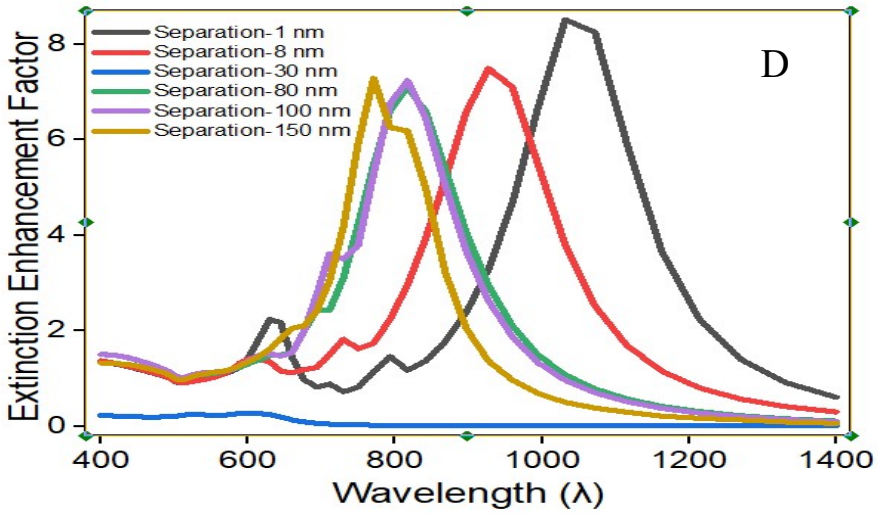

Figure 4.4 (D) FDTD simulation results of 150 nm lengths Au triangle plasmon coupling extinction spectrum, when separation distance, d = 1 nm, 8 nm, 30 nm, 80 nm, 100 nm and 150 nm.

This indicates that a simple variation of separation distance can affect in a great extent of coupling effect. On the other hand, weak coupling occurs from separation distance, d = 30nm, 80nm, 100nm, 150nm (very weak). At length 150nm Au nano plasmon acts like single particle. When extinction distance is 150nm, peak wavelength is around 800nm for extinction. Here extinction enhancement factor decreasing rate around 15.3% for increasing separation.[22]

Cross section enhancement factor as a function of varying separation for a coupling triangular nanoparticle:

In figure 4.4 (E) we can observe cross section enhancement factors for increasing separation. We varied separations from 1nm to 8nm, we got the cross section enhancement factor. Which are summation of absorption and scattering enhancement factors. When separation is less than the extinction enhancement factor are increased. Moreover the extinction enhancement factor are slightly decrease for increasing separation.

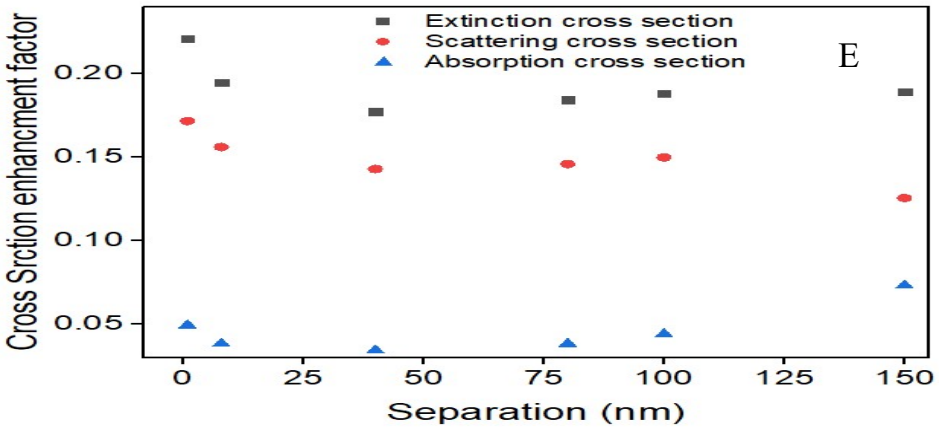

Figure 4.4 (E) coupling effect for l=150 as a function of cross section enhancement factor & strength, when separation distance, d = 1 nm, 8 nm, 30 nm, 80 nm, 100 nm and 150 nm. Absorption in blue line, scattering in red line and extinction in black line.

Observing Comparison of Cross section's spectrum, we can say cross section's area are changes on separation of coupling nanoparticles. In summation, we can represent these results with the help of the table below:

Variations in separations (nm)	Absorption		Scattering		Extinction	
	SPR Peak (nm)	Cross sections (μm^2)	SPR Peak (nm)	Cross sections (μm^2)	SPR Peak (nm)	Cross sections (μm^2)
1	1031.58	0.04945	1031.58	0.1718	1031.58	0.2212
8	927.027	0.0384	927.027	0.1562	927.027	0.1947
30	868.354	0.03437	868.354	0.143	868.354	0.17738
80	816.667	0.03832	816.667	0.146	816.667	0.1844
100	729.787	0.0441	816.667	0.15	816.667	0.1881

Table-4.3: Comparative study of coupled gold nano particles (AuNPs) when varying the couple particles separation in nm. Where column-1 represents variation of length, column-2 represents absorption SPR peak (nm) and cross-sectional area (μm^2), column 3 represents scattering SPR peak (nm) & cross-sectional area (μm^2) and column-4 represents extinction SPR peak (nm) & cross-sectional area (μm^2).

Transmission and reflection of coupling triangular nanoparticle where separations are varying:

Figure-4.4 (F) shows the couple Au nanoparticle transmission properties by varying their separation (d =1nm, 8nm, 30nm, 80nm, 100nm and 150nm) respectively. We increase separation of coupling particles, transmission are linearly increased.

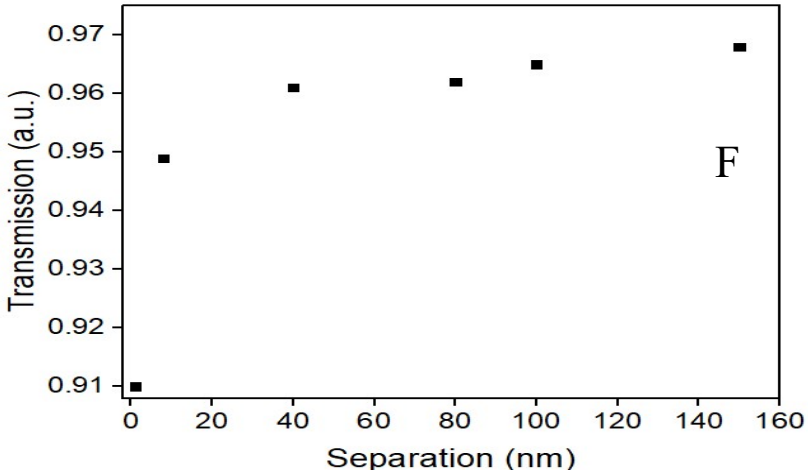

(F)

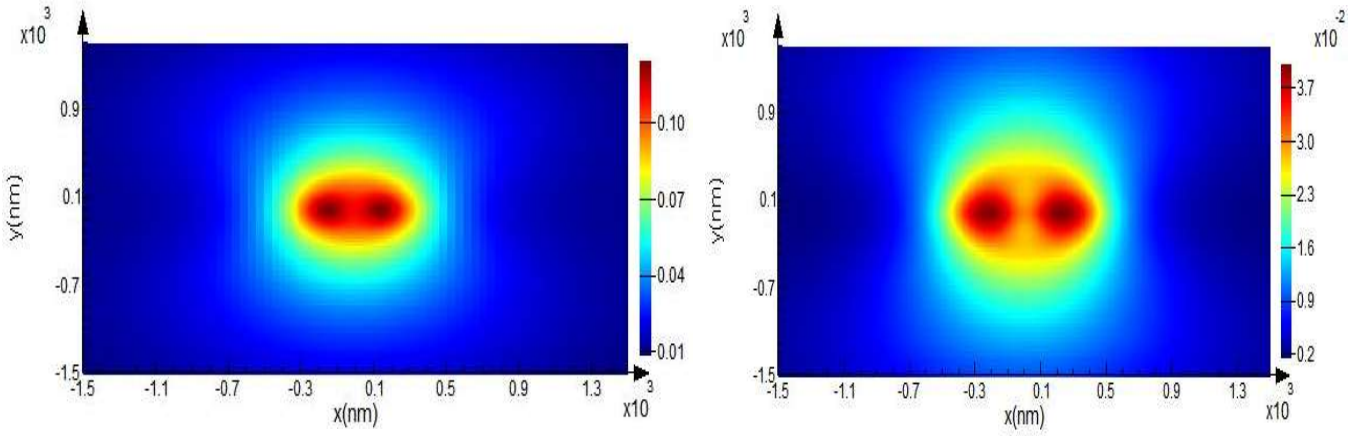

(G) (H)

Figure 4.4 (F) Transmission vs various separation of coupling particles, where length=150 and separation distance are d = 1 nm, 8 nm, 30 nm, 80 nm, 100 nm and 150 nm. (G) E plane image of transmission for separation of coupling particles, where length=150 and separation distance are d = 1 nm. (H) E plane image of transmission for separation of coupling particles, where length=150 and separation distance are d = 128 nm.

In figure-4.4 (I) reflection has been plotted against coupling particles separation. It is seen that reflection are linearly decreased with increasing separation.

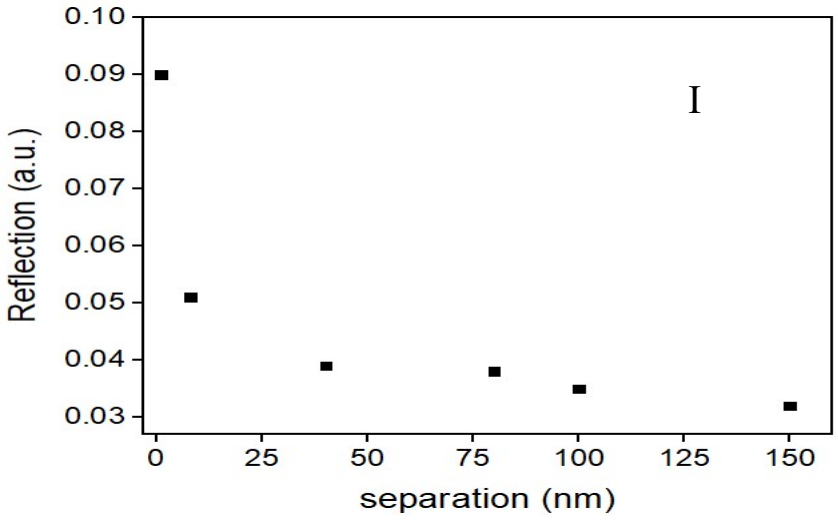

(I)

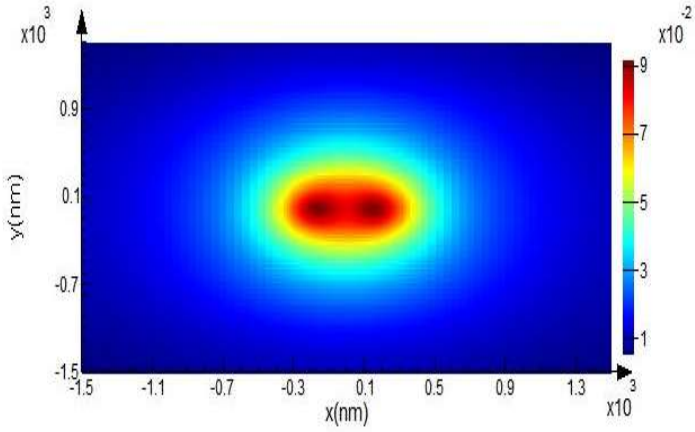

(J)

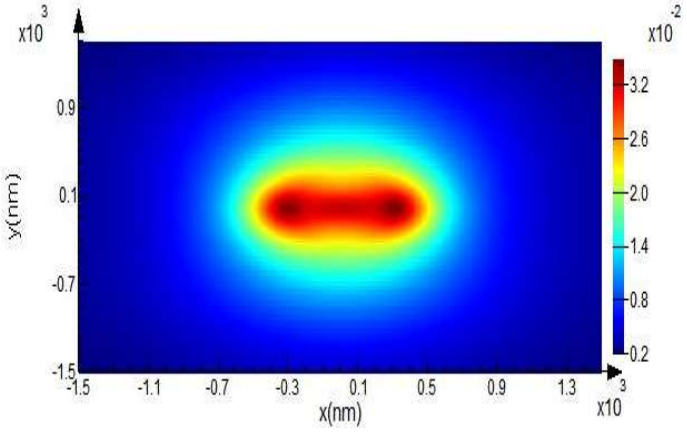

(K)

Figure 4.4 (I) Reflection vs various separation of coupling particles, where length=150 and separation distance are d = 1 nm, 8 nm, 30 nm, 80 nm, 100 nm and 150 nm. (J) E plane image of reflection for separation of coupling particles, where length=150 and separation distance are d = 1 nm. (K) E plane image of reflection for separation of coupling particles, where length=150 and separation distance are d = 128 nm.

4.4.3 Field enhancement of 150 nm length gold (Au) nano particles – FDTD simulation specification

Figure.3.5 (A-F) shows the spatial distribution of electric field as a function of incident light, when the incident E-field is polarized along the axis of two 150nm radius gold (Au) nano particle. [36]

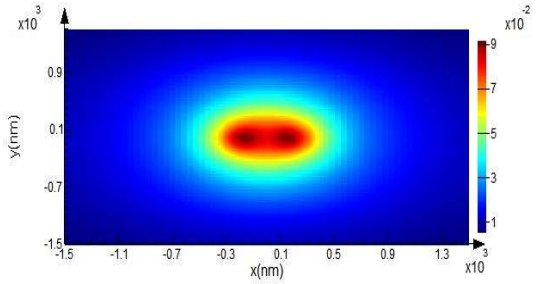

(A) Separation = 1 nm

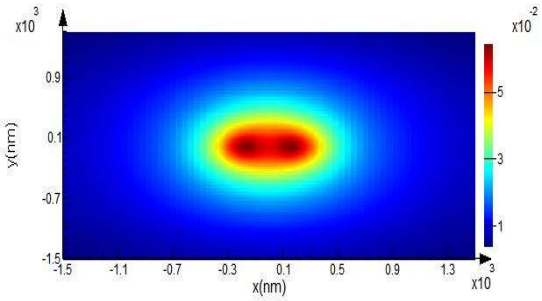

(B) Separation = 8 nm

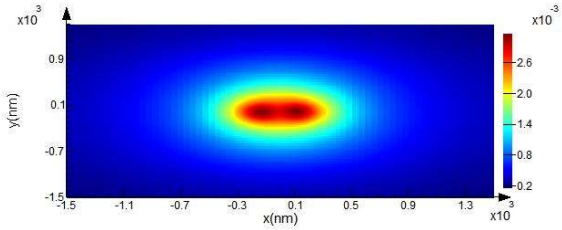

(C) Separation = 30 nm

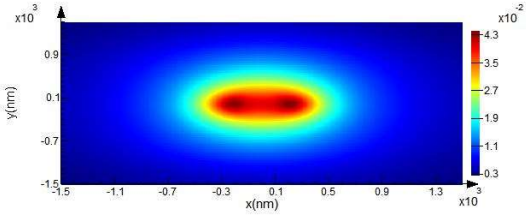

(D) Separation = 80 nm

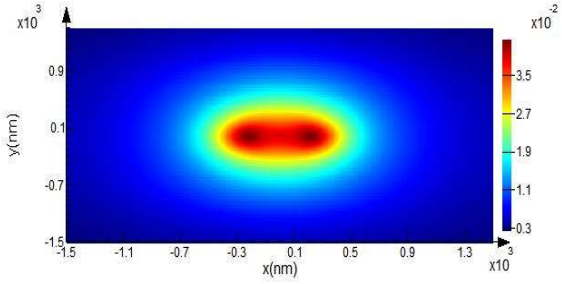

(E) Separation =100 nm

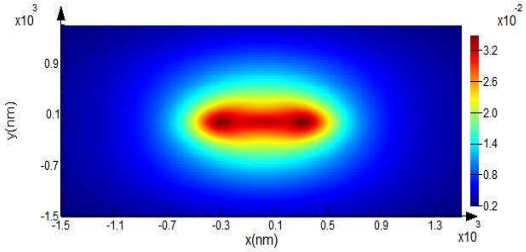

(F) Separation =150 nm

Figure 4.5. Field enhancement of 150 nm length gold (Au) Nano triangle when separation distance is varying. (A) For 1 nm, (B) for 8 nm, (C) for 30 nm, (D) for 80 nm (E) for 100 nm, (F) for 150 nm of XY plane respectively with the scattering peak value

Here, we can observe with figure 4.5 (A-F) and figure 4.4 (B), that the electric field enhancement is varying from 9 $\times 10^{-2}$ a.u. to 3.2 $\times 10^{-2}$ a.u. gradually when spacing between the gold Nano triangle are increasing from 1nm to 150nm. Figure-4.5 (A) shows electric field enhancement intensity of 0.9 $\times 10^{-2}$ au when separation distance is 1nm between the two-nano gold at resonance peak 1031.58nm. Figure- 4.5 (B) shows an electric field enhancement intensity of 5×10^{-2} au when the separation distance is 8nm at resonance peak 927.027nm. Furthermore, Figure-4.5 (C) shows an electric field enhancement intensity of 2.6×10^{-2} au when the separation distance is 30nm at resonance peak 601.75nm. Figure 4.5 (D) shows an electric field enhancement intensity of 4.3×10^{-2} au when the separation distance is 80 nm at resonance peak 816.667nm. Figure-4.5(E) shows an electric field enhancement intensity of 3.5×10^{-2} au when the separation distance is 100nm at resonance peak 816.667nm. Figure-4.5 (F) shows an electric field enhancement intensity of 3.2 $\times 10^{-2}$ au when the separation distance is 150nm at resonance peak 770.786nm. Here, we can clearly observe that electric field enhancement decreasing rate was 66 % with increasing separation. Because the separation distance is smaller the electric field enhancement is greater which is due to near field. It shows far field characteristics as a result the electric field is too weak compared to near field intensity.

Here we can be note that by varying the separation distance in x-axis, we get a clear change in electric field intensity. While we are changing the separation, distance from 1 nm to 4 nm the change in y-axis is almost vertical which is due to near field effect. However, after separation distance of 150nm there is very little change in electric field intensity and the electric field is too weak compared to near field as far-field strength decreases inversely with the distance from the source

4.4.4 Conclusion

In this chapter, we observed that when we varied the length of a single triangular nanoparticle from 60nm to 240nm then the absorption enhancement factor decrease by 8 times, scattering enhancement factor increase by 13 times and extinction efficiency also increse by 1.4 times, We also observed a red shift of SPR and increased intensity when we increased the length from 60nm to 240nm. Secondly, remarkable thing was when we varied the length of a couple triangular nanoparticle from 100nm to 300nm then the absorption, scattering and extinction efficiency also respectively decrease by 5.66 times, 0.68 times and 0.53 times. We also observed a red shift of SPR and increased intensity when we increased the length from 100nm to 300nm. Extinction efficiencies decreasing rate was 0.55 times for increasing particles length. Sphere peaks increasing rate was double for increasing particles length. Lastly, we varied the separation of a couple triangular nanoparticle from 1nm to 150nm when the absorption enhancement factor increase by 87%, scattering enhancement factor decrease by 27.3% and extinction efficiency also decrease by 15.3%. Observing Comparison of Cross section's spectrum, we can say cross section's area are changes on separation of coupling nanoparticles. In case of transmission are slightly increase with increasing separation and reflection are slightly decrease with increasing separation. For coupling particle, far field characteristics of electric field are too weak compared to near field intensity. This result will be helpful to observe the optical property of dipole nanoparticle which will be discussed in next section.

Chapter 5

Performance analysis of optical (dipole) antenna

5.1 Introduction

In this chapter we investigated the optical property of coupled dipole gold (Au) nano particle by finite difference time domain (FDTD) simulation. In this study we observed the optical cross section and field enhancement for coupled dipole Au nanoparticle as a function of separation.

5.2 Characterization of dipole nanoantenna

We have observed the optical property response of a pair of gold dipole nano-antennas on a glass substrate by varying the inter particle separation in nanometer scale. In previous chapter, we observed the transmission, the reflection, and the absorption spectrum of a gold dipole, and also observed parameter like, far-field and near-field, field enhancement. Our observation techniques are used based on the finite difference time domain (FDTD) simulation software.

5.3 Simulation Setup-FDTD

In this chapter, we used dipole from structures. We simulated nano particle of gold (Au) by FDTD software. Here, we choose gold (Au) nano particle-Johnson and Christy. In case of objects, we selected dipole glass substrate (refractive index 1.51). We changed particles length units to nanometer as our work involved nanostructures. The material of the structures faced tip to tip is gold (Au) of fixed height.

We fixed dipole particles length at 400nm, width at 100nm and height at 50nm. And we changed separation in different nm (1, 4, 8, 16, 32, and 64,128).

In our simulations we set mesh accuracy at 2nm. We choose anti- symmetric, symmetric and PML boundary condition. We have used total-field scattered-field (TFSF) source with a wavelength range from 300nm to 3000nm. It must be noted that, we have been placed the

source perpendicular (TE) to the z axis of the structure. We have used time-domain monitors, index monitors and Frequency-domain power monitors. We added two analysis groups, named 'total' and 'scat'. [22]

5.4 Simulation results and discussions

5.4.1 Dipole antenna simulation using FDTD

Here we take dipole particles of gold, each about 400nm long, width 100nm and height 50nm, whose tips face each other. We observed the absorption/ scattering/ extinction cross sectional coupling effect when separation distance is from 1nm-128nm, FDTD simulation method has been used. We fixed dipole particles length at l= 400nm and changes separation in different nm (1, 4, 8, 16, 32, 64, 128). We plotted extinction σ_{ext}, absorption σ_{abs}, and scattering σ_{scat} cross sections for dipole Au nanoparticles. We know the optical and electronic properties of gold nanoparticles are tunable by changing their separation. [37]

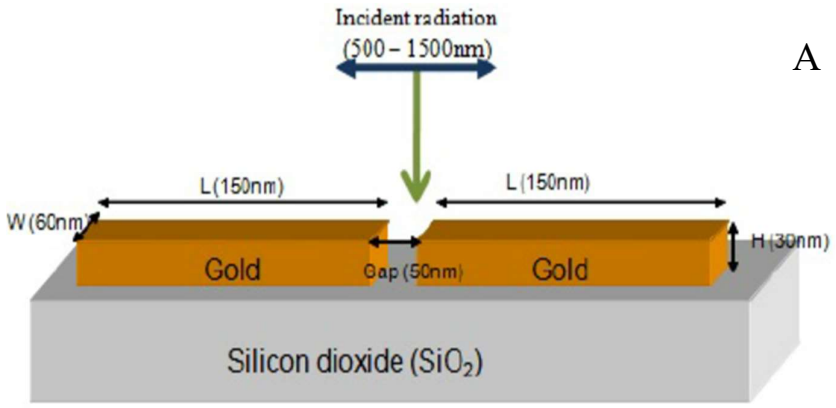

Figure: 5.1(A) Schematic diagram of dipole nanoantenna

Absorption enhancement factor as a function of varying separation for a coupling dipole nanoparticle:

Figure- 5.1 (B) shows the absorption coupling effect when varying their coupling distance. It shows clearly when the separation increases the red shift (longer wavelength) of the surface plasmon resonance from around 1.5×10^{-6} nm to 2.5×10^{-6} nm. As usual the red shift is due to

coupling of plasmonic near field. In case of coupling effect of dipole particle, absorption cross sectional area varies from 5×10^{-18} nm to 1×10^{-17} nm when the separation decreases from 128nm to 1nm, which can be an observation of strong coupling and weak coupling.

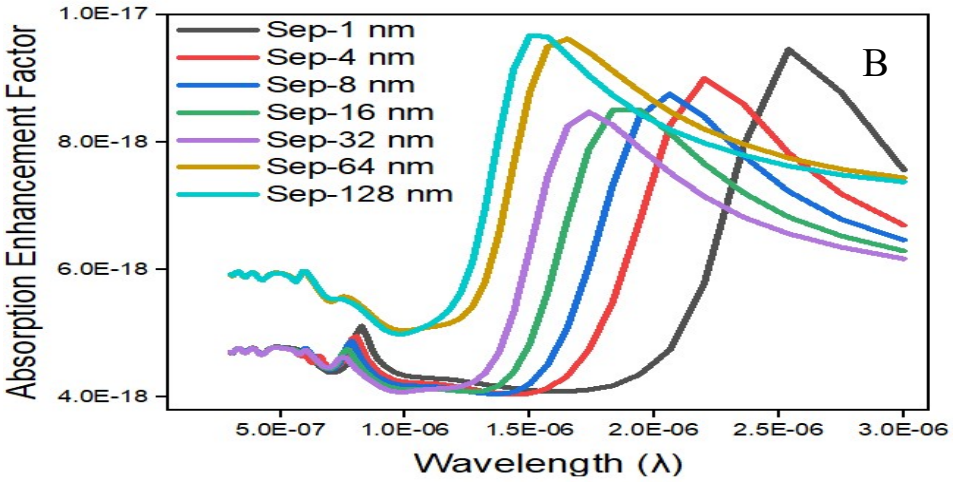

(B)

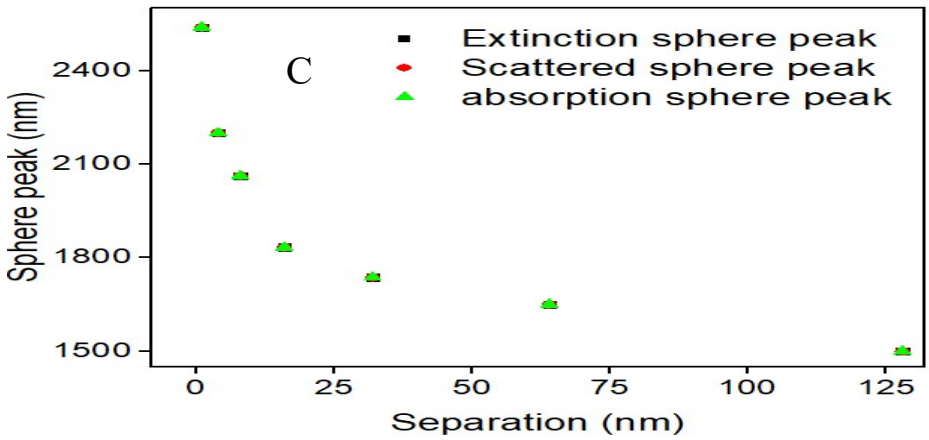

(C)

Figure 5.1 (B) FDTD simulation results of 400 nm lengths, width 100 nm and height 50 nm of Au dipole plasmon coupling absorption enhancement factor, when separation distance, d = 1 nm, 4 nm, 8 nm, 16 nm, 32 nm, 64 nm and 128 nm (C) Plasmon absorption, scattering and extinction coupling effect – strong coupling to weak coupling of 400 nm length dipole (peak wavelength vs coupling separation).

For absorption, the highest strong coupling is shown when peak value of wavelength is around 2538.46nm (figure 5.1 (C)). When separation distance is 4nm, 8nm, 16nm and 32nm, peak value of wavelength is respectively 2200nm, 2062.5nm, 1833.3nm and 1736.84nm (figure 5.1 (C)). This indicates that a simple variation of separation distance can affect in a great extent of coupling effect. Weak coupling occurs from separation distance, d = 64nm, 128nm (very

weak). Ironically, at separation of 128nm Au nano plasmon acts like single particle and peak wavelength is around 1500nm for absorption. Here absorption enhancement factor's increasing rate is around 2.1% for increasing separation.

Scattering enhancement factor as a function of varying separation for a coupling dipole nanoparticle:

Figure- 5.1 (D) and figure-5.1 (C) show the scattering coupling effect when varying their coupling separation.

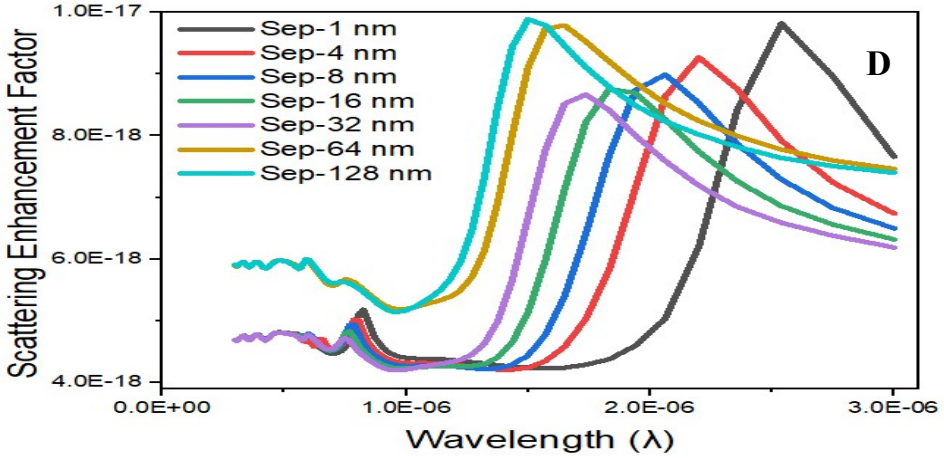

Figure 5.1 (D) FDTD simulation results of 400 nm lengths, width 100 nm and height 50 nm of Au dipole plasmon coupling scattering enhancement factor, when separation distance, d = 1 nm, 4 nm, 8 nm, 16 nm, 32 nm, 64 nm and 128 nm.

In graph when the separation decreases, there has been a red shift (longer wavelength) of the surface plasmon resonance from around 1.5×10^{-6} nm to 2.5×10^{-6} nm. There is an improvement in scattering cross sectional area from 5×10^{-18} nm to 1×10^{-17} nm.

For scattering, the highest strong coupling is shown when peak value of wavelength is around 2538.46nm (Figure 5.1 (C)). When separation distances are 4nm, 8nm, 16nm and 32nm, peak values of wavelength are respectively 2200nm, 2062.5nm, 1833.3nm and 1736.84nm (figure 5.1 (C)). This indicates that a simple variation of separation distance can affect in a great extent of coupling effect. Weak coupling occurs from separation distance, d = 64nm and 128nm (very weak). Here scattering enhancement factor slightly increased for increasing separation.[22]

Extinction enhancement factor as a function of varying separation for a coupling dipole nanoparticle:

As we know extinction spectrum is a summation of absorption and scattering spectrum. We investigated the plasmon coupling of 400nm diameter AuNP dimer using FDTD simulation. Fig. 5.1 (E) found red shift in SPR peak with decreasing inter–particle distance (weak coupling region) and similar as previous the red shift is due to coupling of plasmonic near field in weak coupling region.

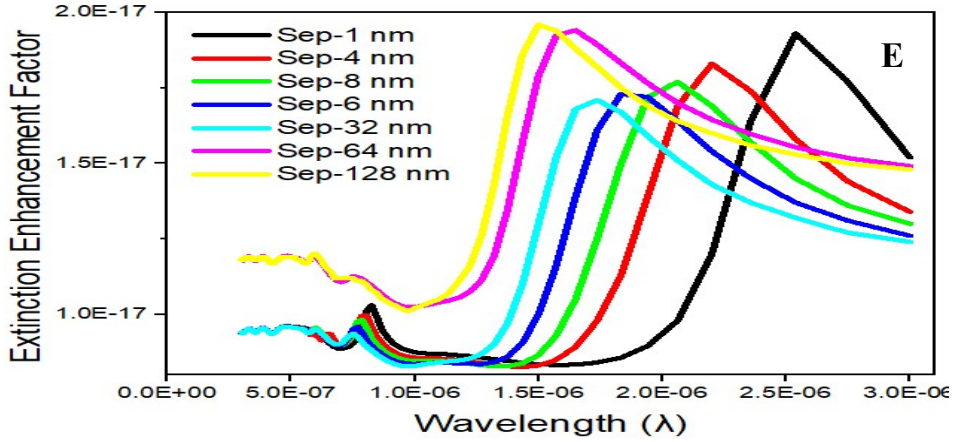

Figure 5.1 (E) FDTD simulation results of 400 nm lengths, width 100 nm and height 50 nm of Au dipole plasmon coupling extinction enhancement factor, when separation distance, d = 1 nm, 4 nm, 8 nm, 16 nm, 32 nm, 64 nm and 128 nm.

When separation distances are 4nm, 8nm, 16nm and 32nm, peak values of wavelength are respectively 2200nm, when separation distance is 1nm, peak value of wavelength is 2538.46nm (Figure 5.1(C)). Weak coupling occurs from separation distance, d = 64nm, 128nm, (very weak).

Cross section spectrum as a function of varying separation for a coupling dipole nanoparticle:

In figure 5.1(F) we can observe cross section enhancement factors for increasing separation. When separations are 1nm to 30nm, we got cross sections at lowest value. If we observed

extinction enhancement factors lines then we can see extinction enhancement factors are increasing with increasing separation.

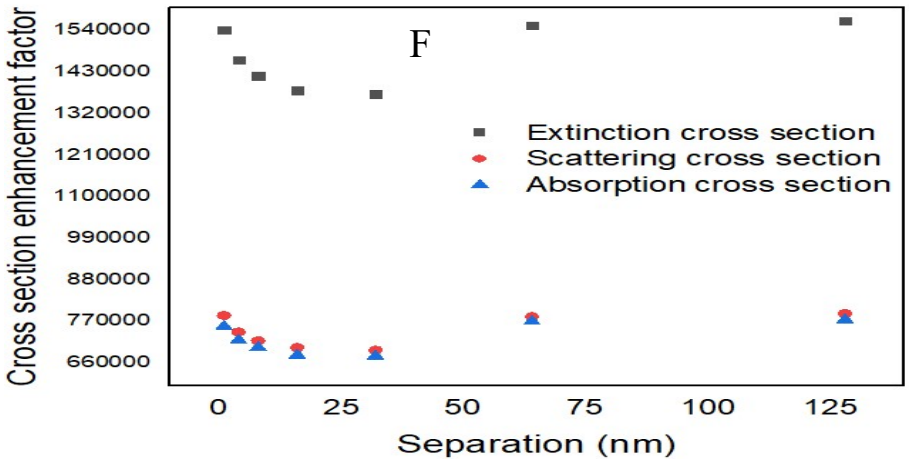

Figure 5.1 (F) coupling effect for of 400 nm lengths, width 100 nm and height 50 nm of Au dipole as a function of cross section enhancement factor & strength, when separation distance, d = 1 nm, 4 nm, 8 nm, 16 nm, 32 nm, 64 nm and 128 nm. Absorption in blue line, scattering in red line and extinction in black line.

Here, absorption is highlighted in blue line, scattering in red line and extinction in black line. Observing comparison of cross section's spectrum, we can say cross section's area are changed due to change of separation. In summation, we can represent these results with the help of the below table.

Variations in separations (nm)	Absorption		Scattering		Extinction	
	SPR Peak (nm)	Cross sections (μm^2)	SPR Peak (nm)	Cross sections (μm^2)	SPR Peak (nm)	Cross sections (μm^2)
1	2538.46	756964	2538.46	785512	2538.46	1.54E+06
4	2200	720328	2200	741845	2200	1.46E+06
8	2062.5	700959	2062.5	718817	2062.5	1.42E+06
16	1833.33	680669	1833.33	700732	1833.33	1.38E+06
32	1736.84	678031	1736.84	693850	1736.84	1.37E+06
64	1650	770100	1650	782273	1650	1.55E+06
128	1500	774285	1500	791129	1500	1.57E+06

Table-4.4: Comparative study of dipole gold nano particles (AuNPs) when varying the dipole particles separation in nm. Where column-1 represents variation of length, column-2 represents absorption SPR peak (nm) & cross-sectional area (μm^2), column 3 represents scattering SPR peak (nm) & cross-sectional area (μm2) and column-4 represents extinction SPR peak (nm) & cross-sectional area (μm^2).

Transmission and reflection of coupling dipole nanoparticle where separations are varying:

Figure-5.1 (G) shows the dipole Au nanoparticle transmission properties by varying their separation (d =1nm, 4nm, 8nm, 16nm, 32nm, 64nm and 128nm) respectively.

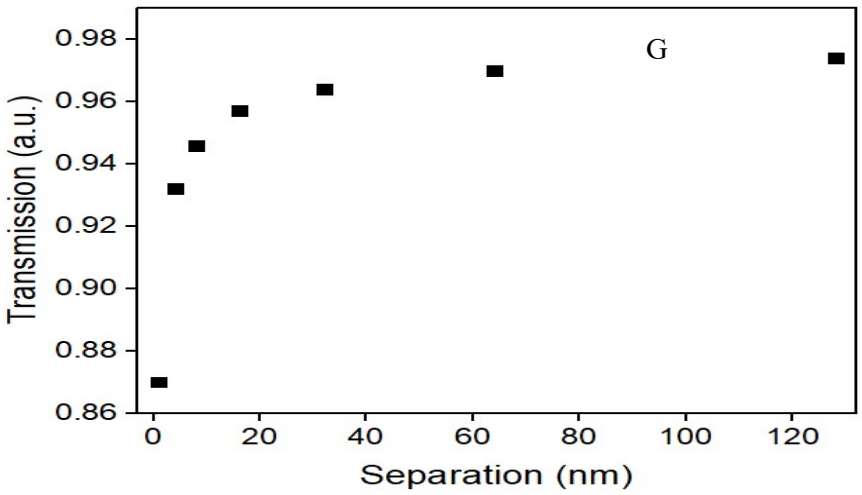

(G)

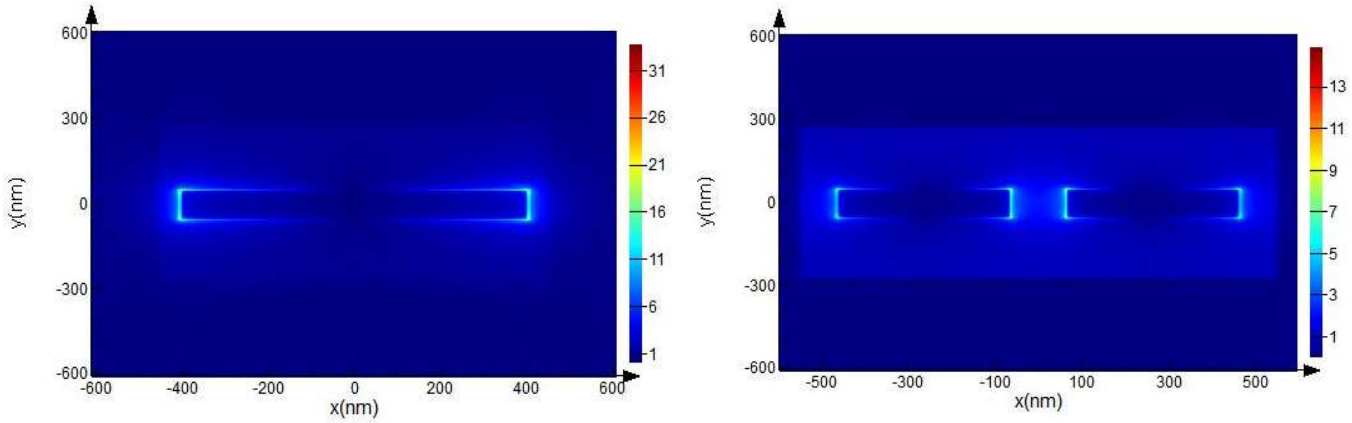

(H) (I)

Figure 5.1 (G) Transmission vs various separation of coupling dipole particles, where 400 nm lengths, width 100 nm, height 50 nm and separation distance are d = 1 nm, 4 nm, 8 nm, 16 nm, 32 nm, 64 nm and 128 nm. (H)E plane image of transmission for coupling dipole particles, where 400 nm lengths, width 100 nm and height 50 nm and separation distance are d = 1 nm.(I)E plane image of Transmission for coupling dipole particles, where 400 nm lengths, width 100 nm and height 50 nm and separation distance are d = 128 nm.

With increasing separation of coupling particles, transmission is linearly increased. Transmission increasing rate around 1.11 times for increasing separation. In figure-5.1 (J) reflection has been plotted against coupling particles separation. It is seen that reflection are linearly decreased with increasing separation. At 128nm separation of coupling particle, reflection shows minimum value.[38] Observing the result from figure-4.4 (H), it can be concluded that, reflection decreasing rate was 0.21 times for increasing separation.

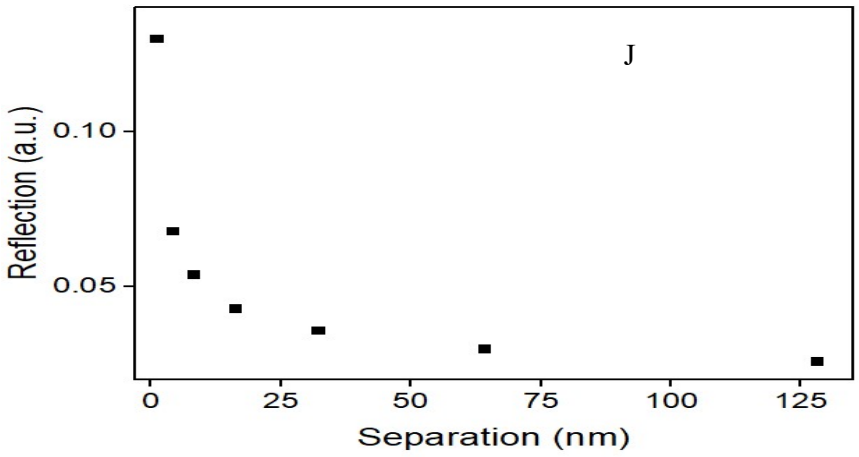

(J)

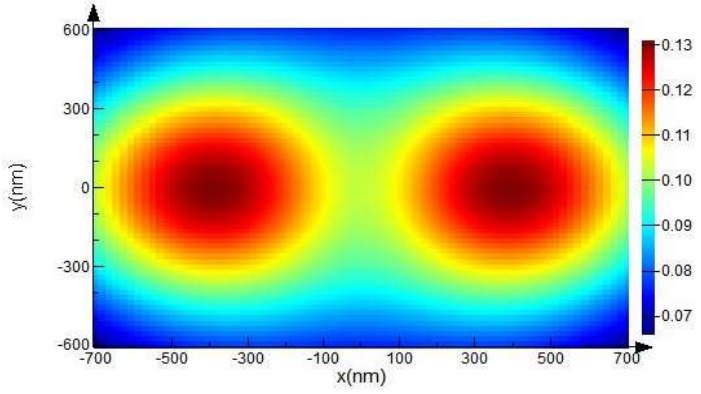

(K)

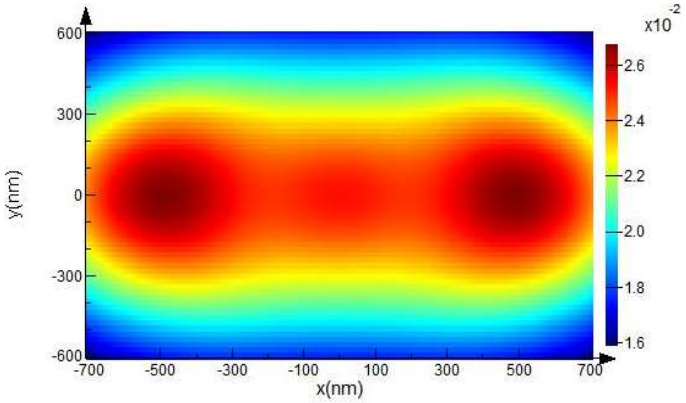

(L)

Figure 5.1 (J) Reflection vs various separation of coupling dipole particles, where 400 nm lengths, width 100 nm, height 50 nm and separation distance are d = 1 nm, 4 nm, 8 nm, 16 nm, 32 nm, 64 nm and 128 nm. (K) E plane image of reflection for coupling dipole particles, where 400 nm lengths, width 100 nm and height 50 nm and separation distance are d = 1 nm.(L) E plane image of reflection for coupling dipole particles, where 400 nm lengths, width 100 nm and height 50 nm and separation distance are d = 128 nm.

5.4.2 Field enhancement of 400nm lengths, width 100nm and height 50nm gold (Au) dipole nano particles – FDTD simulation specification

Figure 5.2 (A-G) shows the spatial distribution of Electric field as a function of incident light, when the incident E-field is polarized along the axis of two 400nm radius gold (Au) nano particle. [36]

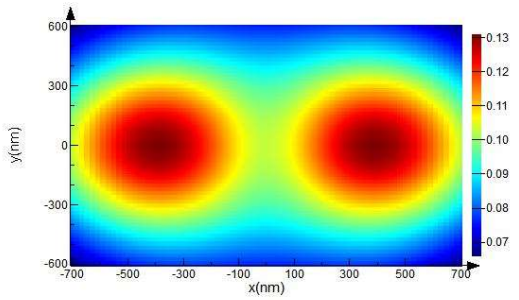

(A) Separation = 1 nm

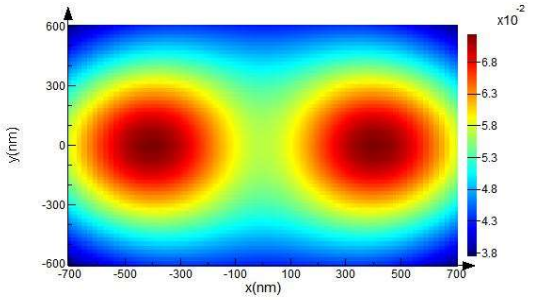

(B) Separation = 4 nm

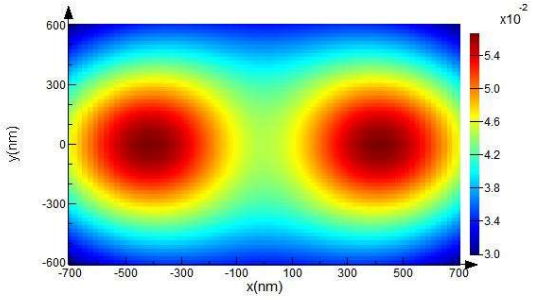

(C) Separation = 8 nm

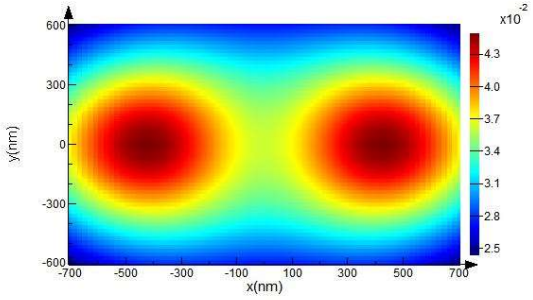

(D) Separation = 16 nm

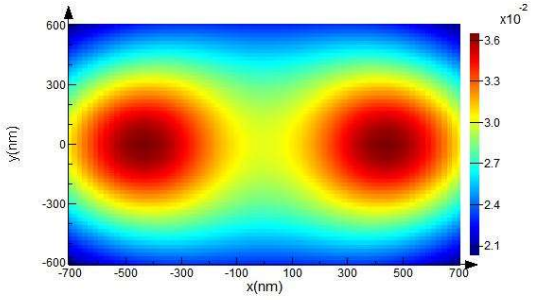

(E) Separation =32 nm

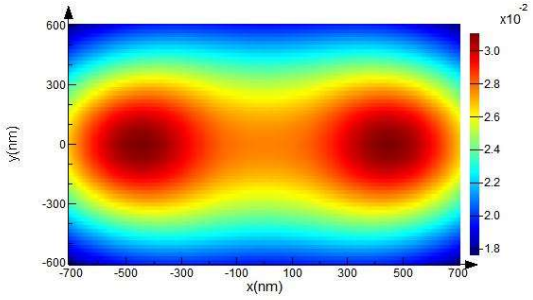

(F) Separation = 64 nm

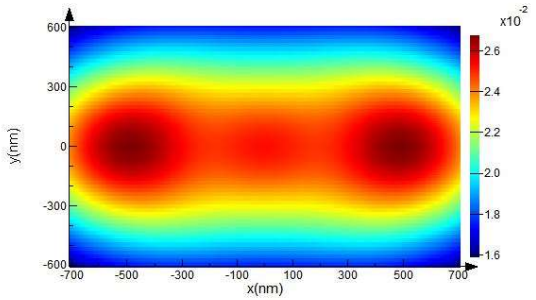

(G) Separation =128 nm

Figure 5.2. Field enhancement of 400 nm lengths, width 100 nm and height 50 nm gold (Au) nano dipole when separation distance is varying. (A) for 1 nm, (B) for 4 nm, (C) for 8 nm, (D) for 16 nm (E) for 32 nm, (F) for 64 nm and (G) for 128 nm of XY plane respectively with the scattering peak value.

Here, we can observe with figure 5.2 (A-G) and figure 5.1 (C) that, the electric field enhancement is varying from 0.13 a.u. to 2.6 $\times 10^{-2}$ au gradually when spacing between the gold nano dipole are increasing from 1nm to 128nm. Figure-5.2 (A) shows electric field enhancement intensity of 0.13 au when separation distance is 1nm among the dipole gold at resonance peak 2538.46nm. Figure- 5.2 (B) shows an electric field enhancement intensity of 6.8×10^{-2} au when the separation distance is 4nm at resonance peak 2200nm. Furthermore, figure-5.2 (C) shows an electric field enhancement intensity of 5.4×10^{-2} au when the separation distance is 8nm at resonance peak 2062.5nm. Figure 5.2 (D) shows an electric field enhancement intensity of 4.3×10^{-2} au when the separation distance is 16nm at resonance peak 1833.33nm. Figure-5.2 (E) shows an electric field enhancement intensity of 3.6×10^{-2} au when the separation distance is 32nm at resonance peak 1736.84nm. Figure-5.2 (F) shows an electric field enhancement intensity of 3.0 $\times 10^{-2}$ au when the separation distance is 64nm at resonance peak 1650 nm. Figure-5.2 (G) shows an electric field enhancement intensity of 2.6 $\times 10^{-2}$ au when the separation distance is 128nm at resonance peak 1500nm. Here, we can clearly observe that electric field enhancement decreasing rate was 100% with increasing separation. Because of smaller separation distance, the electric field enhancement is greater which is due to near

field. It shows far field characteristics as a result the electric field is too weak compare to near field intensity.[39]

Here we can be noted that, by varying the separation distance in x-axis, we get a clear change in electric field intensity. While we are changing the separation distance from 1nm to 4nm, the change in y-axis is almost vertical which is due to near field effect. However, after separation distance of 128nm there is very little change in electric field intensity and the electric field is too weak compared to near field as far-field strength decreases inversely with the distance from the source.

5.5 Conclusion:

In this chapter, we varied the separation of a dipole nanoparticle from 1nm to 128nm and then the absorption enhancement factor increase by 2.1%, scattering enhancement factor increase slightly and extinction efficiency are also increase slightly. Observing comparison of cross section's spectrum, we can say cross section's area are changed on separation of coupling nanoparticles. In case of transmission increasing rate around 1.11 times for increasing separation and reflection decreasing rate around 0.21 times for increasing separation. For coupling particle, far field characteristics of electric field are too weak compared to near field intensity. This result will be helpful to observe the optical property of coupled triangular nanoparticle.

CHAPTER 6

Performance analysis of RF (patch and probe) antenna

6.1 Introduction

In this chapter we investigated performance of patch and probe antenna by finite difference time domain (FDTD) simulation. In this study, we observed the performance of different kind of antennas by tuning their dimensions.

6.2 Characterization of patch antenna

In this chapter, we simulated coaxial-fed rectangular patch antenna mounted over an infinite PEC ground plane. Patch antennas are actually microstrip antenna. We observed patch antennas parameter like, near field, directivity (E & H plane), gain, port power, return loss and impedance. We performed finite difference time domain (FDTD) simulations in order to analyze the parameters.[40]

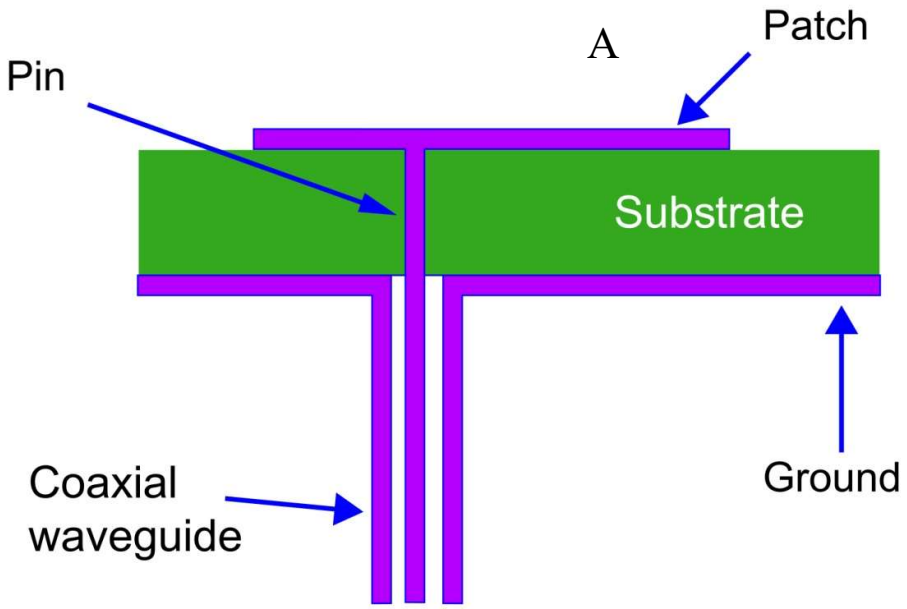

Basically, patch antenna is a type of low-profile radio antenna. Patch antenna can be in various size and shapes. It consists of planer rectangular, circular, metallic ground plane.

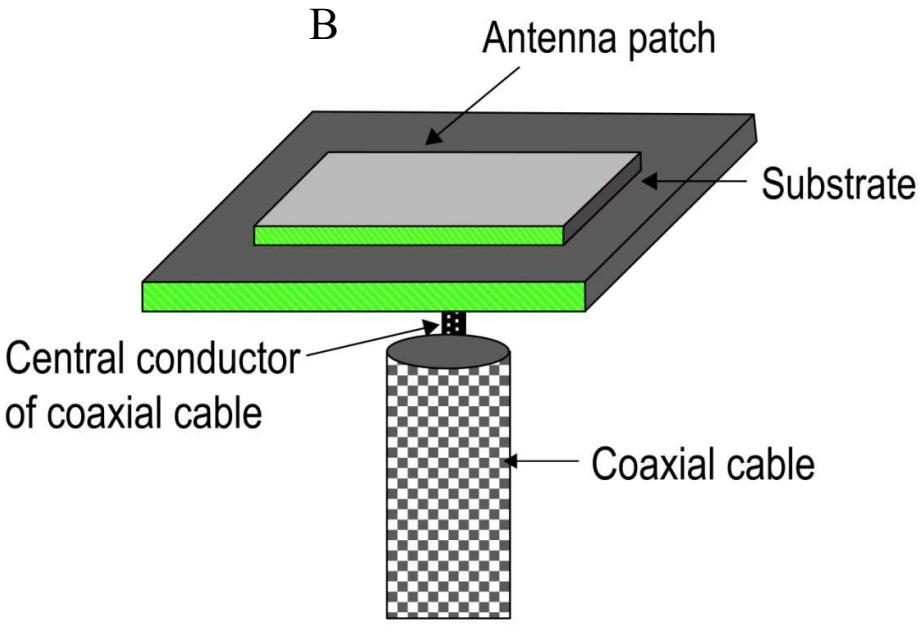

Figure: 6.1: (A) Schematic diagram of former patch antenna (B) coaxial-fed rectangular patch antenna mounted over an infinite PEC ground plane.

Here we simulate a coaxial-fed rectangular patch antenna which mounted over by an infinite PEC (perfect electric conductor) ground plane. From figure 6.1, we can see PEC mounted on a substrate that is stranded on a metallic ground plane. It's used in MHz to THz range frequencies applications, when size, weight, cost, reliability, and aerodynamic performance are obligations. [41]

In FDTD simulations, we used directivity analysis group to find antenna's return loss, directivity, and far-field patterns. When a large object mounted electrically, then ground plane can be considered as infinitely large with low frequencies and a perfect electric conductor (PEC). In this situation, patch antenna is starting excitation by coaxial pin, which is using in bottom of PEC. Coaxial pin extending out of the ground plane and terminating on the top patch.

From the theory relies on transmission line and cavity model, we know the patch antenna as an array of two radiating apertures of width (slots) separated by a transmission line of length L.

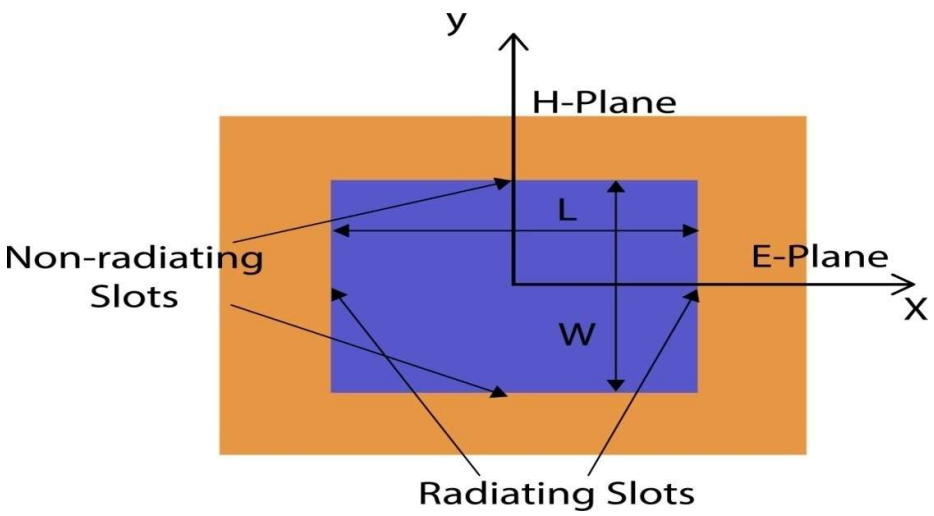

Figure: 6.2: Schematic diagram of coaxial-fed rectangular patch antenna.

In figure 6.2 we can see two non-radiating slots and two radiating slots. When mode TM^{x}_{010} is excited, then the radiation from each slot along with the patch's width add constructively in phase which is known as a radiating slot. Same as when the radiation from each slot along the length adds destructively out of phase that is known as non-radiating slot. Here TM^{x}_{010} is patch's dominant. By relating the fields on the slots to an equivalent current density and radiation equation, we can find the total directivity pattern and far fields.[42]

6.3 Simulation Setup-FDTD

In our simulation we took rectangular sheet of width (y span) 12.86mm and length (x span) 10.06mm. Sheet stand on a rectangular substrate of 10.06mm X 12.86mm X 1.588mm possessing a refractive index of 1.48. Here substrate ground plane constructed from a 2D rectangular sheet, which extended out the simulations domain's X-Y plane, rendering infinite. We use two concentric rings forms the coaxial waveguide's interior vacuum region and outer PEC conductor. Inner PEC conductor surrounded by these rings which act as a circular. The

coaxial waveguide extends out of the bottom (z min) FDTD boundary. To have an impedance of 50 Ω at the expected frequency, the x position of the feed must be optimized and the inner conductor radius a = 0.19107m and outer conductor radius b=1mm are selected.

Here the coaxial waveguide's model intersects the ground plane at z=0 and its inner conductor passes through the substrate that's why we need to manually select the mesh value for these objects.

In our simulation mesh order is assigned as inner conductor = 1, outer conductor =2, ground=3 and substrate=4 (and coax dielectric).

We used index monitor to show the surface conductivity in the X-Z plane at y=0 and verifies the patch is being properly fed by the coaxial waveguide. We placed a port near the bottom edge of the simulation region which is used to inject and measure the coaxial TEM mode over a frequency range of 8GHz to 15GHz.

We set a mesh for override region to ensure high enough resolution to give far field result. We set mesh accuracy of 4 for the rest of the simulation region.

We specified PML all boundaries at least λ0/4 thick so that no reflections will occur outside the directivity analysis group's monitors. Here role of the directivity analysis group is used to setup the monitors and find the directivity of the patch antenna. In the analysis group's setup variable tab, the x, y, and z span are chosen so that the monitors are at least λ/4 away from the edge of the patch antenna.

6.4 Result and analysis

6.4.1 Reflection

Figure- 6.3 (A) shows the port power effect when varying their antennas dimensions. It shows clearly input; output of power verses frequency graph is vice versa.

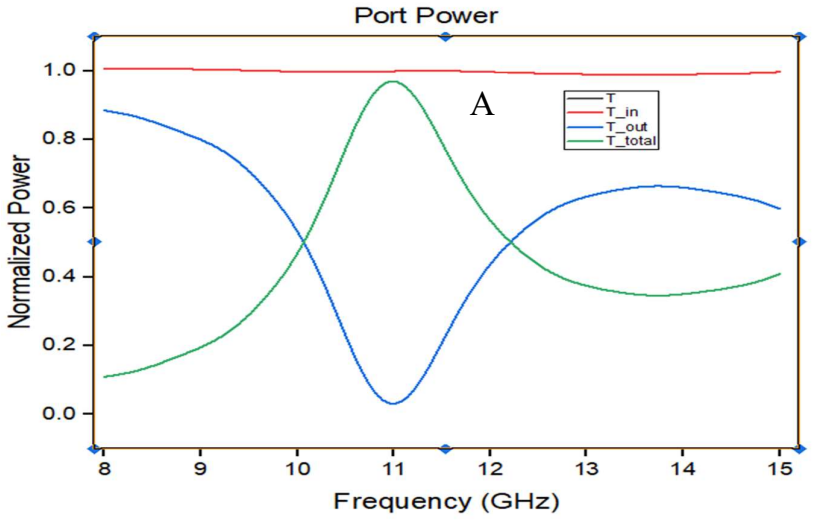

Figure: 6.3 Port power (power vs. frequency) of co-axial waveguide patch antenna.

In port power analysis if we increase frequency, we can see, peak at 11 GHz and at the output port power result is reverse.[43]

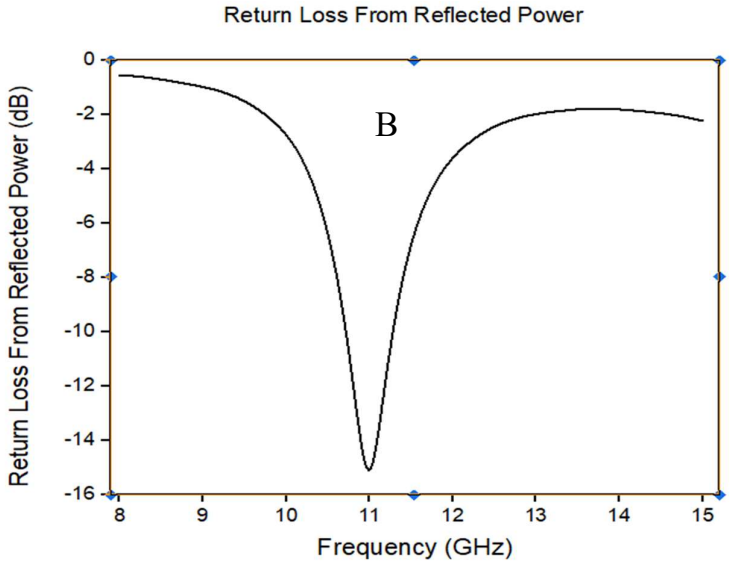

(B)

In figure 6.4 (B) & (C) shows return loss of reflected power and input impedance. The simulated patch antenna's resonant frequency of 11GHz is within 0.8% of the theoretical resonance of 10GHz.

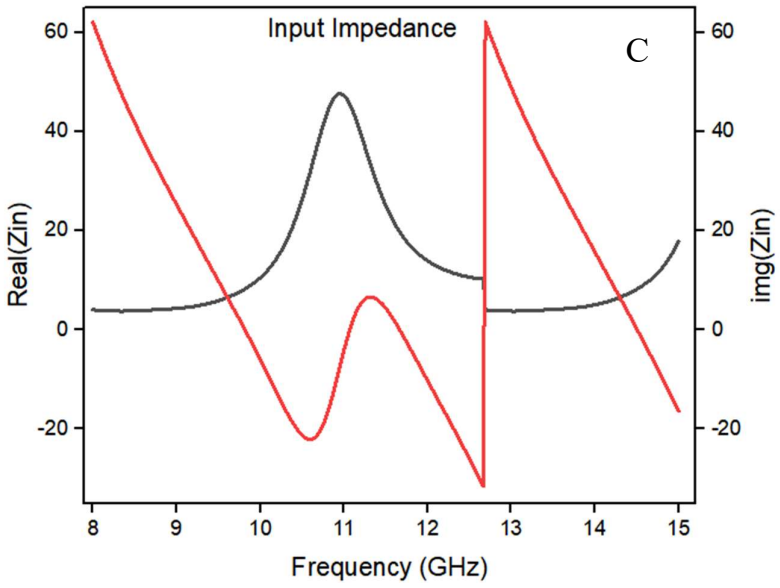

(C)

Figure: 6.4 (B) Return loss from reflected power & (C) input Impedance of co-axial waveguide patch antenna.

This level of match is quite excellent since the theory does not account for the reactive input impedance. In fact, we see in figure that the input resistance reaches its peak near 11GHz. The antenna's input impedance is shown in the figures (C) above, which has 48.19 Ω characteristic impedance at the resonance frequency, very close to the theoretical value of 50 Ω.[44]

6.4.2 Directivity pattern

We use directivity analysis group to calculate the far fields at the resonant frequency. We set far field θ and ϕ resolutions are set to 1deg and 10deg respectively, which can accurately capture the directivity's variation θ and ϕ planes.

In figure 6.5 (D) shows near field power. We see in the figure; the input power reaches its peak near 11GHz.

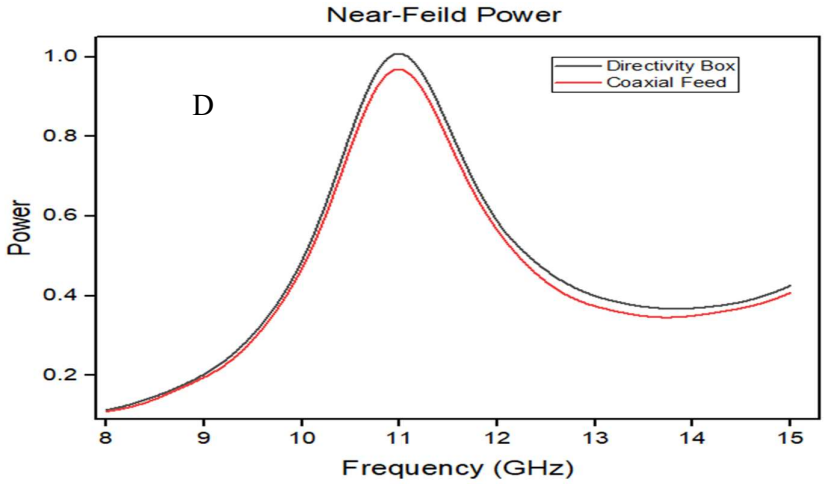

Figure: 6.5 (D) Near-Field power of Co-axial waveguide patch antenna.

Figure 6.6 (E) & (F) shows the script that generates plots of the antenna's directivity in the E-plane (X-Z cut) and H-plane (Y-Z cut). After observing figure 6.5 (E) of E-plane, we can say one thing about D theta polarization, which is our FDTD simulation result match with traditional antenna theory and design. But it shows differences because of a number of assumptions in the theory.

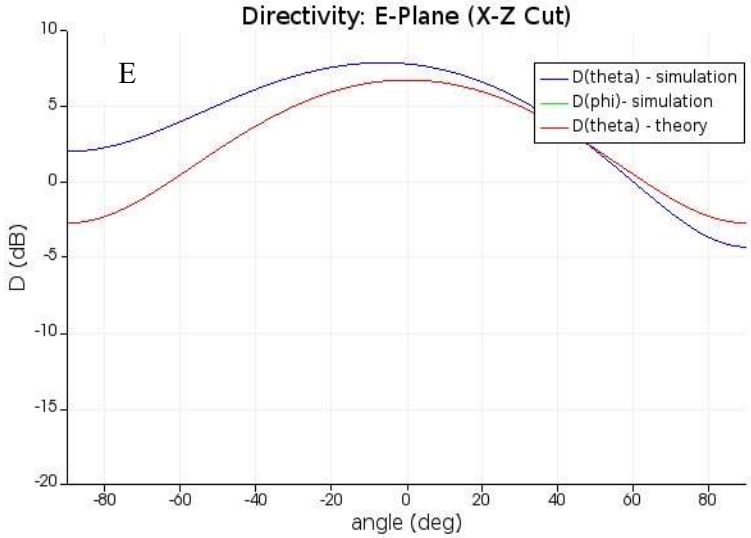

(E)

One important factor in graph (E) is – the D theta polarization is well below -80 dB in the E-plane and its matches with the theory. In E plane, asymmetry occurred in FDTD directivity because of feed which is positioned asymmetrically. In the theory, this asymmetry is not considered. Additionally, in this simulation, substrate over the ground plane changed the magnitude and phase of the image and break down the assumptions in the theory's use of image theory to derive the directivity. This has the largest effect near grazing (θ=90deg) in the E-plane.[45]

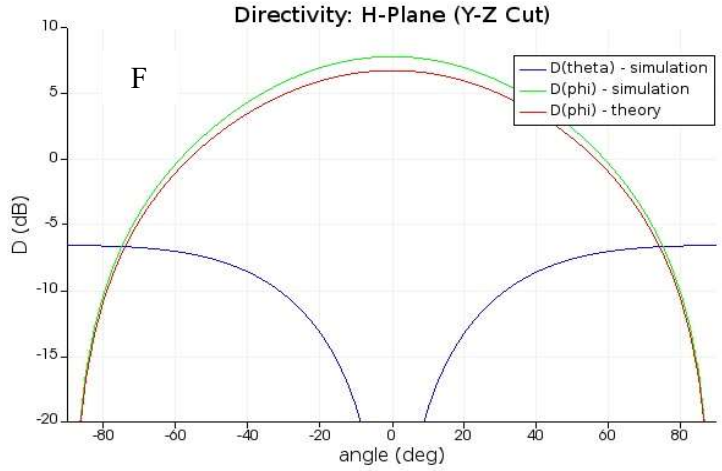

(F)

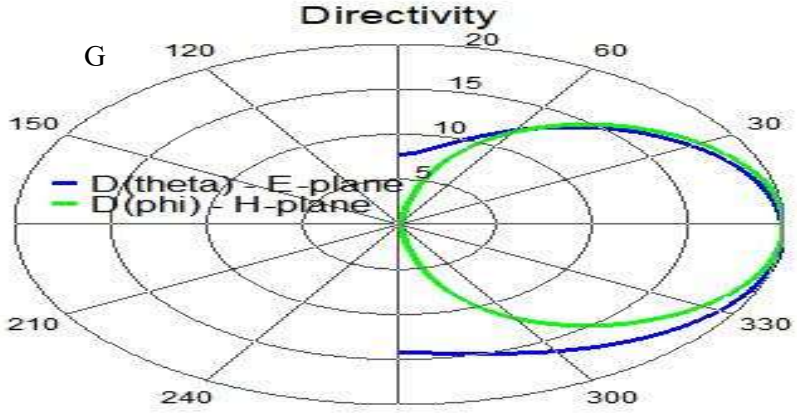

(G)

Figure: 6.6 (E) Directivity E-plan (X-Z Cut) & (F) Directivity H-plan (Y-Z Cut) and (G) Directivity of co-axial waveguide patch antenna.

About H-plane, our FDTD simulation results extremely close to traditional antenna theory and design. As expected, the H-plane is unaltered by the presence of the substrate. Furthermore, the asymmetry of the feed does not affect D theta. [46]

6.5 Characterization of probe antenna

In this chapter, we simulated rectangular probe antenna mounted over a finite and infinite PEC ground plane. We simulated X-band (WR-90) rectangular open-ended-waveguide-probe (OEWG) antenna. This model recommended frequency range 8.20MHz to 12.4MHz. Probe waveguide antennas are used in a wide variety of application. Probe antennas have high power handling capability, low loss, high directivity, and near constant electrical performance. Also, these antennas have low gain variation across their operating frequency. We know waveguide antenna is one of the parts of aperture antenna. This type of antennas edge of a transmission line terminated with an opening radiates energy. This opening radiates acts like an aperture which makes it an Aperture antenna.[47] . As per previous section we observed probe antennas parameter like, near field, directivity (E & H plane), gain, port power, return loss & impedance. We performed finite difference time domain (FDTD) simulations to analyze the parameters.

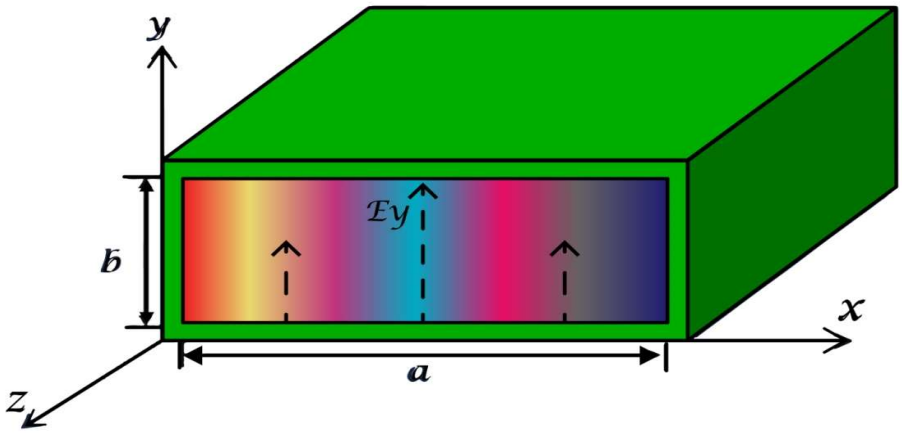

Figure: 6.6 (H) Schematic diagram of rectangular probe antenna

Here rectangular probe antenna mounted on a finite and infinite PEC ground plane. We use directivity analysis group to investigate radiation pattern and radiation efficiency.

The rectangular probe antenna is simple construction and well-known for near-field and far-field response. Traditionally in rectangular probe antenna design, a coaxial pin is used to excite the waveguide. As per previous section TE10 mode is used which dominant the field polarization and magnitude. In aperture-type antenna, generated fields on the open aperture are act like source of the far fields. That's why in our simulation when the probe antenna is mounted on an infinite ground plane, the radiation equation can be directly applied to find the theoretical far-fields. In case of finite ground plane, the far-fields must be approximated using diffraction theory.[44]

Here in our FDTD simulation we use two terms. First, the antenna is mounted on an infinite ground plane. Second, the antenna is mounted on a finite ground plane.

6.6 Simulation Setup-FDTD

In This simulation we took vacuum filled rectangular waveguide of width b=20.86mm and a=8.16mm. Here vacuum filled rectangular waveguide surrounded by a PEC wall which thickness was 2.5mm. We used constructed structure for Rectangle structure. PEC sheet of ground plane extends to the outside of simulation region. We took it as infinite ground plane simulation. Additionally, we took PEC sheet of ground plane in finite dimension simulation which are g_x=40mm and g_y=20mm.

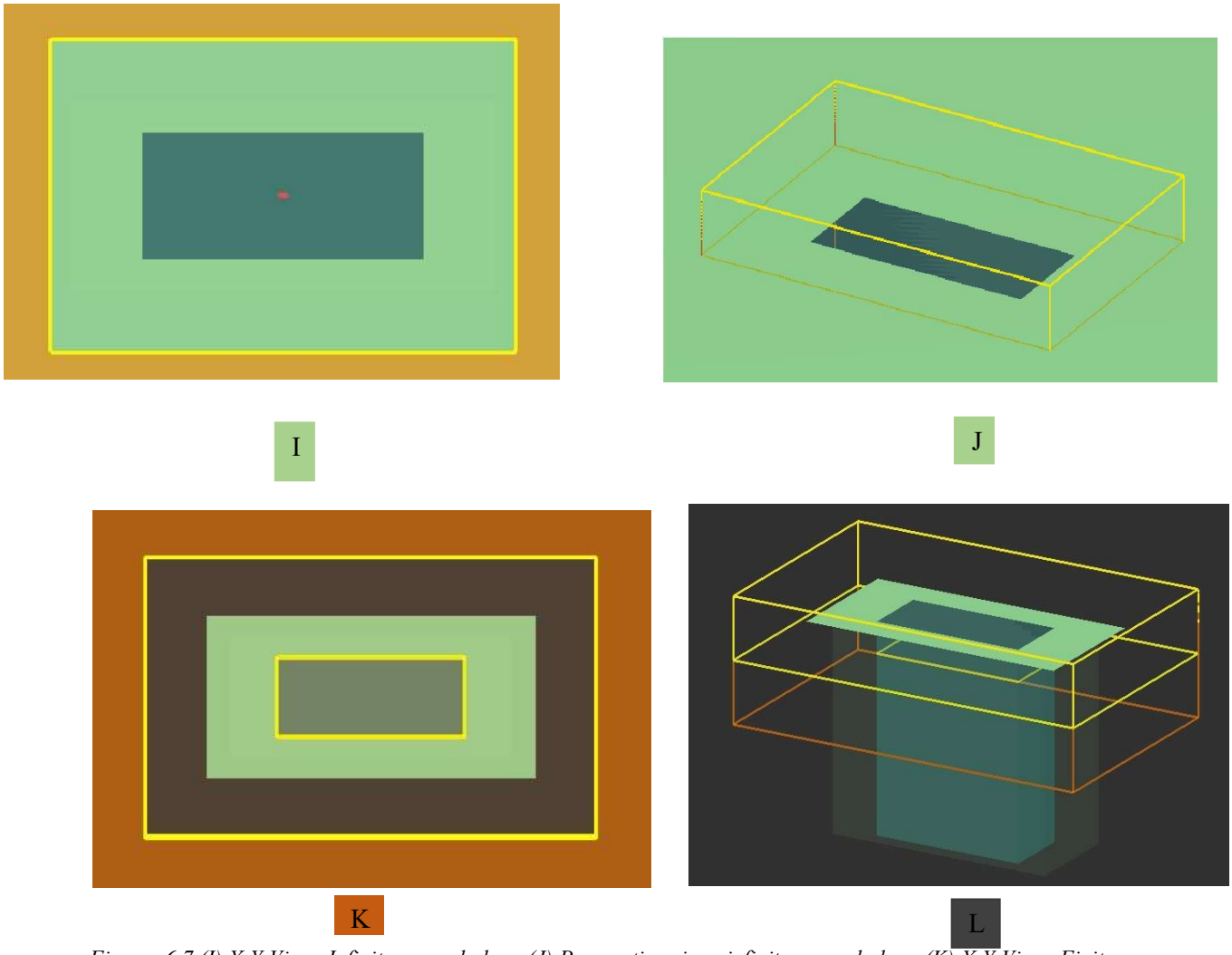

Figure: 6.7 (I) X-Y View: Infinite ground plane (J) Perspective view: infinite ground plane (K) X-Y View: Finite ground plane (L) Perspective view: finite ground plane of rectangular open-ended waveguide probe antenna.

In this simulation we took Directivity analysis group to setup the monitors and find the far fields of the OEWG antenna. As usual we use analysis group to setup Variable tab x, y, and z span. In analysis group, monitors are at least λ/4 away far from the edge of the open aperture for infinite ground plane or the edge of the finite ground plane. We set variable infinite ground plane either 1 or variable finite ground plane 0. Same way we set down sampling variable at 1, that's why down sampling doesn't occur on the monitors. We set source window to 0 for infinite ground plan.

In the case of finite ground plane simulation, we must allow the user to select a window. That's way we can avoid contribution of calculated far fields and radiated power in the directivity

analysis group. In directivity analysis group's parameters we set source window=1, window width 20.86mm, window height 8.16mm, window center (i,j)=(0,0), and window surface=z1.

To excite and measure the rectangular open-ended-waveguide-probe (OEWG) antenna we took TE10 mode port. This port is placed inside the waveguide's PEC walls near the bottom edge of the region. The TE_{10} mode is injected at 10GHz, which is above the mode's cutoff frequency at 6.56GHz.

We set a mesh for override region to ensure high enough resolution to give far field result. We set mesh accuracy of 4 for the rest of the simulation region. We specified PML all boundaries at least λ0/4 thick such that no reflections will occur outside the Directivity analysis group's monitors.

6.7 Result and analysis

6.7.1 Infinite ground plane

In our simulation script we added two step simulation setups. First one for infinite ground plane and second one is for finite ground plane. Here we use script file to run simulation file and generate result.

In this simulation set up works step by step. We modified directivity analysis group and FDTD region for each simulation. Both simulations take separate time for run. This occurs for mesh setting.

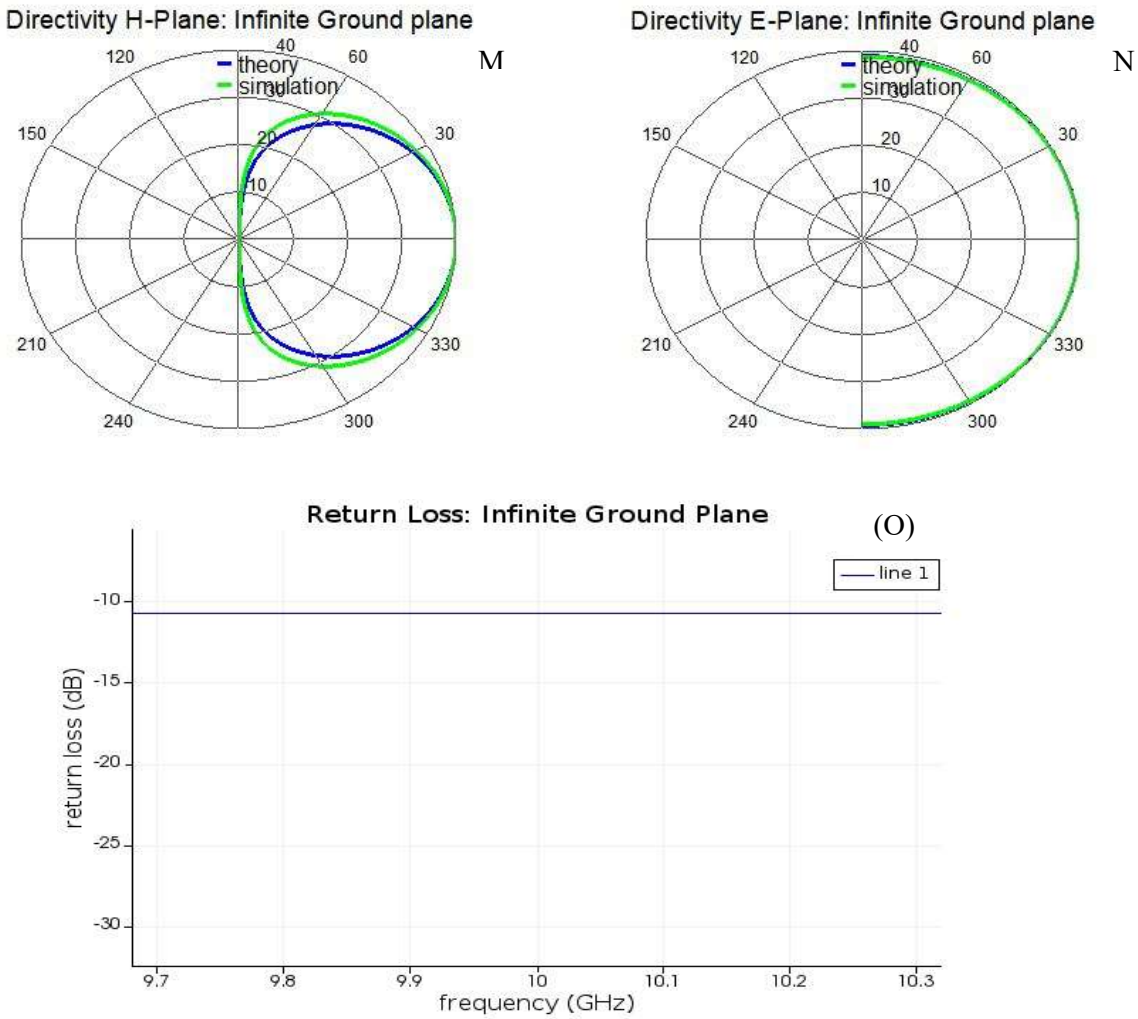

Figure: 6.8: (M) Directivity H-Plane (N) Directivity E-Plane (O) Return loss of rectangular open-ended waveguide probe antenna for Infinite ground plane.

After run simulation we found directivity pattern for H- plane and E- plane these are shown in figure 5.8 (M), (N) respectively. In figure 5.8 (M) & (N) shown H-plane corresponds to the X-Z plane and E-plane corresponds to the Y-Z plane. In the infinite ground plane, all the energy doesn't deviate forward direction and the pattern is only plotted from [-90, 90] degrees. The return loss is about 13dB.[43]

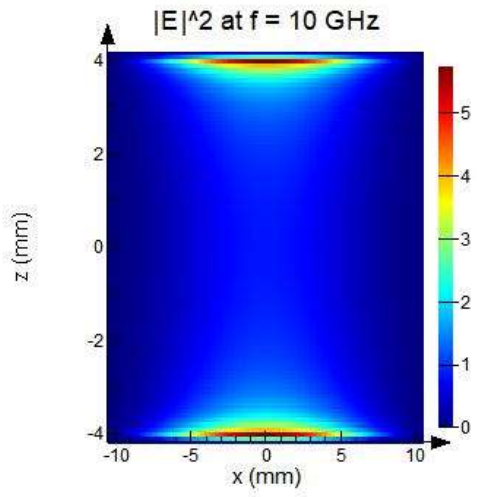

Figure: 6.9: (P) Aperture fields of rectangular open-ended waveguide probe antenna for infinite ground plane.

In theory we assume that the aperture fields are the ideal TE10 mode profile. From above figure 5.9 (P) our simulated aperture fields are shown. It differs from traditional directivity theory. Because, when transitioning from waveguide to free space, there are weak excitation occurs in other modes. These causes played main role of deviation between theoretical and simulated directivity patterns in the H-plane. It shows nearly 1.8dB difference in the total directivity. The radiation efficiency, which is taken as the ratio of accepted power over radiated power is at its expected value of 100%. Here no metallic or dielectric losses are present.

6.7.2 Finite ground plane

As previous section we know in finite ground plane for E plane alters radiative power. So here the open-ended waveguide probe for a finite ground plane, the size of the ground plane significantly alters the radiated power.

In figure 5.10 (Q), we can see H-plane beam width smaller than the E-plane beam width. The directivity pattern shows the expected pattern with a large main lobe.

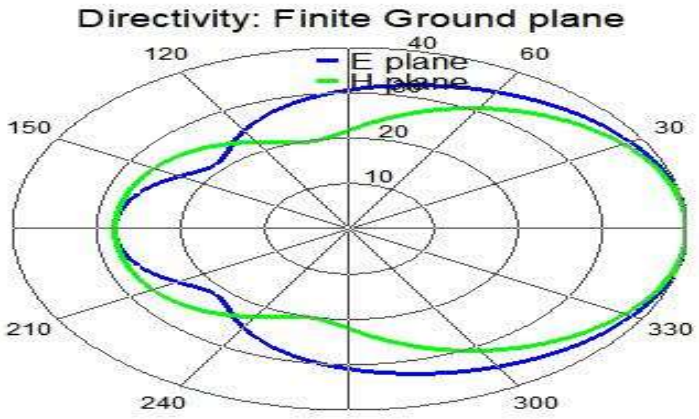

Q

Figure: 6.10: (Q) Directivity of rectangular open-ended waveguide probe antenna for finite Ground Plane.

Our radiation energy is 100% that's why we can assure that the source window is functioning correctly. Here directivity analysis group is subtracting the source's field's power contribution to the total radiated power calculation. As a result, we can accurately find the radiation efficiency.

6.8 Conclusion:

In this chapter, firstly we learned about patch antenna's parameter. We found, with decreasing dimension of antenna peaks (near field power, input impedance and I/P-O/P port power cutting frequency) are increased. Cutting frequency increasing rate is 1%. About directivity, results don't show any change with a little bit decreasing of dimensions. E-plane is altered by the presence of the substrate, but H-plane is unaltered by the presence of the substrate. The main disadvantage of these antennas is their relatively large size. The polarization can be either circular or linear depending on the design of the patch.

Lastly, we learned about directivity radiation pattern for infinite ground plane and finite ground plane. Moreover, we learned an open-ended waveguide probe's efficiency in both infinite and finite ground plan and we got accurate radiation energy. If we change dimensions of rectangle of probe antenna then radiation pattern, return loss, near-field power can be tuned. This observation will be helpful for further experiment.

Chapter 7

Conclusion

7.1 Thesis summary

In this thesis, we have reviewed several observations about nano antenna and RF antenna. Our main focus was on characterization of optical nano antenna and analyzing parameter of RF antenna.

We classify our thesis into six chapters. We arranged our first chapter with fundamental concept of RF and nano antenna which is primarily theory part. We focused on those theories whatever is required in subsequent chapters. Major topics are antenna parameters, surface plasmon resonance, localized surface plasmon resonance, absorption, scattering and extinction theory, plasmon hybridization theory for nano antenna etc. The second chapter is highlighted regarding simulation techniques theory and method while our simulation method is FDTD.

In third chapter, we present our observation about the optical property of single and coupled (bowtie nano antenna) gold (Au) nano particle by finite difference time domain (FDTD) simulation. In this study we observed the optical cross section and field enhancement for single and coupled Au nanoparticle as a function of diameter, size and separation. When we varied the length of a single and bowtie triangular nanoparticle, the absorption, scattering and extinction efficiency also respectively increase by certain times. We also observed a red shift of SPR and increased intensity when we increased the length. Again, we varied the separation of a couple triangular nanoparticle then the absorption, scattering and extinction efficiency also increased. But observing comparison of cross section's spectrum, we can say cross section's areas are changed on separation of coupling nanoparticles. In case of transmission and reflection, field strengths are decreased for increasing separation. Coupling particle, far field characteristics of electric field are too weak compared to near field intensity.

In Fourth chapter, similarly we observed optical property of dipole gold (Au) nano particle by finite difference time domain (FDTD) simulation. Here we varied the separation of a dipole nanoparticle then the absorption, scattering and extinction efficiency also increased. About observing comparison of cross section's spectrum, we can say cross section's areas are changed on separation of coupling nanoparticles.

In Fifth chapter, we investigated the parameter of patch and probe antenna by finite difference time domain (FDTD) simulation. In this study, we observed how antenna parameters can be tuned by changing their dimensions. First, we learned about patch antenna's parameter. We observed that, with decreasing dimension of antenna, peaks (of near field power, input impedance and I/P-O/P port power cutting frequency) are increased. About directivity, results don't show any change with a little bit decreasing of dimensions. E-plane is altered by the presence of the substrate, but H-plane is unaltered by the presence of the substrate. Secondly, we learned about rectangle probe antennas directivity radiation pattern for infinite ground plane and finite ground plane. Moreover, we learned an open-ended waveguide probe's efficiency in both infinite and finite ground plan and we got accurate radiation energy. If we change dimensions of rectangle of probe antenna then radiation pattern, return loss, Near-field power can be tuned.

That's all from our observation. Hopefully, we can say, our observation can considerable in the upcoming innovation of antenna application.

7.2 Challenges

In this paper we discussed about optical properties of nanostructure, and we varied nanoparticles size, shape, and separation. And highlighted about antenna parameters which can be tuned by changing their dimensions. We find some results. All our observation is based on our simulation technique. Simulation technique is an imitative representation of the functioning

of one system or process. Simulation modeling solves real-world problems. Actually, it's a virtual platform. In real life, some challenges can arise. May be our results became little bit different. If we investigated all experiment physically in laboratory, our results would be more accurate. It cannot be possible to fabricate any particle properly in simulation techniques which may another reason of inaccurate results.[48]

Our 2nd challenge is hardware accessories of computer. To find high resolution simulation result, it must be needed high configuration processor, graphics card, RAM etc. Our computer is not much higher than what we needed.

7.3 Future work

The ever-increasing high-tech demand cannot be full filled by nanotechnology in current world. In last two decades, there are significant progress in development of plasmonic nanoantenna technology. Because of individualistic and versatile optical functionalities it can be engineered with remarkable flexibility. [49]

Nanoantenna plays a vital role in many fields like, Optical Wireless Link, Wireless power transfer, Nanoantenna for Terahertz Detection, Nanoantenna for Nanophotonic Application, Mobile Communication, Bio imaging, radar technology etc.

In our paper, we choose Gold (Au) as a material. In nano antenna, we changed nano particles size, separation between particles and observed their results. Same way, if we want to change material with particles dimensions then there can be thousand ways to modify particles optical characterization for any invention. In case of RF antenna, we analyzed rectangular patch and probe antennas parameter. An antenna's performance depends on its parameter. This parameter can be tuned by changing of antennas material and dimensions.

In near future, all sectors may be dependent on nano technology. If we concentrate on nano particles fabrication and material choice, then we can use nano particles in uncounted way and uncounted applications.

7.4 Thesis conclusion

In our thesis, we started our discussion with RF antenna plasmonic nano antenna and also some basic theory regarding antenna. We talk through about FDTD software simulation method. Our target is characterization of nano antenna through FDTD simulation techniques. We started our investigation with triangle gold (Au) single particle. Sequentially we investigated bowtie antenna, dipole antenna. To observe absorption, scattering, extinction efficiency, transmission, reflection, field strengths and far field characteristics, we varied particles dimensions and separation between them. Hence, we got some increasing and decreasing rate of particle properties characteristics. Moreover, we knew that how to tune particle properties characteristics.

Lastly, we talked about antenna parameters. We discussed about patch and probe antenna. We changed our antennas dimensions to tune antennas parameter such as antennas radiation pattern, Gain, Directivity, effect of cutting frequency, input impedance etc.

In subject to conclude, we have shown nano optical antennas design and characterization which can be useful for any antenna research and application.

References

[1] L. Lin, Zheng, Yuebing, "Optimizing plasmonic nanoantennas via coordinated multiple coupling," *Scientific Reports,* vol. 5, 2015.

[2] E. D. O. a. K. Guven, "Scattering Suppression and Absorption Enhancement in Contour Nanoantennas," 2015.

[3] A. Kumar, K. H. Hsu, P. Chaturvedi, H. Ma, J. Xu, and N. X. Fang, "Fabrication and Optical Characterization of Bowtie Antennas," in *2008 8th IEEE Conference on Nanotechnology*, 2008, pp. 98-99.

[4] H. M. Sandip Gajera, N. Patel, "Comparative Analysis of Microstrip Line and Coaxial Feeding Technique for Rectangular Microstrip Patch Antenna," *Semantic Scholar,* 2013.

[5] A. P. A. K. Arya, and M. V. Kartikeyan*, "Microstrip patch antenna with skew-F shaped DGS for dual band operation," *Progress In Electromagnetics Research M,*

, vol. 19, , pp. 147–160, 2011.

[6] P. Kumar, L. Kansal, G. Gaba, and M. Baz, "A comprehensive study of RF antennas," *International Journal of Pure and Applied Mathematics,* vol. 118, pp. 755-764, 01/01 2018.

[7] O. Tutorial. (2006). *Learn Antenna Theory*. Available: contact@tutorialspoint.com www.tutorialspoint.com

[8] R. Solutions. (August 22nd, 2017). *RF Basics: Antenna Types and Characteristics*. Available: https://www.rfsolutions.co.uk/blog/rf-basics-antenna-types-and-characteristics/

[9] C. I. Votis, P. Kostarakis, and A. A. Alexandridis, "Design, Analysis, and Measurements of an Antenna Structure for 2.4 GHz Wireless Applications," *International Journal of Antennas and Propagation,* vol. 2010, p. 796154, 2010/12/13 2010.

[10] A. I. D. N. H. B. Noordin, "Antenna Parameter," vol. 26600 Pekan Pahang Malaysia, Available: hazlina@ump.edu.my

[11] J. Sankar. (August 15, 2016, 1969) Antenna Polarisation. *Electronicsforu.com*. Available: whatisnew@electronicsforu.com

[12] X. Gu and W. Geyi, "Design of a near-field RFID antenna array in metal cabinet environment," *IEEE Antennas and Wireless Propagation Letters,* vol. 18, no. 1, pp. 79-83, 2018.

[13] X. Wang, P. Gogol, E. Cambril, and B. Palpant, "Near-and far-field effects on the plasmon coupling in gold nanoparticle arrays," *The Journal of Physical Chemistry C,* vol. 116, no. 46, pp. 24741-24747, 2012.

[14] E. T.-e. RF. (May 22, 2018). *everythingRF*.

[15] P. Bharadwaj, B. Deutsch, and L. Novotny, "Optical Antennas," *Advances in Optics and Photonics,* vol. 1, pp. 438-483, 11/01 2009.

[16] Z. Jaksic, M. Obradov, S. Vukovic, and M. Belić, "Plasmonic enhancement of light trapping in photodetectors," *Facta Universitatis Series: Electronics and Energetics,* vol. 27, pp. 183-203, 06/01 2014.

[17] A. M. Krasnok, Ivan & Denisyuk, A.I. & Belov, Pavel & Miroshnichenko, Andrey & Simovski, , "Optical nanoantennas.," *Constantin & Kivshar, Yuri. (2013).* vol. Physics-Uspekhi. 56. 539. 10.3367/UFNe.0183.201306a.0561, 2013.

[18] J. Homola, "Surface Plasmon Resonance Sensors for Detection of Chemical and Biological Species," *Chemical Reviews,* vol. 108, no. 2, pp. 462-493, 2008/02/01 2008.

[19] A. García-Etxarri, "Modelization of plasmonic nanoantennas for optical microscopy and surface enhanced spectroscopy," 2010.
[20] J. Cao, E. K. Galbraith, T. Sun, and K. T. V. Grattan, "Comparison of Surface Plasmon Resonance and Localized Surface Plasmon Resonance-based optical fibre sensors," *Journal of Physics: Conference Series,* vol. 307, p. 012050, 2011/08/17 2011.
[21] Y. Chen and H. Ming, "Review of surface plasmon resonance and localized surface plasmon resonance sensor," *Photonic Sensors,* vol. 2, no. 1, pp. 37-49, 2012.
[22] P. K. Jain, K. S. Lee, I. H. El-Sayed, and M. A. El-Sayed, "Calculated absorption and scattering properties of gold nanoparticles of different size, shape, and composition: applications in biological imaging and biomedicine," (in eng), *J Phys Chem B,* vol. 110, no. 14, pp. 7238-48, Apr 13 2006.
[23] E. Prodan, C. Radloff, N. J. Halas, and P. Nordlander, "A Hybridization Model for the Plasmon Response of Complex Nanostructures," *Science,* vol. 302, no. 5644, p. 419, 2003.
[24] S. Baur, S. Sanders, and A. Manjavacas, "Hybridization of Lattice Resonances," *ACS Nano,* vol. 12, 01/04 2018.
[25] X. Lin, N. Wan, L. Weng, H. Zhu, and J. Du, *FDTD method and models in optical education* (14th Conference on Education and Training in Optics and Photonics, ETOP 2017). SPIE, 2017.
[26] S. Gedney, "Introduction to the Finite-Difference Time-Domain (FDTD) Method for Electromagnetics," *Synthesis Lectures on Computational Electromagnetics,* vol. 6, 01/26 2011.
[27] C. Abrudean, M. Panoiu, C. Panoiu, and I. Sora, "Using finite difference time-domain method to simulate the electromagnetic field in a multimode microwave oven," 01/01 2009.
[28] S. Tanev, V. V. Tuchin, and P. Paddon, "Light scattering effects of gold nanoparticles in cells: FDTD modeling," *Laser Physics Letters,* vol. 3, no. 12, pp. 594-598, 2006/12/01 2006.
[29] P. K. Jain, K. S. Lee, I. H. El-Sayed, and M. A. El-Sayed, "Calculated absorption and scattering properties of gold nanoparticles of different size, shape, and composition: applications in biological imaging and biomedicine," *The journal of physical chemistry B,* vol. 110, no. 14, pp. 7238-7248, 2006.
[30] A. Kumar, "Optical nano-antennas: Fabrication, characterization and applications," 01/01 2011.
[31] A. S. M. Mohsin, "Aggregation and Uptake Kinetics of Gold Nanoparticles in Biological Cells, Using Plasmon Coupling and Image Correlation Spectroscopy," 2015.
[32] P. Schuck, D. Fromm, A. Sundaramurthy, G. Kino, and W. Moerner, "Improving the Mismatch between Light and Nanoscale Objects with Gold Bowtie Nanoantennas," *Physical review letters,* vol. 94, p. 017402, 01/14 2005.
[33] A. S. M. Mohsin and M. B. Salim, "Probing the Plasmon Coupling, Quantum Yield, and Effects of Tip Geometry of Gold Nanoparticle Using Analytical Models and FDTD Simulation," *IEEE Photonics Journal,* vol. 10, no. 3, pp. 1-10, 2018.
[34] R. Fernandez Garcia, "Simulation and characterization of optical nanoantennas for field enhancement and waveguide coupling," 2013.
[35] A. S. Mohsin and M. B. Salim, "Probing the intracellular refractive index and molecular interaction of gold nanoparticles in hela cells using single particle spectroscopy," *International journal of nanomedicine,* vol. 13, p. 6019, 2018.

[36] S. Kühn, U. Håkanson, L. Rogobete, and V. Sandoghdar, "Enhancement of Single-Molecule Fluorescence Using a Gold Nanoparticle as an Optical Nanoantenna," *Physical Review Letters,* vol. 97, no. 1, p. 017402, 07/07/ 2006.
[37] H. Fischer and O. Martin, "Polarization sensitivity of optical resonant dipole antennas," *Journal European Optical Society - Rapid Publications vol 3 08018,* vol. 3, p. 8018, 04/30 2008.
[38] B. García-Cámara, F. Moreno, F. González, and O. Martin, "Light scattering by an array of electric and magnetic nanoparticles," *Optics express,* vol. 18, pp. 10001-15, 05/10 2010.
[39] M. A. Mohamed, E. Kuester, M. Piket-May, and C. Holloway, "The field of an electric dipole and the polarizability of a conducting object embedded in the interface between dielectric materials," *Progress In Electromagnetics Research B,* vol. 16, pp. 1-20, 01/01 2009.
[40] S. Farahani, "Chapter 5 - RF Propagation, Antennas, and Regulatory Requirements," in *ZigBee Wireless Networks and Transceivers*, S. Farahani, Ed. Burlington: Newnes, 2008, pp. 171-206.
[41] Z. Li and Y. Rahmat-Samii, *PBG, PMC and PEC ground planes: a case study of dipole antennas*. 2000, pp. 674-677 vol.2.
[42] R. K. Mishra and A. Patnaik, "Neurospectral analysis of coaxial fed rectangular patch antenna," in *IEEE Antennas and Propagation Society International Symposium. Transmitting Waves of Progress to the Next Millennium. 2000 Digest. Held in conjunction with: USNC/URSI National Radio Science Meeting (C*, 2000, vol. 2, pp. 1062-1065: IEEE.
[43] M.-H. Ho, K. Michalski, and K. Chang, "Waveguide Excited Microstrip Patch Antenna theory And Experiment," *Antennas and Propagation, IEEE Transactions on,* vol. 42, pp. 1114-1125, 09/01 1994.
[44] C. A. Balanis, "Antenna Theory and Design," vol. 4th Edition. John Wiley & Sons (2016).
[45] N. Yuan, T. Yeo, X.-C. Nie, Y.-B. Gan, and J. Li, "Analysis of Probe-Fed Conformal Microstrip Antennas on Finite Grounded Substrate," *Antennas and Propagation, IEEE Transactions on,* vol. 54, pp. 554-563, 03/01 2006.
[46] R. Waterhouse, "Small microstrip patch antenna," *Electronics letters,* vol. 31, no. 8, pp. 604-605, 1995.
[47] Z. Wang, S. Fang, and S. Fu, "Wideband dual-layer patch antenna fed by a modified L-strip," *Journal of Microwaves, Optoelectronics and Electromagnetic Applications,* vol. 9, pp. 89-99, 12/01 2010.
[48] K. Shinde, D. M. S. Shah, and P. Patel, *A Review on opportunities and challenges of Nano Antenna for Terahertz Communications*. 2019, pp. 1-6.
[49] S. Sahoo, S. Parveen, and J. Panda, "The present and future of nanotechnology in human health care," *Nanomedicine: Nanotechnology, Biology and Medicine,* vol. 3, no. 1, pp. 20-31, 2007.